



Ultraviolet-activated sodium perborate process (UV/SPB) for removing humic acid from water

Ahmed Jaber Ibrahim ^{a,*}

^a Scientific Research Center, Al-Ayen University, ThiQar 64011, Iraq

ARTICLE INFO:

Received 3 June 2022

Revised form 9 Aug 2022

Accepted 28 Aug 2022

Available online 29 Sep 2022

Keywords:

Absorption,
UV-vis spectrum,
Environment,
Contaminants,
Humic acid

ABSTRACT

Humic acid (HA) has a complex chemical composition and the ability to chelate, adsorb, and exchange ions with organic and inorganic contaminants in bodies of water, which worsens water quality and poses a threat to human health and the environment. In this research, an Ultraviolet-activated sodium perborate (UV/SPB) symbiotic method (UV/SPB) was developed to eliminate humic acid in water. The major synergistic and degradative processes of the humic acid were investigated, as well as the impact of the starting humic acid concentration, sodium perborate dose, and primary pH value on the humic acid elimination. Results indicate that just 0.5 % and 1.5 % of humic acid were eliminated mostly by sole UV and sole sodium perborate (SPB) methods, respectively. More effectively than other methods, UV/SPB removed humic acid with an efficiency of 88.83%. An experiment using free radicals to mask them revealed that the primary catalyst for humic acid removal is the hydroxyl radical generated by sodium perborate activation. The excitation-emission matrix spectroscopy, Ultraviolet-visible absorption (UV-Vis) spectrum, absorbance ratio values, specific Ultraviolet-visible absorbance values (SUVA), and UV/SPB method performance findings demonstrated the UV/SPB method's capability to degrade and mineralize humic acid.

1. Introduction

Humic acid, a non-regular macromolecular polymer formed over a long period by the polymerization of various biological remnants, is the principal component of natural organic matter (NOM) [1]. The complex chemical composition of humic acid and the presence of numerous organic functional groups, including hydroxyl(-OH), carboxyl(-COOH), carbonyl(C=O), methoxy(-O-CH₃), and quinone groups -(C(=O)-), make it able to chemically adsorb, exchange ions, and physical chelation with contaminants in bodies

of water that are both organic and inorganic. This compromises the water quality and endangers the ecosystem and public health [2]. Environmental studies now have one goal figuring out how to eliminate humic acid from water properly and effectively. Physical and chemical oxidation techniques are the primary means of regulating humic acid in water. The coagulation method [3], flocculation method [4], and adsorption method [5] are physical techniques for removing humic acid. However, these techniques transport humic acid into the solid phase; further solid waste processing is still necessary. Due to the rapid degradation and mineralization of humic acid, chemical oxidation is of major interest [6]. Commonly used chemical

*Corresponding Author: Ahmed Jaber Ibrahim

Email: ahmed.jibrahim@alayen.edu.iq

<https://doi.org/10.24200/amecj.v5.i03.191>

oxidation processes for treating organic wastewater include the photocatalysis method [7-9], The Fenton oxidation method [10], and the electrochemical oxidation method [11]. Despite this, each of these processes has drawbacks, including difficult reaction conditions and complicated operations. The in situ oxidizing agent sodium perborate (SPB, NaBO_3) is frequently employed. In contrast to sodium percarbonate, cyclic perborate ions ($\text{B}_2\text{O}_8\text{H}_4^{-2}$), which are made up of two peroxide chains lacking BO_3^- anions, are present in sodium perborate instead of being associated with inorganic salt and hydrogen peroxide [12]. After being dissolved in water, sodium perborate creates hydrogen peroxide steadily, making it an effective hydrogen peroxide alternative [13]. Solid sodium perborate is safer, simpler to carry, and easier to store than liquid hydrogen peroxide. The formation of hydroxyl radicals ($\cdot\text{OH}$) can occur during sodium perborate activation across a broad range, which is crucial. The primary methods for sodium perborate activating are ultraviolet light [14] and transitional metal ions [15]. Scientists have utilized UV-activated perborate to remove organic pollutants [13]. Furthermore, the perborate is often used as an oxidant in homogeneous photo-Fenton and heterogeneous Fenton-like reactions to remove colorant and phenolic compounds [12,16]. Of these, the UV-activated process is simple to use, secure, and free of other pollutants, allowing it to effectively stimulate hydrogen peroxide to break down organics in sewage [17,18]. Though UV-activated peroxide as well as the UV-activated sodium perborate (UV/SPB) approach has been used to eliminate organics from water, reports of the elimination of HA using UV-activated SPB are infrequent. To reduce humic acid in an aqueous solution, it was important for this research to construct a UV/SPB symbiotic system (UV/SPB). The influences of the primary humic acid concentration, sodium perborate concentration, and starting pH value on humic acid cleansing were investigated using the practical and effective spectrophotometric approach [19]. Using a free radical masking test, the primary compounds

produced in the symbiotic system for removing humic acid were identified. The degradation process was carefully investigated using UV spectrum, total organic carbon, and 3-dimensional excitation-emission matrix spectroscopic (3D-EEM).

2. Material and Methods

2.1. Chemicals

Every chemical was obtained with the highest level of purity, including humic acid (M.wt 2485 dalton, CAS1415-93-6, Merck Millipore Co., USA), Sodium perborate (NaBO_3 , SPB, CAS10486-00-7, Weifang Haizhiyuan Chemistry and Industry Co., China), Sodium sulfate (Na_2SO_4 , CAS7757-82-6, Tokyo Chemical Industry Co., Japan), Sodium hydroxide (NaOH , CAS1310-73-2, Weifang Haizhiyuan Chemistry and Industry Co., China), Sulfuric acid (H_2SO_4 , CAS7664-93-9, Merck Millipore Co., USA), Sodium carbonate (Na_2CO_3 , CAS497-19-8, Merck Millipore Co., USA), Sodium dihydrogen phosphate (NaH_2PO_4 , CAS7558-80-7, Tokyo Chemical Industry Co., Japan), Sodium nitrate (NaNO_3 , CAS7631-99-4, Merck Millipore Co., USA), Sodium bicarbonate (NaHCO_3 , CAS144-55-8, Weifang Haizhiyuan Chemistry and Industry Co., China), Sodium chloride (NaCl , CAS7440-23-5, Weifang Haizhiyuan Chemistry and Industry Co., China), and Tertiary butanol (TBA, CAS75-65-0, Merck Millipore Co., USA).

2.2. Experiment

The humic acid removal studies were carried out at 25°C. The UV led (16 W, 254 nm) was positioned above the beaker at a length of 3.5 cm. The magnetic stirrer held the beaker, which served as the chemical reactor. In this study, the UV irradiation was estimated to be 35.2 Jm cm^{-2} for an hour. A certain amount of the humic acid solution was diluted to 100 mL before the experiment. The sodium perborate was then added to the HA-imitated wastewater, and light irradiation started the reaction. 2.5 mL aliquots were taken out at predetermined intervals to measure the absorbance. Every experiment was run at least twice. Tertiary butanol was utilized as the scavenger to confirm the

creation of hydroxyl radicals.

2.3. Analysis and Procedure

To determine the effectiveness of the humic acid removal process, the solution's absorbance was measured using a UV-vis spectrophotometer and an external reference technique at a wavelength of 254 nm [20]. The mathematics formula read in Equation 1 as follows:

$$\text{HA elimination efficiency} = (C_0 - C_t / C_0) \times 100 \% \quad (\text{Eq.1})$$

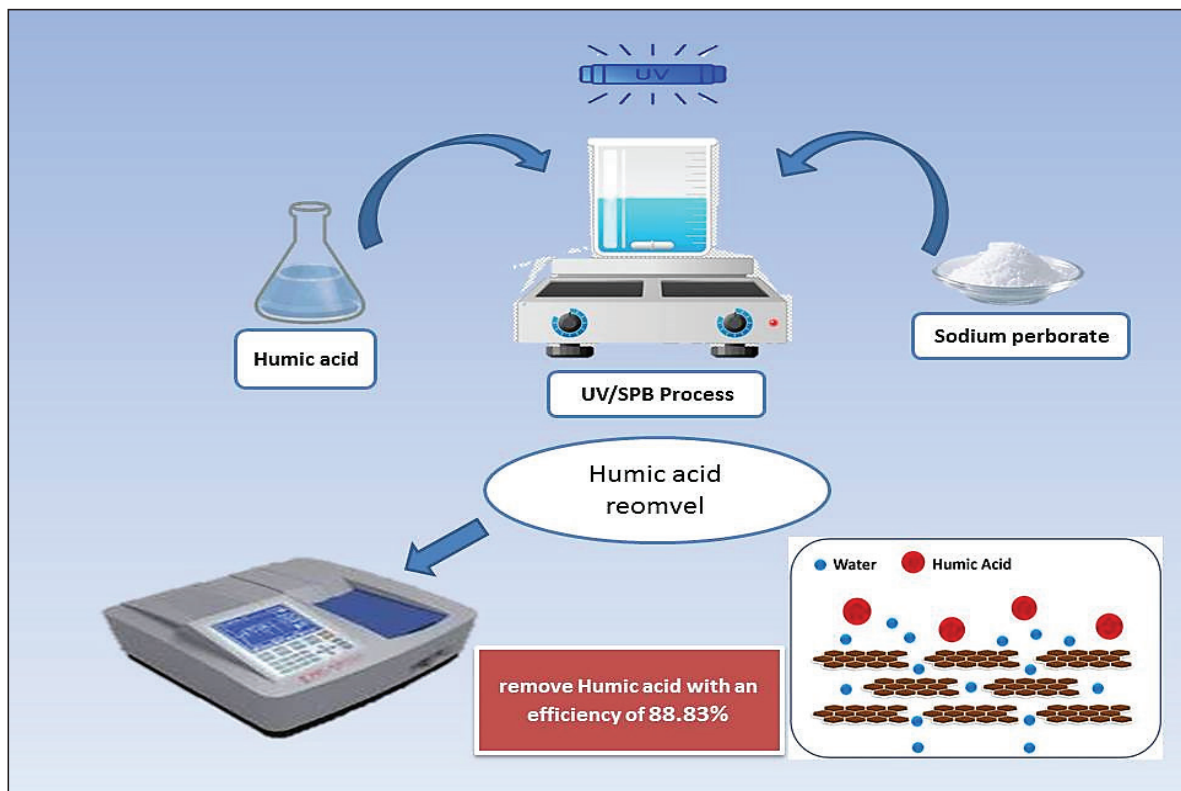
where C_t represents the humic acid quantity at the time of treatment t , and C_0 represents the initial humic acid quantity.

A variety of distinct UV-vis adsorption patterns were used to determine the change in the humic acid molecule structure. absorbance values were determined by spectrophotometer at wavelengths

(nm) at 203, 250, 253, 254, 365, 436, 465, and 665, respectively [21]. To characterize the changes in the humic acid molecule structure, continuous variations in the solution's absorbance range (200-800 nm) were also examined (Schema 1). A TOC tester was used to measure total organic carbon (TOC). A_x (sample absorbance at x nm) and TOC were used to determine specific UV absorbance (SUVA $_x$) which was shown in (Equation 2) [22].

$$(\text{SUVA}_x) = (A_x / \text{TOC}) \times 100\% \quad (\text{Eq.2})$$

The mechanism of the humic acid degradation was investigated using the 3D-EEM spectrum. The corresponding apertures were 10 and 5 nm, respectively, while the wavelength limits for the emission and stimulation ranges were (280-550 nm) and (200-400 nm), respectively.



Schema 1. Removal procedure for the humic acid and determined by the UV-Vis spectrophotometer

3. Results and discussion

3.1. Study of the humic acid elimination by UV/SPB process

3.1.1. Performance comparison of the humic acid elimination in various systems

First, three processes—UV, SPB, and UV/SPB—were examined for their ability to remove the humic acid, as shown in Figure 1. The following were the experimental parameters: starting pH 3, 10 mg L⁻¹ of the humic acid, 1 mmol L⁻¹ of Sodium perborate, and 10 mg L⁻¹ of the humic acid.

The single UV treatment took 1 hour to remove 0.5 % of the humic acid, which was barely eliminated. The single sodium perborate treatment had a negligible effect on the removal of the humic acid, with a decolorization ratio of 1.5% after an hour. The UV/SPB process had a higher decontamination efficiency of 88.83 % than the other two processes, which rose by a smaller amount. In addition, when the humic acid was removed using UV light and hydrogen peroxide

with the same molecular weight, the elimination ratio was only 40.2 % after 1 hour (60 min). It has the same effect as hydrogen peroxide when Sodium perborate is dissolved in water (Equation 3) [12], which is why it is frequently employed for in situ chemical oxidation. Hydrogen peroxide was produced in the only Sodium perborate system, but because it cannot be activated to produce hydroxyl radicals, very little humic acid was eliminated. In the UV/SPB system, hydrogen peroxide produced from Sodium perborate can generate hydroxyl radicals after being exposed to UV (Equation 4) [14], This might oxidize and damage the functional groups in the structure of the molecule of the humic acid.

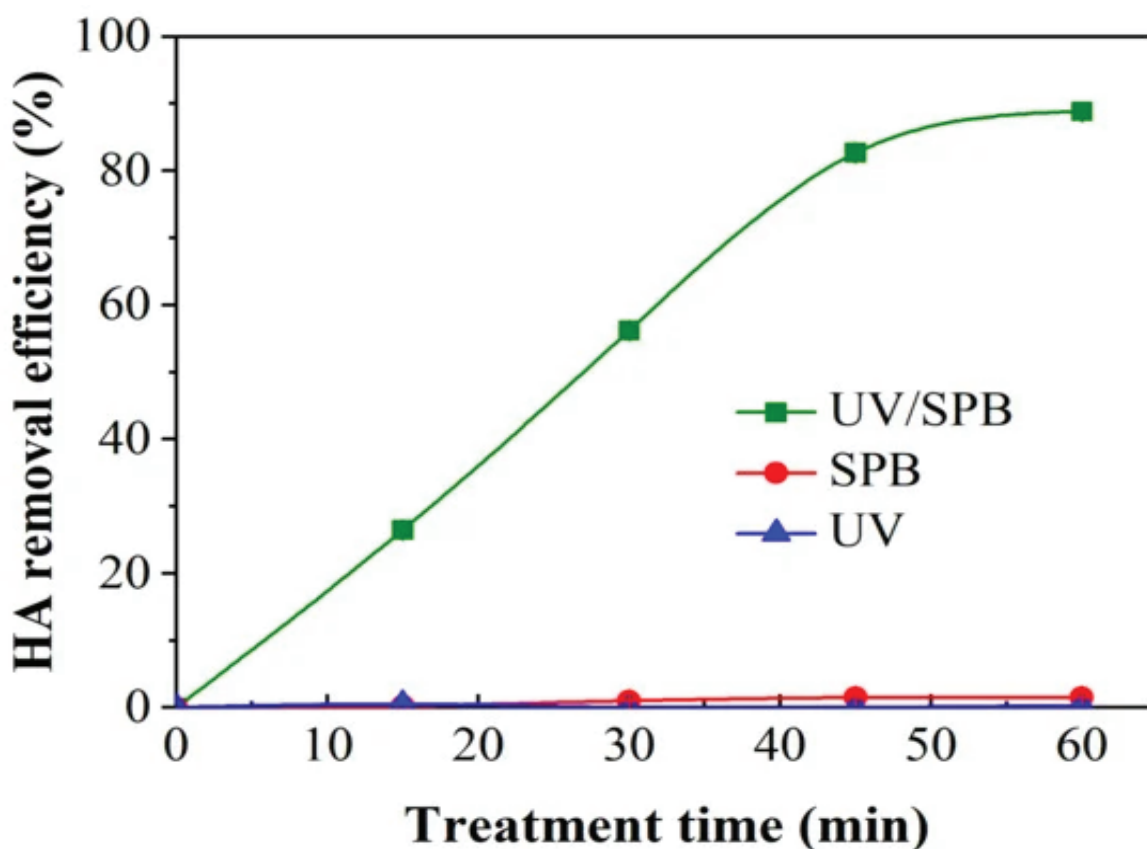
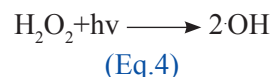
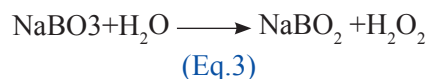


Fig. 1. Performance comparative of humic acid elimination in various systems

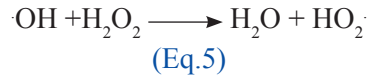
3.1.2. Humic acid concentration effect

Figure 2a illustrates the impact of the humic acid concentration on the humic acid elimination by the UV/SPB system. The optimized parameters were the sodium perborate concentration of 1 mmol L⁻¹ and primary pH of 3. The elimination ratio dropped as the humic acid primary concentration raised. After 1 hour, the elimination ratio dropped from 89.81% to 70.81% when the humic acid content increased from 5 to 15 mg L⁻¹.

Because there weren't enough oxygen radicals generated by the system to completely oxidize all of the pollutants in the solution, it proved that the oxygen radicals generated during the UV/SPB system were continually used. Additionally, as humic acid concentration gradually increased, the competition between humic acid molecules and oxygen radicals grew more intense. Further, the increased humic acid content would absorb more UV rays [23], preventing hydrogen peroxide activation and the subsequent generation of hydroxyl radicals ($\cdot\text{OH}$), which resulted in a decrease in the elimination of the humic acid.

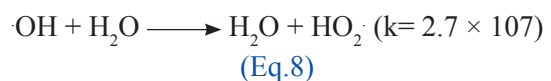
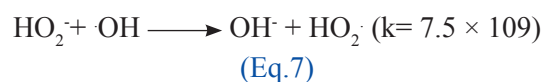
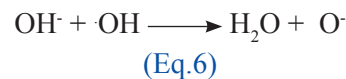
3.1.3. Effect of sodium perborate concentration

Reactive radicals are produced by the Sodium perborate (SPB), which is important for the symbiotic mechanism. Investigations were done on the effect of Sodium perborate concentration on humic acid removal (Figure 2b). A concentration of humic acid of 10 mg L⁻¹ and a pH of 3 was used in the test. After 1 hour, the Sodium perborate concentration was increased from 0.25 to 1.0 mmol L⁻¹, and the humic acid elimination ratio increased from 53.0 to 88.83 %. The number of active oxygen radicals in the system was increased with an increase in Sodium perborate concentration, which aided in the elimination of humic acid. Nevertheless, In excess, Sodium perborate would hunt the hydroxyl radical and produce the peroxy hydroxyl radical ($\text{HO}_2\cdot$) (Equation 5) [24]. peroxy hydroxyl radical has a weaker redox potential than hydroxyl radical. Consequently, the reduction in humic acid elimination was caused by the excess Sodium perborate (2 mmol L⁻¹).



3.1.4. Primary pH effect

Figure 2c illustrates the impact of various initial pH levels on the elimination of humic acid following UV/SPB processing. The Sodium perborate concentration was 1 mmol L⁻¹ and the humic acid concentration was 10 mg L⁻¹ during the experiment. After 1 hour, the pH value increased from 3 to 11, while the humic acid elimination fell from 88.83% to 58.4%. Strongly acidic conditions render the humic acid molecule neutral, resulting in more photochemical activity than under neutral or basic conditions. The pH has an impact on the redox potential Energy_(OH, H₂O) as well. The redox of Energy_(OH, H₂O) decreases from 2.61 V to 2.14 V as pH rises from 3 to 11 [25]. The alkaline state would cause the hydroxyl radical to undergo a reaction (Equation 6-8) that would change it into O \cdot (E = 1.78 V), which had a lower oxidation capability than the hydroxyl radical. When the pH reaches 11, the main form of hydrogen peroxide changes to HO_2^- , which reacts with hydroxyl radical ($\cdot\text{OH}$) at a faster rate than hydrogen peroxide does [27], therefore going to lead using more hydroxyl radical in the process.



3.1.5. Elimination of humic acid in various water bodies

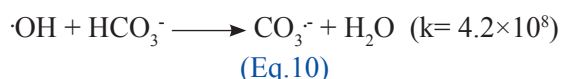
Figure 2d shows how the UV/SPB system removes humic acid from various water bodies. Following a one-hour reaction, the amounts of humic acid removed from tap water, lake water, and DI (deionized water) were 88.83%, 59.63%, and 47.53 %, respectively. It shows that both tap water and lake water prevented humic acid from being eliminated. These were the underlying causes. First, the hydroxyl

radical produced by the UV/SPB process would face competition from other naturally occurring organic substances in the lake. Second, the attendance of several anions in both tap water and lake water may limit the action of the oxidizing agents, decreasing the effectiveness of removing humic acid.

3.1.6. Common anions' influence on water

Figure 3a illustrates how common anions including HCO_3^- , CO_3^{2-} , NO_3^- , SO_4^{2-} , Cl^- , and H_2PO_4^- affect the removal of humic acid by the UV/SPB process. When the Carbonate anion (CO_3^{2-}) concentration was dropped from 1 to 10 mmol L^{-1} , as shown in Figure 3a, the elimination efficiency dropped from 63.7 to 44.9 %. The cause of the decline in humic acid elimination was that the hydroxyl radical produced by the process was used by Carbonate anion (CO_3^{2-}) to create $\text{CO}_3^{\cdot-}$ with a low oxidation capability (Equation 9) [28].

$\cdot\text{OH} + \text{CO}_3^{2-} \longrightarrow \text{CO}_3^{\cdot-} + \text{OH}^-$ ($k = 4.2 \times 10^8$) (Eq.9)
According to Figure 3b, the humic acid elimination efficiency rapidly declined from 74.2 to 53.5 % during 1 hour when the HCO_3^- concentration rose from 1 to 10 mmol L^{-1} . The system also converted hydroxyl radicals into $\text{HCO}_3^{\cdot-}$ (Equation 10). In addition, the HCO_3^- addition would result in a rise in the pH of the solution [29].



In Figure 3c, the elimination of humic acid reduced from 84.1 % to 79.9 % as the chlorine anion (Cl^-) was increased from 1 to 30 mmol L^{-1} . more excess chlorine anion would use more hydroxyl radicals and create more chlorine radicals (Equation 11,12). Therefore, the decrease in humic acid elimination was caused by the loss in oxidation capability [30].

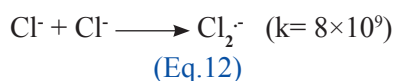


Figure 3d shows that the humic acid elimination ratio decreased with increasing Nitrate anion (NO_3^-) addition. The humic acid elimination was reduced to 33.4 % when 20 mmol L^{-1} of Nitrate anion was introduced. Reactive nitrogen species (NO_2^\cdot) ($E_0 = 0.867 \text{ V}$), can be produced when UV ray activated Nitrate anion which has reduced oxidation capability and also would be damaged through the UV/SPB process (Equation 13-15) [31]. Additionally, Nitrate anion could use hydroxyl radical immediately (Equation 16) [32].

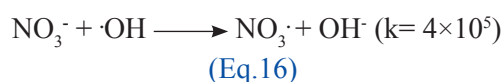
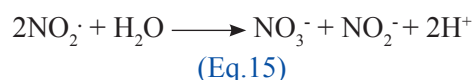
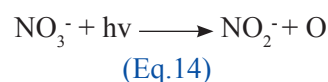
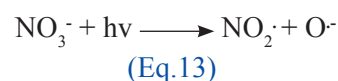
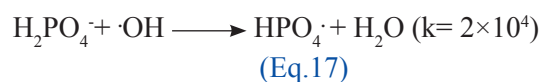


Figure 3e demonstrates that the humic acid elimination activity was unaffected by the rise in sulfate anion (SO_4^{2-}) quantity. The sulfate anion concentration was increased to 20 mmol L^{-1} , which resulted in an 88.0 % increase in humic acid elimination effectiveness. The literature claims that sulfate anion does not interact with the reactive species produced in the system [33,34]; hence it has no impact on eliminating humic acid. As shown in Figure 3f, the increase of H_2PO_4^- anion little affected the humic acid elimination. The humic acid removal efficiency decreased from 86.3 % to 82.4 % as the Dihydrogenphosphate anion (H_2PO_4^-) level increased from 10 to 30 mmol L^{-1} . Although Dihydrogenphosphate anion and hydroxyl radical can combine to generate the hydrogen phosphate radical (HPO_4^\cdot) (Equation 17) [35], The elimination of humic acid wouldn't be impacted because of the highly sluggish reaction rate.



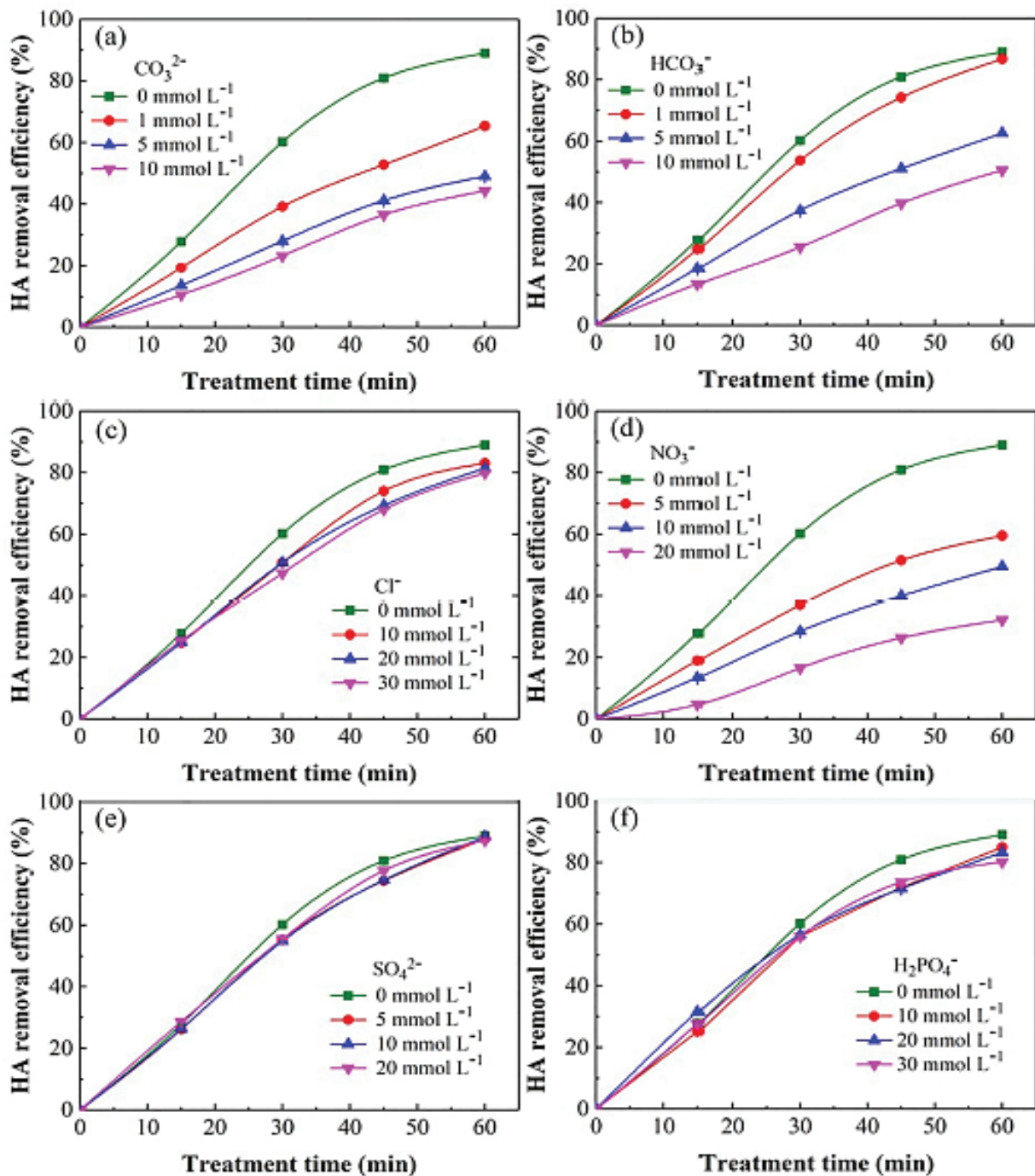


Fig. 2. Effect of several factors during UV/SPB system on Humic acid elimination:

- a) Humic acid concentration, b) Sodium perborate concentration,
c) primary pH, d) UV/SPB elimination of Humic acid in various waterbodies

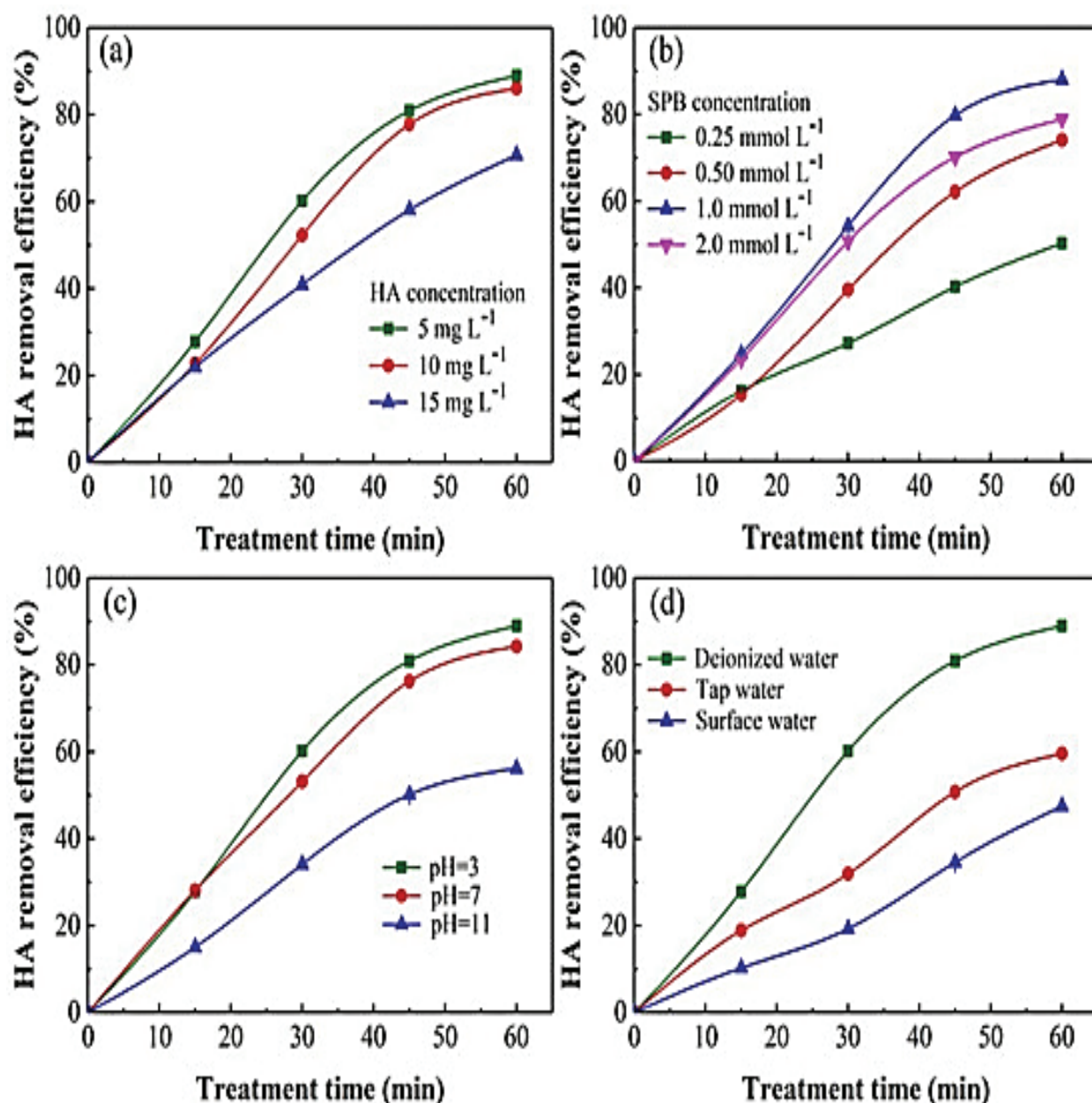


Fig. 3. Common anions' effects on the elimination of humic acid in UV/SPB process

3.2. Mechanism of UV/SPB humic acid elimination

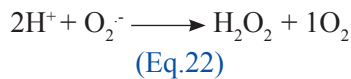
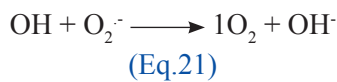
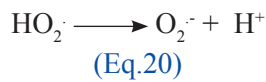
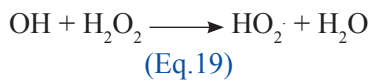
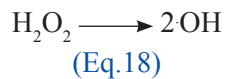
3.2.1. Examining Scavenging

Tertiary butanol (TBA) had the ability to remove hydroxyl radical from the process of oxidation ($k_{TBA, OH} = 3.8-7.6 \times 10^8$) [36]. The effect of Tertiary butanol adding on the elimination of humic acid in the UV/SPB process is shown in Figure 4. The

empirical parameters were starting pH 3, humic acid concentration of 10 mg L⁻¹, and Sodium perborate dosage of 1.0 mmol L⁻¹. The humic acid elimination was constrained by the addition of Tertiary butanol, as shown in the figure, which decreased from 16.5 to 11.5 % with the addition of Tertiary butanol and increased from 0.05 to 0.5 mol L⁻¹.

According to its testimony, hydroxyl radical may

be the primary oxidizing agent in the symbiotic system. After the addition of Tertiary butanol, the removal of humic acid was not entirely inhibited, which may be because the HO_2 generated by the breakdown of hydrogen peroxide (H_2O_2) could likewise produce other activated particles, including superoxide anion radicals ($\text{O}_2^{\cdot-}$) and singlet oxygen ($^1\text{O}_2$) (Equation 18-22) [37,38], which also have some oxidation ability and cannot be entirely repressed by Tertiary butanol.



3.2.2. Mechanism of humic acid degradation

The humic acid molecule structure changes may be reflected in the absorbance ratios [39]. Figure 5a depicts the development of these ratios in the UV/SPB mechanism. The value of absorbance ratio (253/203) declined from 0.98 to 0.44 with a rise in reaction time, showing the durability of functional groups (such as carboxyl [-COOH] and carbonyl groups [-C=O]) in humic acid aromatic structure gradually decreased. The absorbance ratio (250/365) increased from 2.42 to 3.20, which indicated that the humic acid molecular weight had been reduced. The humic acid chromophore was damaged by the absorbance ratio (254/436) rising from 4.63 to 5.60. The absorbance ratio (465/665) dropped from 3.5 to 1.0, demonstrating the loss of aromaticity in humic acid.

The humic acid molecule's structural differences can also be seen in the UV-visible absorption spectra. Figure 5b depicts the evolution of the humic acid absorption spectrum in the UV/SPB process over time. Implies that hydroxyl radical produced in the UV/SPB process damaged the chromophore groups and double bond structure (C=C) of humic acid, as well as oxidizing the

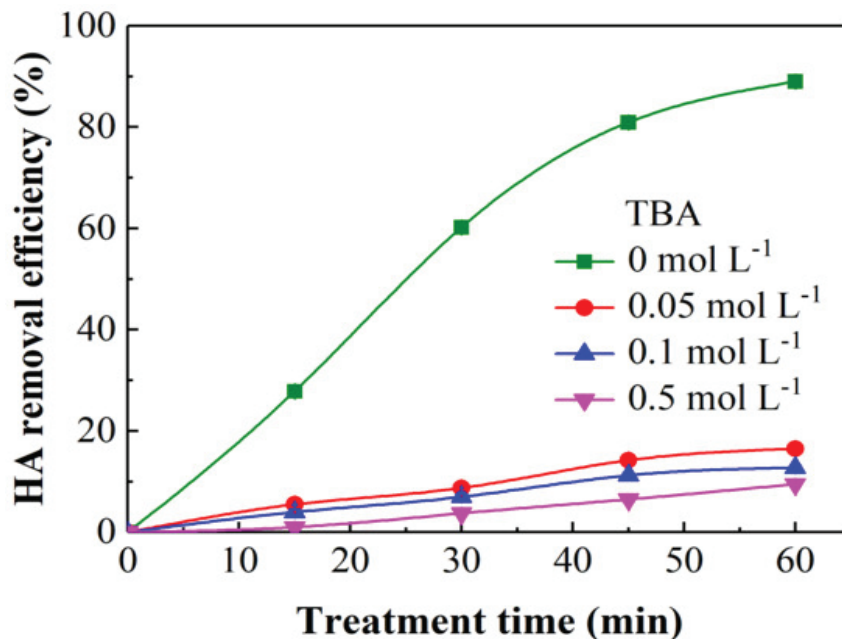


Fig. 4. Tertiary butanol addition's effect on humic acid removal

unsaturated ketone, the absorption edge of humic acid at 200-250 nm, becomes weaker with time. Additionally, the absorption edge shifted to the region of short wavelengths, a phenomenon known as blue shift. This proved that the carbon atom substitution process took place in the carbonyl group (C=O) of the humic acid chromophore [40]. Linearly expanded quinone groups and unsaturated carbons make up humic acid and fulvic acid. When specific substituent groups were used to replace the carbon atom of a chromophore, such as a carbonyl group (C=O), the absorption edge would shift to a low amplitude. In general, specific ultraviolet absorbances (SUVA) (254, 280, 365, and 436) were chosen to describe the mineralization and decomposition of natural organic matter. Where SUVA-365 nm denotes the molecular volume, SUVA-436 nm denotes the chromophore situation in natural organic matter, SUVA-280 nm denotes the stability of the aromatic system, and SUVA-254 nm denotes the molar mass [39].

After one hour of UV/SPB treatment, Figure 5c demonstrates that the SUVA-254 and SUVA-280 values decreased with time, indicating that the molar mass of organic compounds decreased and the basic aromatic framework was destroyed. The decrease in SUVA-365 showed that as the process developed, the volume of organic molecules dropped. The lowering value of SUVA-436 demonstrated that different oxidizing agents

destroyed the functional groups and chromophores. Additionally, the total organic carbon (TOC) in the process decreased from 7.139 to 2.440 mg L⁻¹ and the mineralization efficiency increased to 65.81 %, showing that the majority of humic acid had been converted into water (H₂O) and carbon dioxide (CO₂). UV spectrum and total organic carbon findings demonstrated that the UV/SPB symbiotic therapy could successfully break down the intricate chemical composition of humic acid.

Figure 6 displays the outcomes of further investigating the humic acid degradation process in the UV/SPB process using 3D-EEM. The intricacy of the spectral reaction and the scanning sample led to the division of the scanning spectrum into five sections. According to the structure of heterocyclic amino acids in natural organic matter, the I and II range can indicate aromatic proteins in organic molecules [40]. The III region in the humus structure denotes fulminate-like compounds connected to hydroxyl (-OH) and carboxyl (-COOH) groups. Region IV's coverage area reflects the tiny molecular structure of organic materials [35]. A humic-like fluorescence is shown by the V area. The fluorescence density of the five locations whole decreased and slowly vanished from 0 to 15 minutes (Fig. 6a and 6b) and 1 hour (Fig. 6c), moreover demonstrating that the humic acid molecular formula was broken down and mineralized in this cooperative system.

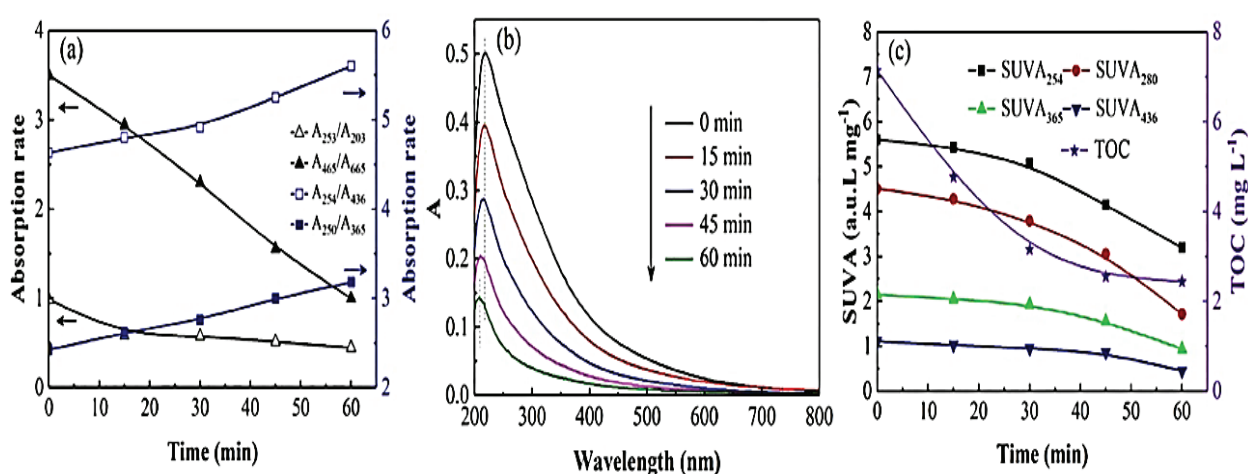


Fig. 5. (a) Ultraviolet absorption level, (b) Ultraviolet-visible spectrum, (c) SUVAx and TOC content for humic acid degradation

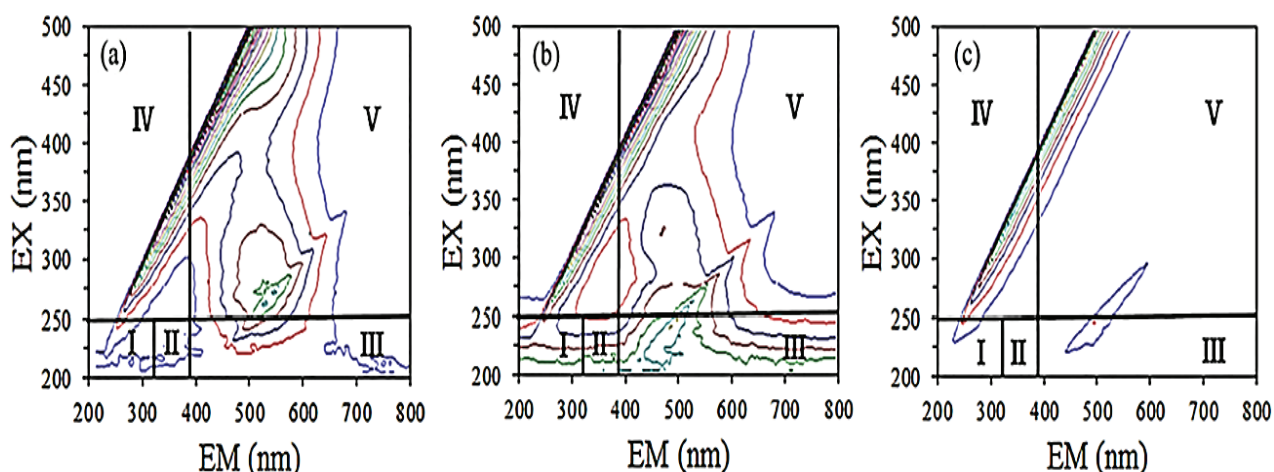


Fig. 6. humic acid's time-changing 3D-EEM spectra in the UV/SPB mechanism
(a) 0 min, (b) 15 min, (c) 1 hour (60 min)

4. Conclusions

The UV/SPB synergistic technique was developed in this work to eliminate humic acid from water, and the experimental findings showed that the procedure could efficiently degrade humic acid. The humic acid elimination effectiveness was 88.83 % after 1 hour of therapy under the experimental parameters of 10 mg L⁻¹ humic acid concentration, 1 mmol L⁻¹ Sodium perborate dose, and initial pH 3. When compared to DI (deionized water), the humic acid was eliminated far less effectively in tap and lakes water. The anion effect studies proved that, aside from SO₄⁻², Cl⁻, and H₂PO₄⁻, the carbonate anion (CO₃⁻²), bicarbonate anion (HCO₃⁻), and nitrate anion (NO₃⁻) exhibited varying degrees of humic acid elimination inhibition. By using masking tests, it was determined that the primary chemical responsible for removing humic acid was the hydroxyl radical produced by Sodium perborate activation. Results from the UV-vis spectrum, absorbance ratio, specific UV absorbance (SUVA), and 3D-EEM together demonstrated that the symbiotic mechanism could decompose and mineralize humic acid in water effectively.

5. Acknowledgements

This research is supported by the Physical Chemistry

Lab., Chemist Department, College of Education for Pure Science (Ibn-al Haitham), University of Baghdad.

6. References

- [1] J. Ryu, J. Jung, K. Park, W. Song, B. Choi, J. Kweon, Humic acid removal and microbial community function in membrane bioreactor, *J. Hazard. Mater.*, 417 (2021) 126088. <https://doi.org/10.1016/j.jhazmat.2021.126088>.
- [2] L. Cui, Y. Zhang, K. He, M. Sun, Z. Zhang, Ti4O7 reactive electrochemical membrane for humic acid removal: Insights of electrosorption and electrooxidation, *Separ. Purif. Tech.*, 293 (2022) 121112. <https://doi.org/10.1016/j.seppur.2022.121112>.
- [3] Y. Yue, G. An, L. Lin, H. Demissie, X. Yang, R. Jiao, D. Wang, Design and coagulation mechanism of a new functional composite coagulant in removing humic acid, *Separ. Purif. Tech.*, 292 (2022) 121016. <https://doi.org/10.1016/j.seppur.2022.121016>.
- [4] X. Huang, Y. Wan, B. Shi, J. Shi, Effects of powdered activated carbon on the coagulation-flocculation process in humic acid and humic acid-kaolin water treatment, *Chemosphere*, 238 (2019) 124637. <https://doi.org/10.1016/j.chemosphere.2019.124637>.

- [5] Y. Chen, Y. Qian, J. Ma, M. Mao, L. Qian, D. An, New insights into the cooperative adsorption behavior of Cr(VI) and humic acid in water by powdered activated carbon, *Sci. Total Environ.*, 817 (2022) 153081. <https://doi.org/10.1016/j.scitotenv.2022.153081>.
- [6] S. Lee, Y. Roh, D.-C. Koh, Oxidation and reduction of redox-sensitive elements in the presence of humic substances in subsurface environments: A review, *Chemosphere*, 220 (2018) 86–97. <https://doi.org/10.1016/j.chemosphere.2018.11.143>.
- [7] V. Oskoei, M. H. Dehghani, S. Nazmara, B. Heibati, M. Asif, I. Tyagi, S. Agarwal, V. K. Gupta, Removal of humic acid from aqueous solution using UV/ZnO nano-photocatalysis and adsorption, *J. Mol. Liq.*, 213 (2016) 374–380. <https://doi.org/10.1016/j.molliq.2015.07.052>.
- [8] E. Doustkhah, M. Esmat, N. Fukata, Y. Ide, D. A. Hanaor, M. H. N. Assadi, MOF-derived nanocrystalline ZnO with controlled orientation and photocatalytic activity, *Chemosphere*, 303 (2022) 124932. <https://doi.org/10.1016/j.chemosphere.2022.134932>.
- [9] B. Hashemzadeh, H. Alamgholiloo, N.N. Pesyan, E. Asgari, S. A. heikhmohammadi, J. Yeganeh, H. Hashemzadeh, Degradation of ciprofloxacin using hematite/MOF nanocomposite as a heterogeneous Fenton-like catalyst: A comparison of composite and core-shell structures, *Chemosphere*, 281 (2021) 130970. <https://doi.org/10.1016/j.chemosphere.2021.130970>.
- [10] B. Huang, C. Qi, Z. Yang, Q. Guo, W. Chen, G. Zeng, C. Lei, Pd/Fe₃O₄ nanocatalysts for highly effective and simultaneous removal of humic acids and Cr(VI) by electro-Fenton with H₂O₂ in situ electro generated on the catalyst surface, *J. Catal.*, 352 (2017) 337–350. <https://doi.org/10.1016/j.jcat.2017.06.004>.
- [11] T. Maqbool, Q.V. Ly, K. He, L. Cui, Y. Zhang, M. Sun, Z. Zhang, Reactive electrochemical ceramic membrane for effective removal of high concentration humic acid: Insights of different performance and mechanisms, *J. Membr. Sci.*, 651 (2022) 120460. <https://doi.org/10.1016/j.memsci.2022.120460>.
- [12] C. Zhang, Y. Dong, B. Li, F. Li, Comparative study of three solid oxidants as substitutes of H₂O₂ used in Fe (III)-oxalate complex mediated Fenton system for photocatalytic elimination of reactive azo dye, *J. Clean. Prod.*, 177 (2018) 245–253. <https://doi.org/10.1016/j.jclepro.2017.12.211>.
- [13] H.R. Sindelar, M.T. Brown, T.H. Boyer, Evaluating UV/H₂O₂, UV/percarbonate, and UV/perborate for natural organic matter reduction from alternative water sources, *Chemosphere*, 105 (2014) 112–118. <https://doi.org/10.1016/j.chemosphere.2013.12.040>.
- [14] J. Gao, J. Song, J. Ye, X. Duan, D.D. Dionysiou, J.S. Yadav, M.N. Nadagouda, L. Yang, S. Luo, Comparative toxicity reduction potential of UV/sodium percarbonate and UV/hydrogen peroxide treatments for bisphenol A in water: An integrated analysis using chemical, computational, biological, and metabolomic approaches, *Water Res.*, 190 (2021) 116755. <https://doi.org/10.1016/j.watres.2020.116755>.
- [15] D. Habibi, M.A. Zolfigol, M. Safaiee, A. Shamsian, A. Ghorbani Choghamarani, Catalytic oxidation of sulfides to sulfoxides using sodium perborate and/or sodium percarbonate and silica sulfuric acid in the presence of KBr, *Catal. Comm.*, 10 (2009) 1257–1260. <https://doi.org/10.1016/j.catcom.2008.12.066>.
- [16] F. LACSA, Oxidative degradation of phenol via heterogeneous Fenton-Like reaction over Fe-ZSM5 catalyst using sodium perborate and sodium percarbonate as oxidants, Ph.D. Thesis, Ateneo de Manila University, Metro Manila, Philippines (2017). <https://archium.ateneo.edu/theses-dissertations/30>
- [17] X. Chang, T. Lin, J. Mo, H. Xu, H. Tao, W. Liu, Coagulation combined with ultraviolet irradiation activated sodium percarbonate as pretreatment prior to ultrafiltration: Analysis

- of free radical oxidation mechanism and membrane fouling control, *Chemosphere*, 287 (2022) 132049. <https://doi.org/10.1016/j.chemosphere.2021.132049>.
- [18] J. Gao, R.F. Nunes, K. O'Shea, G.L. Saylor, L. Bu, Y.-G. Kang, X. Duan, D.D. Dionysiou, S. Luo, UV/Sodium percarbonate for bisphenol A treatment in water: Impact of water quality parameters on the formation of reactive radicals, *Water Res.*, 219 (2022) 118457. <https://doi.org/10.1016/j.watres.2022.118457>.
- [19] A.H. Alminshid, H.A. Alalwan, H.A. Abdulghani, M.M. Mohammed, Spectrophotometric study of ephedrine hydrochloride in drug using molecular absorption UV-Visible, *Spectrochim. Acta. Mol. Biomol. Spectros.*, 270 (2022) 120828. <https://doi.org/10.1016/j.saa.2021.120828>.
- [20] X.-F. Zhou, J.-P. Liang, Z. Z.-L. hao, H. Yuan, J.-J. Qiao, Q.-N. Xu, H.-L. Wang, W.-C. ang, D.-Z. Yang, Ultra-high synergetic intensity for humic acid removal by coupling bubble discharge with activated carbon, *J. Hazard. Mater.*, 403 (2021) 123626. <https://doi.org/10.1016/j.jhazmat.2020.123626>.
- [21] Y. Cui, J. Yu, M. Su, Z. Jia, T. Liu, G. Oinuma, T. Yamauchi, Humic acid removal by gas-liquid interface discharge plasma: Performance, mechanism and comparison to ozonation, *Environ. Sci. Water Res. Tech.*, 5 (2019) 152–160. <https://doi.org/10.1039/C8EW00520F>.
- [22] D. Yuan, J. Tang, Z. Nie, S. Tang, Study on humic acid removal in water by ultraviolet activated sodium percarbonate, *J. Yanshan Univ.*, 45 (2021) 220–226. <https://doi.org/10.3390/coatings12070885>
- [23] X. Li, B. Wu, Q. Zhang, D. Xu, Y. Liu, F. Ma, Q. Gu, F. Li, Mechanisms on the impacts of humic acids on persulfate/Fe²⁺-based groundwater remediation, *Chem. Eng. J.*, 378 (2019) 122142. <https://doi.org/10.1016/j.cej.2019.122142>.
- [24] C. Tan, N. Gao, Y. Deng, Y. Zhang, M. Sui, J. Deng, S. Zhou, Degradation of antipyrine by UV, UV/H₂O₂ and UV/PS, *J. Hazard. Mater.*, 260 (2013) 1008–1016. <https://doi.org/10.1016/j.jhazmat.2013.06.060>.
- [25] G.V. Buxton, C.L. Greenstock, W.P. Helman, A.B. Ross, Critical review of rate constants for reactions of hydrated electrons, hydrogen atoms and hydroxyl radicals (OH/O) in Aqueous Solution, *J. Phys. Chem. Ref. Data.*, 17 (1988) 513–886. <https://doi.org/10.1063/1.555805>.
- [26] S. Tang, D. Yuan, Y. Rao, M. Li, G. Shi, J. Gu, T. Zhang, Percarbonate promoted antibiotic decomposition in dielectric barrier discharge plasma, *J. Hazard. Mater.*, 366 (2019) 669–676. <https://doi.org/10.1016/j.jhazmat.2018.12.056>.
- [27] D. Das, A. Bordoloi, M.P. Achary, D.J. Caldwell, R.P. Suri, Degradation and inactivation of chromosomal and plasmid encoded resistance genes/ARBs and the impact of different matrices on UV and UV/H₂O₂ based advanced oxidation process, *Sci. Total Environ.*, 833 (2022) 155205. <https://doi.org/10.1016/j.scitotenv.2022.155205>.
- [28] D. Yuan, C. Zhang, S. Tang, Z. Wang, Q. Sun, X. Zhang, T. Jiao, Q. Zhang, Ferric ion-ascorbic acid complex catalyzed calcium peroxide for organic wastewater treatment: Optimized by response surface method, *Chin. Chem. Lett.*, 32 (2021) 3387–3392. <https://doi.org/10.1016/j.ccllet.2021.04.050>.
- [29] J. Fang, Y. Fu, C. Shang, The Roles of Reactive Species in Micropollutant Degradation in the UV/Free Chlorine System, *Environ. Sci. Tech.*, 48 (2014) 1859–1868. <https://doi.org/10.1021/es4036094>.
- [30] L. Cai, L. Li, S. Yu, J. Guo, S. Koppers, L. Dong, Formation of odorous by-products during chlorination of major amino acids in East Taihu Lake: Impacts of UV, UV/PS and UV/H₂O₂ pre-treatments, *Water Res.*, 162 (2019) 427–436. <https://doi.org/10.1016/j.watres.2019.07.010>.
- [31] Y. Ji, C. Zeng, C. Ferronato, J.-M. Chovelon,

- X. Yang, Nitrate induced photodegradation of atenolol in aqueous solution: Kinetics, toxicity and degradation pathways, *Chemosphere*, 88 (2012) 644–649. <https://doi.org/10.1016/j.chemosphere.2012.03.050>.
- [32] Z. Xu, C. Shan, B. Xie, Y. Liu, B. Pan, Decomplexation of Cu(II) EDTA by UV/persulfate and UV/H₂O₂: Efficiency and mechanism, *Appl. Catal. B Environ.*, 200 (2017) 439–447. <https://doi.org/10.1016/j.apcatb.2016.07.023>.
- [33] S. Tang, Z. Wang, D. Yuan, C. Zhang, Y. Rao, Z. Wang, K. Yin, Ferrous ion-tartaric acid chelation promoted calcium peroxide fenton-like reactions for simulated organic wastewater treatment, *J. Clean. Prod.*, 268 (2020) 122253. <https://doi.org/10.1016/j.jclepro.2020.122253>.
- [34] D. Yuan, K. Yang, E. Zhu, X. Li, M. Sun, L. Xiao, Q. Hari, S. Tang, Peracetic acid activated with electro-Fe²⁺ process for dye removal in water, *Coatings*, 12 (2022) 466. <https://doi.org/10.3390/coatings12040466>.
- [35] S. Tang, J. Tang, D. Yuan, Z. Wang, Y. Zhang, Y. Rao, Elimination of humic acid in water: Comparison of UV/PDS and UV/PMS, *RSC Adv.*, 10 (2020) 17627–17634. <https://doi.org/10.1039/D0RA01787F>.
- [36] M. Zhao, Y. Xiang, X. Jiao, B. Cao, S. Tang, Z. Zheng, X. Zhang, T. Jiao, D. Yuan, MoS₂ co-catalysis promoted CaO₂ Fenton-like process: performance and mechanism, *Separ. Purif. Tech.*, 276 (2021) 119289. <https://doi.org/10.1016/j.seppur.2021.119289>.
- [37] M. Cheng, G. Zeng, D. Huang, C. Lai, P. Xu, C. Zhang, Y. Liu, Hydroxyl radicals based advanced oxidation processes (AOPs) for remediation of soils contaminated with organic compounds: A review, *Chem. Eng. J.*, 284 (2016) 582–598. <https://doi.org/10.1016/j.cej.2015.09.001>.
- [38] Y. Xiang, H. Liu, E. Zhu, K. Yang, D. Yuan, T. Jiao, Q. Zhang, S. Tang, Application of inorganic materials as heterogeneous cocatalyst in Fenton/Fenton-like processes for wastewater treatment, *Separ. Purif. Tech.*, 295 (2022) 121293. <https://doi.org/10.1016/j.seppur.2022.121293>.
- [39] T. Wang, G. Qu, J. Ren, Q. Yan, Q. Sun, D. Liang, S. Hu, Evaluation of the potentials of humic acid removal in water by gas phase surface discharge plasma, *Water Res.*, 89 (2016) 28–38. <https://doi.org/10.1016/j.watres.2015.11.039>.
- [40] Y. Li, G. Qu, L. Zhang, T. Wang, Q. Sun, D. Liang, S. Hu, Humic acid removal from micro-polluted source water using gas phase surface discharge plasma at different grounding modes, *Separ. Purif. Tech.*, 180 (2017) 36–43. <https://doi.org/10.1016/j.seppur.2017.02.046>.



A rapid removal of xylene from air based on nano-activated carbon in the dynamic and static systems and compared to commercial activated carbon before determination by gas chromatography

Mostafa Jafarizaveh^a, Akram Tabrizi^a and Farideh Golbabaei^{b,*}

^a MSc. of Occupational Health Engineering, lecturer, Health Faculty, Gonabad University of Medical Sciences, Gonabad, Iran

^{b,*} Professor of Occupational Health Engineering, Department of Occupational Health, Faculty of Health, Tehran University of Medical Sciences, Tehran, Iran

ARTICLE INFO:

Received 5 May 2022

Revised form 12 Jul 2022

Accepted 22 Aug 2022

Available online 28 Sep 2022

Keywords:

Xylene,
Adsorption,
Air,
Nano activated carbon,
Dynamic system,
Gas chromatography

ABSTRACT

As main air pollutants, volatile organic compounds (VOCs) must be paid special attention. In this study, the removal efficiency of xylene from the air was investigated by nano-activated carbons (NACs) as an efficient adsorbent and compared to commercial activated carbons (ACs). In the chamber, the xylene vapor in pure air was generated, stored in the airbag (5 Li), and moved to adsorbents. Then, the xylene vapor was absorbed on the NAC/AC adsorbents and desorbed from it by a heat accessory. The efficiency of xylene removal with NACs and ACs was investigated in the dynamic and static systems based on 100-700 mg L⁻¹ of xylene, flow rates of 100 ml min⁻¹, and 100 mg of adsorbent at a humidity of 32% (25°C). Xylene concentrations were determined by gas chromatography equipped with a flame ionization detector (GC-FID). In the batch system, the maximum absorption capacity for NACs and ACs was obtained at 205.2 mg g⁻¹ and 116.8 mg g⁻¹, respectively. The mean adsorption efficiency for NACs and ACs adsorbents was obtained at 98.5% and 76.55%, respectively. The RSD% for NACs ranged between 1.1-2.5% in optimized conditions. The characterizations of the NACs adsorbent showed that the particle-size range was between 35-100 nm. The results showed that the adsorption efficiency of NACs for removing xylene from the air was achieved more than ACs. The GC-MS validated the proposed procedure in real air samples.

1. Introduction

Xylene is a colorless, aromatic hydrocarbon with a sweet taste that is easily flammable. Xylene is naturally present in petroleum and coal, and as a result of forest fires, it's produced some of it. Xylene is a toxic one-ring aromatic compound that its release in the air can have a significant

effect on the health and well-being of humans and the quality of the air. The permissible exposure limit (PEL or OSHA PEL) for xylene is 100 ppm in the air [1]. One of the main concerns of industrial health experts is the control of volatile organic compounds such as xylene. Activated carbons are broadly defined to include the range of amorphous carbon-based materials and have a high degree of porosity with an extended surface area[2]. Recently, the removal of organic

*Corresponding Author: [Farideh Golbabaei](mailto:Farideh.Golbabaei@tums.ac.ir)

Email: fgolbabaei@sina.tums.ac.ir

<https://doi.org/10.24200/amecj.v5.i03.196>

compounds from the air by various processes such as adsorption, biofiltration and oxidation, has been widely studied. Gholamreza Mousavi et al showed that the xylene and other contaminated air such as benzene were removed from the air by a catalytic ozonation process. This study aims to evaluate the efficiency of activated carbon based on ozone (catalytic ozonation) to remove different concentrations of xylene. The results indicated that the efficiency of catalytic ozonation for removing xylene in the air was higher than single adsorption by AC [3]. In another study, the effect of retention time, ozone dose and relative humidity on the efficiency of the catalytic ozonation process in the removal of xylene from contaminated air were studied by Gholamreza Mousavi et al. They showed that the adsorption capacity of the AC adsorbent improved with the increase of inlet ozone dose as well as gas flow rate[3]. So far, a wide range of adsorbents has been used to separate various compounds from the air. These adsorbents differ in physical and chemical characteristics, such as the shape and size of the cavity, surface area, cavity volume, and surface activity. The superiority of nanoadsorbents over previous adsorbents is due to the nanometric scale, which causes tremendous changes in their physical and chemical properties. Other factors affecting the adsorption of analytes (BTEX) are the much number of adsorption sites and the extreme facilitation of molecular interactions in nanoadsorbents. Bin Gao et al reported developments of VOCs adsorption onto a variety of engineered carbonaceous adsorbents, including activated carbon, biochar, activated carbon fiber, carbon nanotube (CNTs), graphene (NG/NGO) and its derivatives (IL-NG), carbon-silica composites (CSC), ordered mesoporous carbon(OMC), etc. The key factors that influence VOC adsorption are analyzed with a focus on the physiochemical characteristics of adsorbents, properties of adsorbates, and the adsorption conditions[4]. Hamidreza Pourzamani et al investigated the adsorption capacity of nanoadsorbents to remove benzene and xylene

from aqueous solutions. In this study, single-walled carbon nanotubes (SWCNTs), multi-walled carbon nanotubes (MWCNTs), and hybrid carbon nanotubes (HCNTs) were used. This study showed that the efficiency of nanoadsorbents was significant in removing xylene from the air [5]. In another study, the removal of Ortho, Meta, and para-xylene from the air samples was carried out on an oxidized carbon nanotube cartridge as an adsorbent by Le Huu Quynh Anh et al. In this study, the oxidized carbon nanotube with carbonyl groups significantly increased the adsorption capacity of xylene isomers[6]. In another study by Lu et al, the multi-walled carbon nanotubes were oxidized with sodium hypochlorite and used to remove ethyl benzene and para-xylene from aqueous solutions and significantly improved the removal of benzene and para-xylene[7]. Also, Golbabaei et al showed that nano-activated carbon adsorbent has a higher adsorption capacity for xylene removal compared to commercial activated carbon in the static state[8]. The adsorption of BTEX on carbon nanotube cartridges from air samples was reported by Le et al and the results showed that the CNTs had high potential for BTEX adsorption due to their microporous structure and high surface area[9]. They showed that the oxidized CNTs with carbonyl groups increased its adsorption capacity for these isomers [6]. Also, Shahi Ahangar showed that the photocatalytic removal efficiency in the concentrations of 50, 100, and 300 ppm was equal to 87.8%, 98.9%, and 90.8%, respectively [10]. Many researchers used different pilot and nanoadsorbents (Ni-MWCNTs, GQDs, NGO, NG, MSN, ILs, Silica) to remove hazardous pollutants such as toluene, ethyl benzene, mercury, benzene, dust, and hydrogen sulfide from the air [4,11-20]. Finally, according to those mentioned above and the high efficiency of nanoadsorbents compared to other adsorbents in the removal of different materials in the previous studies, a comparison study for adsorption of xylene from the air between commercial activated carbon adsorbent and Nano carbon adsorbent was

obtained to survey the effect of nanoadsorbent in the removal of xylene from the air. The previous studies for removing BTEX from the air reported a low efficiency in the air ambient.

In this study, NACs were used as adsorbent to remove xylene vapor from the air and compared to ACs (NIOSH adsorbent). All effective parameters were optimized. The xylene in pure air was generated in the chamber of pilot for the dynamic process. Also, the effect of temperature on the desorption/desorption of xylene and reusability of NACs or ACs adsorbents was studied. The retention time of nano-activated carbon was also studied and its efficiency was calculated over different days (inter-day and intra-day).

2. Experimental

In this experimental-analytical study, the feasibility of replacing activated carbon with nano-activated carbon for removing xylene vapors from the air was studied. The study was done according to the following steps.

2.1. Instrumental and Reagents

In this study, Gas chromatography equipped with a flame ionization detector was used (Varian 3800, CP7996 with a length of 25 m and a diameter of 0.25 mm). The FID detector was chosen for xylene analysis in gas/liquid. Before injection, the slide the plunger carrier down until it is completely

over the syringe plunger, and tighten the plunger thumb screw finger-tight. The injector temperature was adjusted to 200°C. The column temperature reached from 35°C to 90°C with the speed of 20°C per minute, and the split ratio was adjusted from 2 to 1. The detector temperature tuned at 220°C. Hydrogen gas as a carrier gas was used at a flow rate of 30 ml min⁻¹. A Hamilton syringe was used for sample injection into the injector. Minimum and maximum pressures in psi for inlets and detectors tuned at the bulkhead fitting at the back of the gas chromatograph (100 psi). Finally, according to the peak areas of injecting of different xylene concentration to the GC-FID, a calibration curve was drawn (Fig.1). Agilent 5977B single quadrupole GC/MS based on cost-effective solution including the High-Efficiency Source (HES) for the most challenging detection limit samples was used for the xylene determination and the validation of procedure. Chemicals were acquired from Sigma Aldrich Germany. The mixed xylene (Catalogue Number: 108633, CAS N:1330-20-7, ACS, 99.5% purity) and para-xylene (Catalogue Number: 108684, CAS N:106-42-3, ACS, 99.7%) was procured from Merck. The standard solutions of xylene were made based on the procedure. In this study, the activated carbon (ACs) and Nano-activated carbon adsorbents (NACs) were prepared from Iranian Research Institute of the Petroleum Industry (RIPI, size <100 nm).

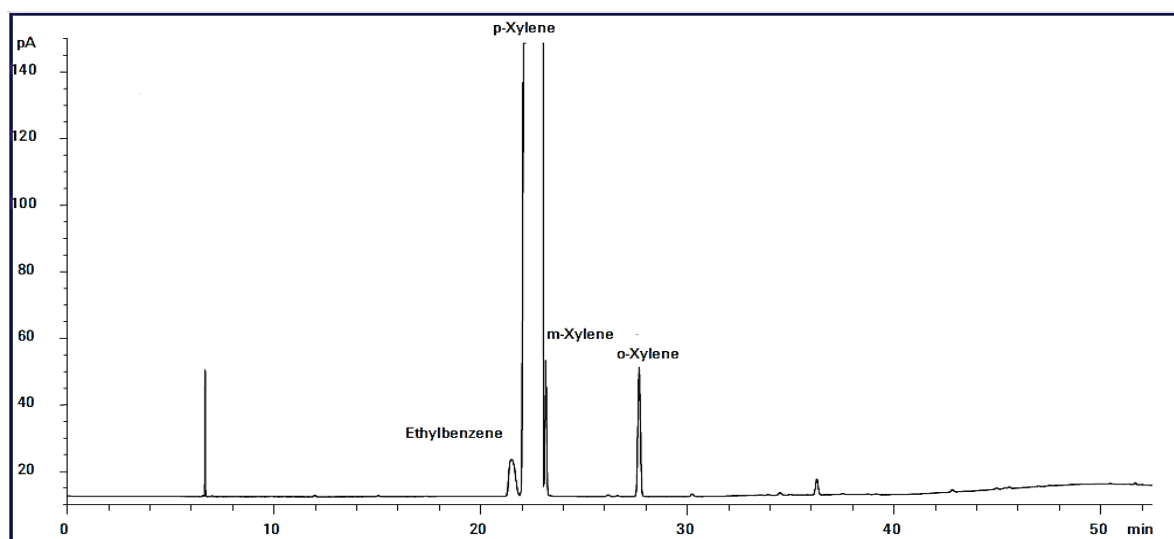


Fig.1. Peak area of GC-FID for species of xylene

2.2. Characterizations

The nano-activated carbon specification was investigated by Transmission Electron Microscopy (TEM), Electron Microscopy Scanning (SEM), and X-Ray Diffraction (XRD) at the Iranian Research Institute of the Petroleum Industry (RIPI). X-ray diffractions (PW 1840, Phillips, Netherland) based on radiation source of Cu-K α . The morphologies of the NACs were achieved by scanning electron microscopy (SEM) and transmission electron microscopy (TEM), respectively (PW3710, CM30, Philips, Netherland). SEM and TEM of NACs showed Nano size below 100 nm.

2.3. Absorption procedure

In this study, according to the NIOSH method [21], various concentrations of xylene (purchased from Merck Company) were prepared in a range of 10 to 300 mg L⁻¹ in sampling bags (Tedlar). Then, using a syringe, 400 microliters from the air existent in the sample bags were taken. In dynamic procedure, the different xylene concentration in

pure air was made in the chamber of pilot. (Fig.2). The standard solution of xylene vapored in the chamber, mixed with pure air, and moved to a PVC storage bag (1-5 Li) at 25°C. GC-FID has measured the certified reference gas of xylene. Then the xylene gas moved to NACs sorbent and AC with a flow rate from 100 mL up to 300 mL per min. After xylene absorption on the NACs/ACs adsorbents, the xylene was released from the adsorbent by heating up to 150°C. Then xylene concentration was determined by GC-FID. In the static system, the absorption xylene based on AC and NACs was achieved by a closed GC vial. In the static state, various concentrations of xylene were injected into the vial containing 5.0 mg adsorbent. Then 400 μ l of air from the vial was injected into the GC, and the adsorption capacity of the NACs/ACs adsorbents was calculated according to Equation 1.

$$q_e = \frac{(C_0 - C_e) \times V}{m}$$

(Eq. 1)

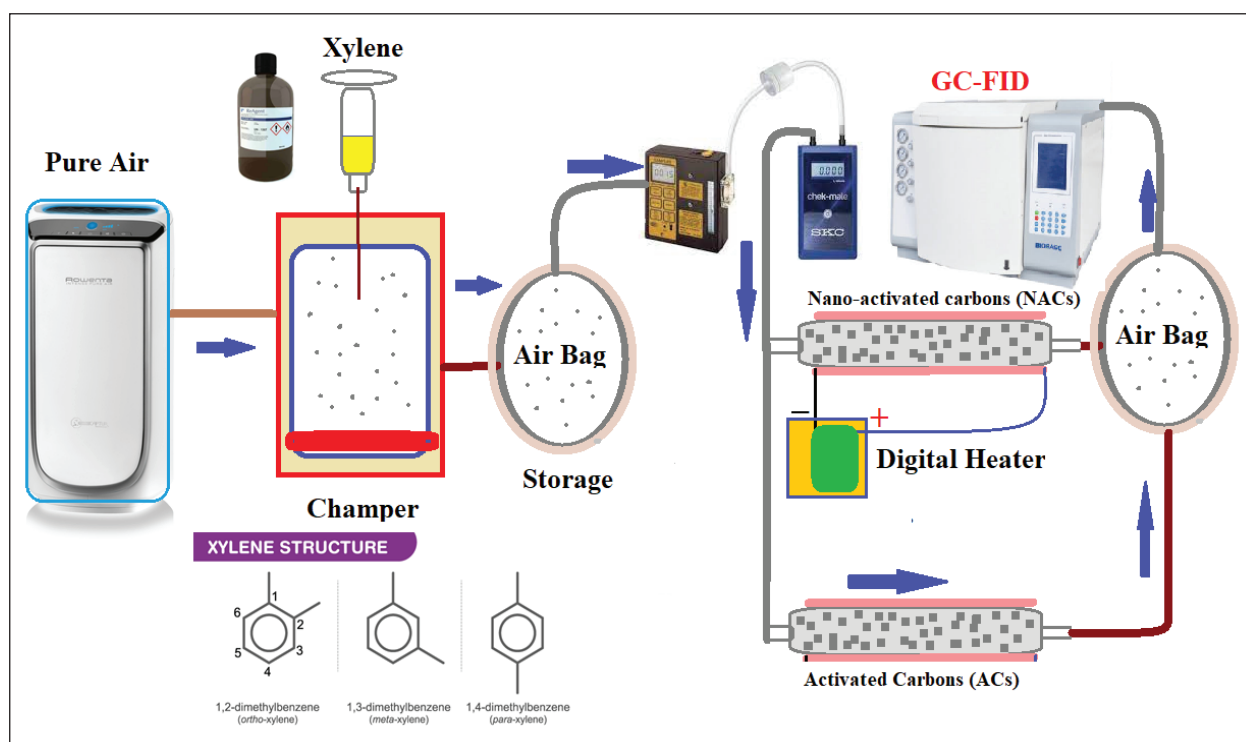


Fig.2. A schematic of the dynamic absorption system

3. Results and Discussion

3.1. Absorption efficiency and the effect of various factors on NACs

In this study, the different concentrations of 50, 200, 450, and 700 mg L⁻¹ of xylene were injected by syringe into the chamber (Impinger) in presence of pure air. Then, the micro personal sampling pump (SKC, 20-300 ml min⁻¹) in different flows (100, 200, and 300 ml min⁻¹) passed the air containing xylene from the impinger into a sample bag (1 or 3 liters). In this experiment, at the beginning of every test, the impinger was heated to warm the air inside, and xylene was steamed completely. Finally, after filling the sample bag, the air inside it was taken by GC gas syringe and injected into GC-FID, and then, the results were analyzed. After assuring the mixing of xylene with inlet air into the designed pilot, the adsorbent was placed after the sampling bag. The amount of weight of adsorbent was 100, 150, and 200 mg. During this experiment, the adsorption of various concentrations of xylene in different air flows and amounts of adsorbent mass were investigated. The experiments were carried out at constant moisture and an ambient temperature (25 °C). It should be noted that these experiments were carried out for two activated carbon and Nano activated carbon, and adsorption efficiency was calculated after a sampling time of 30 minutes (Equation 2). Each experiment was repeated five times, and the efficiency was obtained below Equation 2.

$$\text{Efficiency (\%)} = (C_i - C_f) / (C_i) \times 100 \quad (\text{Eq. 2})$$

C_i : initial xylene concentration and C_f : xylene concentration after passing from the adsorbent.

3.2. The storage stability of NACs

In this stage, to determine xylene adsorbed Nano-activated carbon, the 300 mg L⁻¹ of xylene was passed on adsorbent (100 mg) with a flow of 100 ml min⁻¹. After the adsorption of xylene on NACs or ACs, two ends of the adsorbent tube

were sealed with paraffin and stored at 0 °C, and the adsorbent was analyzed at different times (in terms of days), and the efficiency was calculated according to Equation 3

$$\text{Removal Efficiency (RE)} = A_f / A_i \times 100 \quad (\text{Eq. 3})$$

(A_f = Final analysis for xylene concentration adsorbed on adsorbent after distinct duration A_i : initial analysis for xylene concentration adsorbed on adsorbent).

3.3. Repeatability of NACs

Nano-activated carbon (NACs) recovery and its reusability were studied in this study. For this purpose, the nano activated carbon adsorbent was used in the dynamic system. The adsorbent's efficiency was obtained in a concentration of 300 mg L⁻¹ from xylene in a flow rate of 100 ml min⁻¹ and 100 mg of adsorbent. After xylene adsorption on NACs adsorbent, the xylene desorbed from NACs by the thermal accessory. The results showed that the recovery decreased after 16 times of adsorption/desorption. So, 16 times was considered as the number of reusability of adsorbent. The analysis for NACs or ACs was done three times (Mean of three determinations of samples \pm confidence interval; $P = 0.95$, $n = 10$). In this study, the mean values of the results are presented.

3.4. Data analysis and images

To analyze the data and compare the efficiency of various adsorbents for the removal of xylene, the SPSS software version 16 was used. Nano-activated carbon was analyzed utilizing TEM, XRD and SEM. The XRD, SEM, and TEM of activated carbon (ACs) and Nano activated carbon (NACs) are shown in Fig. 3a-e. The particle size of Nano-activated carbon was obtained below 100 nm by SEM and 30 nm by TEM. Also, XRD images showed a cubic structure of Nano activated carbon and activated carbon.

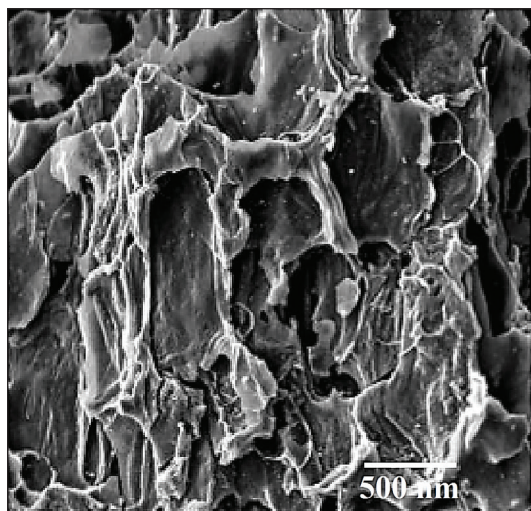


Fig.3a. SEM of activated carbon (ACs)

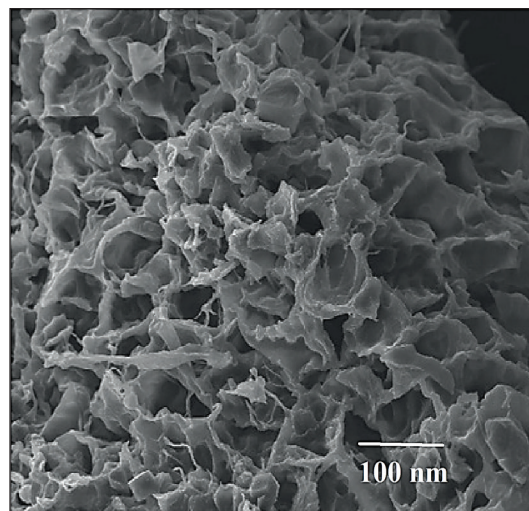


Fig.3b. SEM of Nanoactivated carbon (NACs)

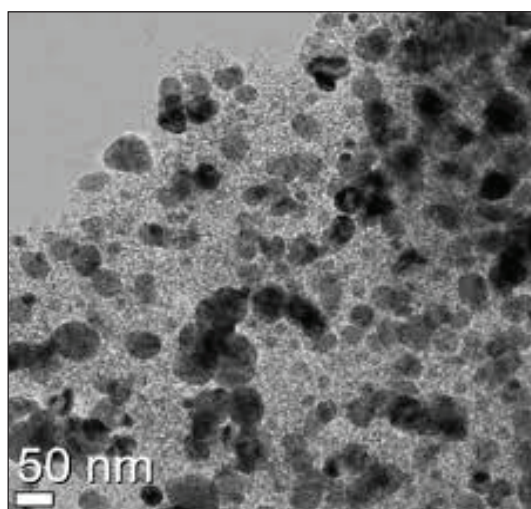


Fig.3c. TEM of activated carbon (ACs)

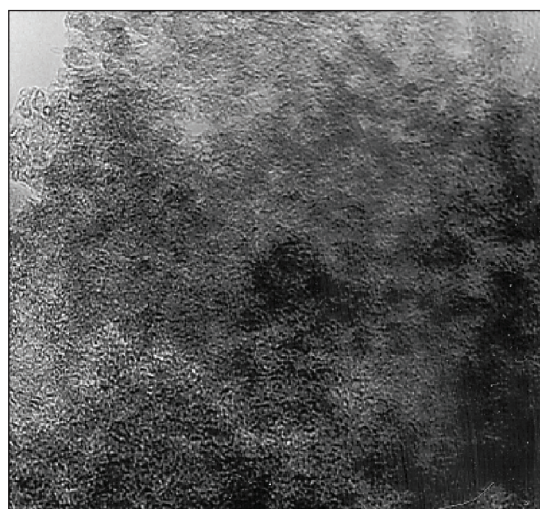


Fig.3d. TEM of Nanoactivated carbon (NACs)

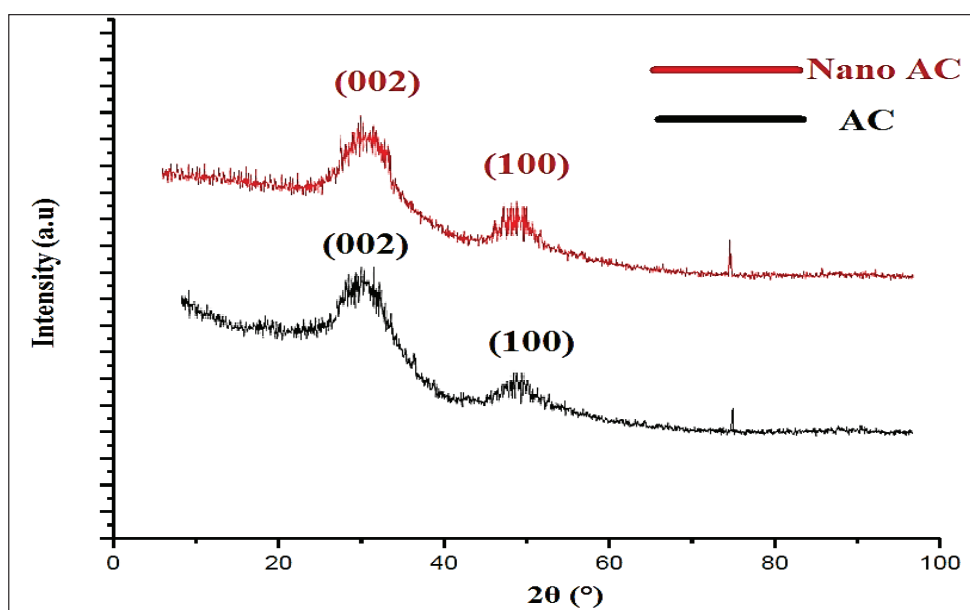


Fig.3e. XRD of activated carbon (ACs) and Nano activated carbon (NACs)

3.5. Adsorption Performance

The descriptive analysis of the adsorption efficiency (%) for NACs and AC is shown in Table 1. As can be seen, the average value of the adsorption efficiency of NACs is higher than AC (respectively 98.48 and 76.55). The statistical analysis of the results showed that the difference between the mean efficiency in Nano activated carbon and activated carbon was insignificant. (P-value =0.474). Linear regression was used to analyze the variables. In this analysis, the linear relationship between the dependent variable (adsorption efficiency, %) and independent variables (x1: xylene concentration, mg L⁻¹), (X2: air flow rate, ml min⁻¹) and (x3: adsorbent mass, mg) was investigated. The multi-linear regression equation was obtained as Equation 4 (R_{AC}: Activated carbon efficiency, R_{NAC}: Nano carbon Active Adsorbance Adsorption Efficiency).

$$R_{CA}=75.598-0.027x_1-0.042x_2+0.087x_3$$

$$R_{NCA}=98.737-0.024x_1-0.057x_2+0.09x_3$$

(Eq. 4)

Regarding the nano activated carbon adsorbent, the value of R² was 0.9895 in the activated carbon adsorbent equal to 0.9524. The correlation between the adsorption efficiency of NAC and ACs obtained experimentally. The linear regression equation obtained from the adsorptions results of xylene

by nano activated carbon and activated carbon adsorbents which were shown that there was a high correlation between them (correlation coefficient: 0.833) .

3.6. Effect of xylene concentration

In this study, the adsorption efficiency of xylene by NAC and ACs adsorbents in various xylene concentrations at optimized conditions such as the flow rate of 100 ml min⁻¹ and 200 mg of absorbance was evaluated. First, the adsorption efficiency was constant and then, decreased by increasing the xylene concentration. The adsorption efficiency in the activated carbon adsorbent (ACs) was decreased significantly more than NACs adsorbent. At concentrations of 50, 100, 450 and 700 mg L⁻¹, the removal efficiency of NACs and ACs for 10 analyses was obtained (99.8%, 99.4%, 97.6% and 95.8%) and (77.4%, 75.9%, 69.2% and 60.1%), respectively.

3.7. Effect of flow rate

According to the results, the adsorption efficiency was decreased with an increasing flow rate. The effect of flow rate on activated carbon efficiency is higher than Nano activated carbon. At flow rates of 100, 200, and 300 ml min⁻¹ with 200 mg adsorbents and xylene concentration of 100-200 mg L⁻¹, the removal efficiency of nano-activated carbon was equal to 98.5%, 94.3%, and 90.6%, respectively and for ACs was achieved 76.5%, 67.3% and 52.6%, respectively (Fig.4).

Table 1. Descriptive and analytical analysis of adsorbent efficiency of Nano activated carbon and activated carbon (P-value=0.474)

Adsorbent type	Number	AEA	SD	SE	CI (95%)	
					Lower limit	Upper limit
NACs	36	98.48	10.27	1.7	97.2	99.8
AC	36	76.55	10.03	1.67	67.4	85.7
Average	72	87.49	10.08	1.18	82.3	92.75

AEA: Adsorption Efficiency Average

SD: Standard Deviation

SE: Standard Error

CI: Confidence Interval

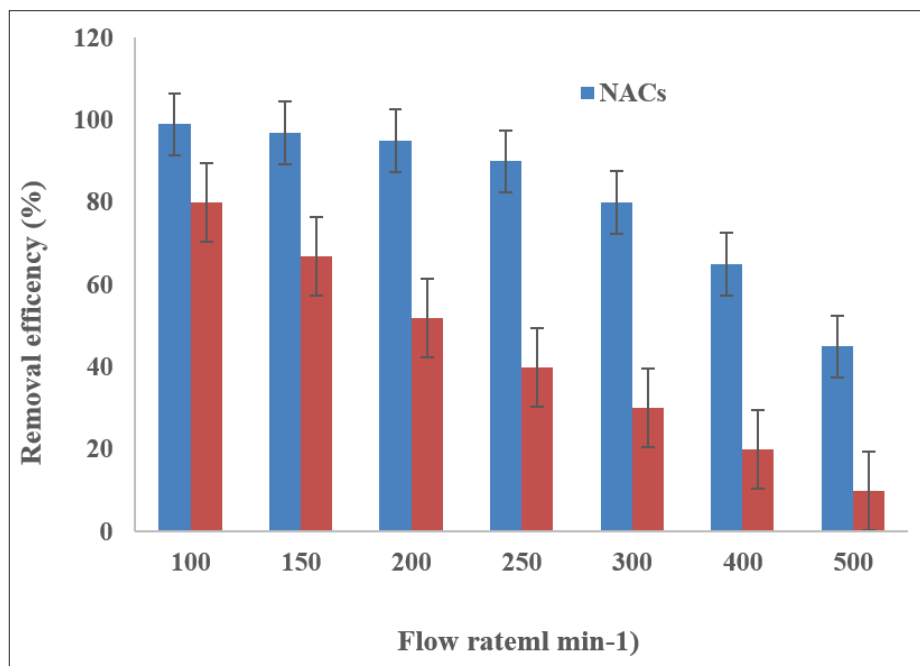


Fig.4. Effect of flowrate on removal efficiency of xylene by NACs and ACs adsorbents

3.8. Effect of adsorbent mass

According to the result, by increasing adsorbent, the removal efficiency of xylene from air increased and then constant. At the adsorbent mass of 100, 150 and 200 mg and concentration of 200 mg L⁻¹ and flow rate of 100 ml min⁻¹, the efficiency of Nano activated carbon was 96%, 97.5%, and 98.5%, respectively. So, 100 mg of NAC was used as optimum amount of adsorbent. (Fig.5)

3.9. The effect of flow rate based on the amount of adsorbent

Figure 6 shows the combined effect of flow rate and the amount of adsorbent mass on the adsorption efficiency of nano activated carbon at various concentrations. As shown in Figures 5 and 6, by increasing amount of adsorbent and decreasing airflow rate, the adsorption efficiencies were increased.

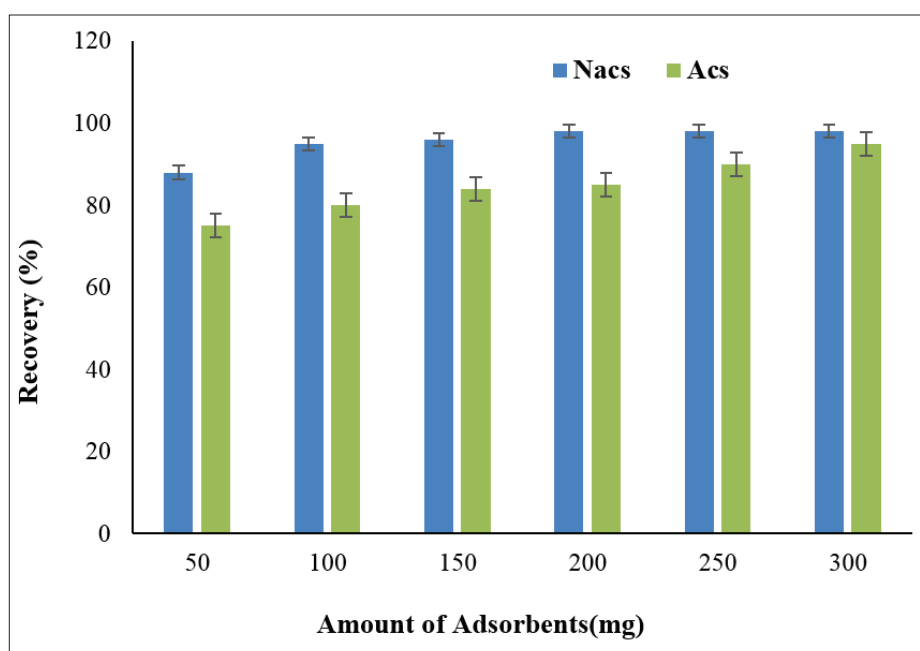


Fig.5. Effect of amount of NACs and ACs adsorbents on removal efficiency of xylene

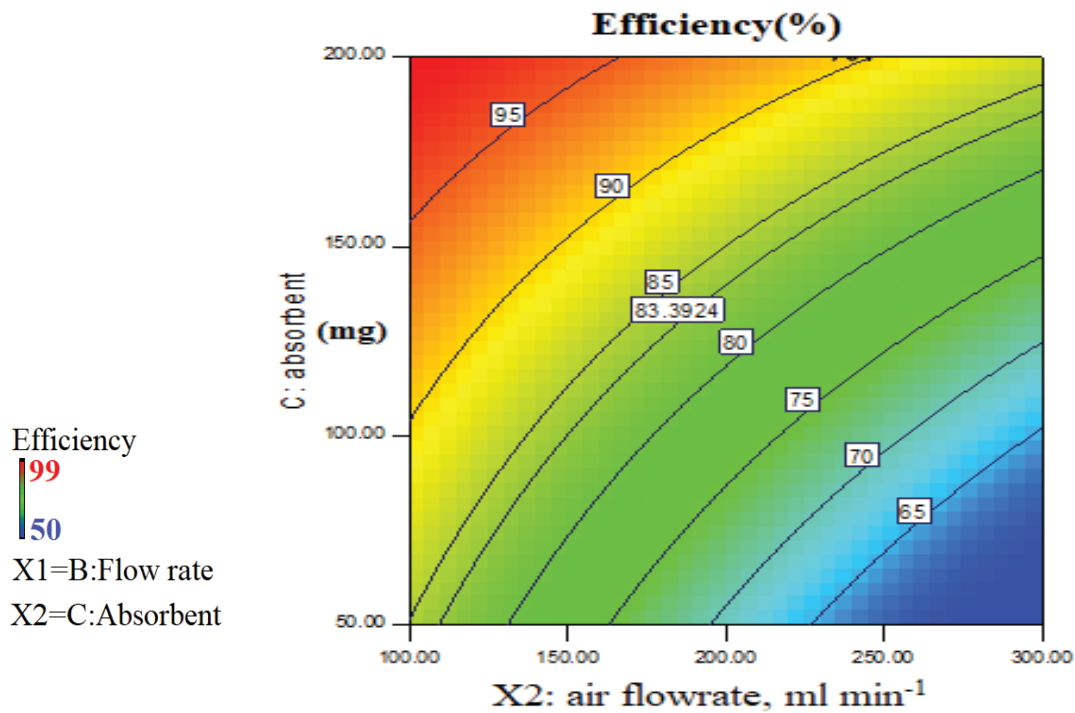


Fig. 6. Combined Effect of airflow and adsorbent mass on the adsorption efficiency of NACs

3.10. The effect of retention time

The effect of retention time of NAC on the xylene removal from air was investigated. Table 2 shows the xylene values added to the NACs and ACs adsorbents after passing pure air containing xylene vapor over it at a flow rate of 100 ml min^{-1} on different days (1, 3, 7, and 21 days). Then, the removal efficiency of the NACs and ACs adsorbents was calculated. The results showed that the retention time on nano-activated carbon was significant.

3.11. Effect of reusing and storage of adsorbent

By thermal accessory, the adsorbent recovered for 30 minutes. After 16 times of adsorption/desorption, the adsorbent efficiency was from 95.9%-99.3% for primary adsorbent. After storing the closed original adsorbent in the refrigerator, it reached 94.5-96.1%. So, it is desirable with good recovery for removal of xylene by NACs in optimized conditions for 10 days storage in the refrigerator (-4°C). After 10 days, the recovery decreased.

Table 2. Results of the retention time for xylene removal from air by NACs (P-value: 0.462-0.513)

Row	XM	AM	XM_2	FR	RT	XM_3	(%) Efficiency
1	8.6	100	108.2	100	1	108.15	99.3
2	8.6	100	108.12	100	3	108.06	99.2
3	8.6	100	108.3	100	7	108.19	98.6
4	8.6	100	107.95	100	21	107.82	98.3

XM_2 : xylene value (mg L^{-1}) + adsorbent mass (mg)

XM_3 : The xylene value (mg L^{-1}) + adsorbent mass after retention time (days)

FR: Flow rate (ml min^{-1})

RT: Retention time (days)

AM: adsorbent mass (mg)

XM: Xylene value (mg L^{-1})

3.12. Discussion

Activated carbon is one of the essential adsorbents for removing volatile organic matter. In this study, nano-carbon adsorbent's efficiency for removing xylene from air compared to activated carbon and other carbon structures. Due to results and comparison of efficiency between NAC and AC adsorbents, NAC adsorbent had better performance and capacity than activated carbon for removing xylene from the air in the optimized conditions (xylene concentration, flowrate, and amount of adsorbent). The average adsorption efficiency of the NAC adsorbent was higher than activated carbon adsorbent in the same conditions (NAC:98.5% and AC:76.5%). The results showed that the difference in efficiency was not statistically significant (p -Value = 0.474). Due to previous studies, the efficiency of nano adsorbents such as CNTs, GO, NG, and CQDs was higher than activated carbon. Golbabaie et al showed that the adsorption capacity of nano-activated carbon for xylene is higher than the activated carbon in the static state. There is a significant difference between the adsorption capacity and recovery of the two adsorbents. In another study by Golbabaie et al, the results showed that the Nanographene had a higher adsorption capacity than nano graphene oxide and activated carbon adsorbents for removing xylene from the air. Also, they showed that the adsorption efficiency of nano adsorbents such as NAC, NG, NGO, and CNTs was higher than AC for removing xylene from the air [22]. Tanju Karanfil et al reported the adsorption of volatile organic pollutants by Nanographene sheet, which was compared to the carbon nanotube, activated carbon, and Nanographene. They introduced these alternative adsorbents to remove industrial organic compounds from water. This study also shows the high performance of the Nano adsorbent [23]. The results showed that increasing the air flow rate and the xylene concentration decreased the removal efficiency. On the other hand, the removal efficiency increased by adding the amount of adsorbents such as NAC or AC. This is due to an increase in retention time and available adsorption sites. Also, the results showed that a flow rate had a more significant effect

on nano-activated carbon than activated carbon. This effect of the airflow rate caused no significant difference between the adsorption efficiency of the activated carbon and the nano-activated carbon. In fact, the study shows that low flow rates give better adsorption because the increase in flow rate actually creates a turbulent stream and the xylene molecules do not have enough time to adsorb onto the adsorbent. The results of flow rate and amount of adsorbent in the present study were similar to the results of Asilian et al. Asilian et al showed that the absorption capacity of xylene for zeolite was decreased up to 1.69 mg g^{-1} by increasing flow rate. Also, in a high flow rate, the time of failure and saturation time decreased in zeolite adsorbent [24]. Asilian also reported that increasing the amount of adsorbent cause to increase the adsorption efficiency. In fact, in this study, adsorption efficiency in low flowrate is was excellent and consistent [24]. Lu et al showed that the carbon nanotube oxidized with sodium hypochlorite had a higher BTEX adsorption than carbon nanotube and granular activated carbon. They showed that the physical and chemical properties of carbon nanotubes such as purity, structural and surface nature after oxidation were significantly improved, which led to a significant increase in BTEX adsorption capacity. Also, Shirkhanloo et al reported that the adsorption capacity of ionic liquid modified on nanographene caused to increase in the toluene removal from the air. The absorption capacity of toluene for IL-NGO was obtained at 126 mg g^{-1} which shows the remarkable favorite efficacy of nanoadsorbent for removing of volatile organic compounds. The modification of nanoadsorbent increased the potential of toluene removal [25]. In the present study, according to the results of experiments in different conditions, the nano-activated carbon showed a higher removal efficiency than activated carbon and competed with the IL/NGO or IL/CNTs. One of the critical factors for adsorbents is the ability to recycle them. Nano adsorbents are the most economical and recyclable. By the proposed procedure, the results showed that the nano-activated carbon can also be recovered by heating and can be reused many times.

4. Conclusion

During the review of previous studies, it has been found that this study is the only one conducted to evaluate the efficiency of nano activated carbon adsorbent in removing xylene. This study showed that the nano activated carbon adsorption efficiency (98.5%) was somewhat higher than the activated carbon (76.5%), this difference was statistically significant. The absorption capacities (AC) for the NACs and ACs adsorbents ranged from 187.6-245.2 mg g⁻¹ and 89.7-132.4 mg g⁻¹, respectively ($n=10$, $m=100$ mg). According to the results, both adsorbents have the potential to be used for removing xylene from the air with favorite efficiency and capacity. As a suggestion, the NACs as a novel adsorbent can be used optimally and more studies are needed in this regard.

5. Acknowledgment

This study has been funded and supported by the Tehran University of Medical Sciences and the research ethics code is **IR.TUMS.REC.1394.176**. The authors would like to thank the Tehran Research Institute of Petroleum Industry and authorities of the Occupational Health Laboratory of Tehran University of Medical Sciences for their contribution.

6. References

- [1] ACGIH, TLVs and BEIs, threshold limit values for chemical substances and physical agents and biological exposure indices, Signature Publications, Cincinnati, 2011. <https://www.acgih.org/science/tlv-bei-guidelines/>
- [2] F. Çeçen, Ö. Aktaş, Activated carbon for water and wastewater treatment: integration of adsorption and biological treatment, John Wiley & Sons, 2011. <https://doi.org/10.1002/9783527639441>.
- [3] H.R. Mokarami, Removal of xylene from waste air stream using catalytic ozonation process, Iran. J. health Environ., 3 (2010) 239-250. <http://ijhe.tums.ac.ir/article-1-105-en.html>
- [4] X. Zhang, B. Gao, A.E. Creamer, C. Cao, Y. Li, Adsorption of VOCs onto engineered carbon materials: A review, J. Hazard. Mater., 338 (2017) 102–123. <https://doi.org/10.1016/j.jhazmat.2017.05.013>.
- [5] B. Bina, M.M. Amin, A. Rashidi, H. Pourzamani, Benzene and toluene removal by carbon nanotubes from aqueous solution, Arch. Environ. Prot., 38 (2012) 3–25. <https://doi.org/10.2478/v10265-012-0001-0>.
- [6] L.H. Quynh Anh, Removal of O,M,P-Xylene from air samples on oxidized carbon nanotubes cartridges, Vietnam J. Sci. Technol., 56 (2018) 226–233. <https://doi.org/10.15625/2525-2518/56/2a/12690>.
- [7] F. Su, C. Lu, S. Hu, Adsorption of benzene, toluene, ethylbenzene and p-xylene by NaOCl-oxidized carbon nanotubes, Colloids Surfaces A Physicochem. Eng. Asp., 353 (2010) 83–91. <https://doi.org/10.1016/j.colsurfa.2009.10.025>.
- [8] M. Jafarizaveh, H. Shirkanloo, F. Golbabaeei, A. Tabrizi, K. Azam, M. Ghasemkhani, Nobel method for xylene removal from air on nano activated carbon adsorbent compared to NIOSH approved carbon adsorbent, J. Health Saf. Work, 6 (2016) 23. <http://jhs.w.tums.ac.ir/article-1-5374-en.html>
- [9] H.Q.A. Le, D.T. Phan, Investigation of BTEX adsorption on carbon nanotubes cartridges from air samples, Appl. Mech. Mater., 889 (2019) 216–222. <https://doi.org/10.4028/www.scientific.net/amm.889.216>.
- [10] H.A. Rangkooy, F. Jahani, A. Siah Ahangar, Effect of the Type of Ultraviolet on the Photocatalytic Removal of Xylene as a Pollutant in the Air Using TiO₂ Nanoparticles Fixed on the activated carbon, J. Occup. Hyg. Eng., 5 (2019) 26–32. <http://johe.umsha.ac.ir/article-1-461-en.html>
- [11] A.A.M. Beigi, M. Yousefi, M. Abdouss, Room temperature imidazolium-based ionic liquids as scavengers for hydrogen sulfide removal of crude oil, Anal. Methods Environ. Chem. J., 1 (2018) 11–22. <https://doi.org/10.24200/>

- amecj.v1.i01.32.
- [12] S.M. Mostafavi, A. Ebrahimi, Mercury determination in work place air and human biological samples based on dispersive liquid-liquid micro-extraction coupled with cold vapor atomic absorption spectrometry, *Anal. Methods Environ. Chem. J.*, 2 (2019) 49–58. <https://doi.org/10.24200/thamecj.v2.i04.81>.
- [13] P. Paydar, A.F. Zarandi, Air Pollution Method: A new method based on ionic liquid passed on mesoporous silica nanoparticles for removal of manganese dust in the workplace air, *Anal. Methods Environ. Chem. J.*, 2 (2019) 5–14. <https://doi.org/10.24200/amecj.v2.i01.52>.
- [14] S.A.H. Mirzahassemi, Environmental Health Analysis: Assessing the emission levels of benzene from the fuel tanks doors of the vehicles in Tehran city, *Anal. Methods Environ. Chem. J.*, 2 (2019) 49–54. <https://doi.org/10.24200/amecj.v2.i01.47>.
- [15] C. Jamshidzadeh, H. Shir Khanloo, A new analytical method based on bismuth oxide-fullerene nanoparticles and photocatalytic oxidation technique for toluene removal from workplace air, *Anal. Methods Environ. Chem. J.*, 2 (2019) 73–86. <https://doi.org/10.24200/amecj.v2.i01.55>.
- [16] A. Vahid, Determination of H₂S in crude oil via a rapid, reliable and sensitive method, *Anal. Methods Environ. Chem. J.*, 2 (2019) 37–44. <https://doi.org/10.24200/amecj.v2.i2.61>.
- [17] M. Bagheri Hosseinabadi, S. Timoori, A. Faghihi Zarandi, Functionalized graphene-trimethoxyphenyl silane for toluene removal from workplace air by sorbent gas extraction method, *Anal. Methods Environ. Chem. J.*, 2 (2019) 45–54. <https://doi.org/10.24200/amecj.v2.i2.63>.
- [18] A. Ebrahimi, A. Salarifar, Air pollution Analysis: Nickel paste on Multi-walled carbon nanotubes as novel adsorbent for the mercury removal from air, *Anal. Methods Environ. Chem. J.*, 2 (2019) 79–88. <https://doi.org/10.24200/amecj.v2.i03.70>.
- [19] M. Arjomandi, H. Shir Khanloo, A Review: Analytical methods for heavy metals determination in environment and human samples, *Anal. Methods Environ. Chem. J.*, 2 (2019) 97–126. <https://doi.org/10.24200/amecj.v2.i03.73>.
- [20] M. Gou, B.B. Yarahmadi, Removal of ethylbenzene from air by graphene quantum dots and multi wall carbon nanotubes in present of UV radiation, *Anal. Methods Environ. Chem. J.*, 2 (2019) 59–70. <https://doi.org/10.24200/amecj.v2.i04.82>.
- [21] P.M. Eller, M.E. Cassinelli, NIOSH manual of analytical methods, 4th ed, Diane Publishing, 1996. <https://doi.org/10.5860/choice.33-2747>.
- [22] A. Tabrizi, F. Golbabaei, H. Shir Khanloo, M. Jafarizaveh, K. Azam, R. Yarahmadi, Evaluation of the adsorption capacity of nano-graphene and nano-graphene oxide for xylene removal from air and their comparison with the standard adsorbent of activated carbon to introduce the optimized one, *J. Heal. Saf. Work*, 6 (2016) 25-34. <http://jhs.w.tums.ac.ir/article-1-5415-en.html>
- [23] O.G. Apul, Q. Wang, Y. Zhou, T. Karanfil, Adsorption of aromatic organic contaminants by graphene nanosheets: Comparison with carbon nanotubes and activated carbon, *Water Res.*, 47 (2013) 1648–1654. <https://doi.org/10.1016/j.watres.2012.12.031>.
- [24] Z. Vahdat Parast, H. Asilian, A. Jonidi Jafari, Adsorption of xylene from air by natural iranian zeolite, *Heal. Scope*, 3 (2014). e17528. <https://doi.org/10.17795/jhealthscope-17528>.
- [25] H. Shir Khanloo, M. Osanloo, O.Q. Dadras, Nobel method for toluene removal from air based on ionic liquid modified nano-graphen, *Int. J. Occup. Hyg.*, 6 (2014) 1–5. <https://ijoh.tums.ac.ir/index.php/ijoh/article/view/89>



Catalytic ozonation process using ZnO/Fe₂O₃ nanocomposite for efficient removal of captopril from aqueous solution

Maryam Dolatabadi ^{a,b}, Ruhollah Akbarpour ^c, Saeid Ahmadzadeh ^{d,e*}

^a Student Research Committee, Kerman University of Medical Sciences, Kerman, Iran.

^b Environmental Science and Technology Research Center, Department of Environmental Health Engineering, School of Public Health, Shahid Sadoughi University of Medical Sciences, Yazd, Iran.

^c MSc student in Environmental Engineering, Islamic Azad University, Estahban branch, Estahban, Iran.

^d Pharmaceutics Research Center, Institute of Neuropharmacology, Kerman University of Medical Sciences, Kerman, Iran.

^e Pharmaceutical Sciences and Cosmetic Products Research Center, Kerman University of Medical Sciences, Kerman, Iran

ARTICLE INFO:

Received 27 Apr 2022

Revised form 23 Jun 2022

Accepted 15 Jul 2022

Available online 28 Sep 2022

Keywords:

Captopril,
Catalytic ozonation,
ZnO/Fe₂O₃ nanocomposite,
Removal,
Aqueous solution

ABSTRACT

The presence of pharmaceutical compounds in aqueous media, even in low concentrations, has caused adverse effects on human, animal, and environmental health. Captopril is a widely used pharmaceutical compound detected in the environment at different concentrations. Because of the concern and problems caused by the presence of captopril in water and the aquatic ecosystem, it appears necessary to remove it from the environment. The current study investigated captopril removal by a catalytic ozonation process using ZnO/Fe₂O₃ nanocomposite as a low-cost catalyst. The effects of variables such as ZnO/Fe₂O₃ nanocomposite dosage (0.5-2.5 g L⁻¹), solution pH (3-11), initial captopril concentration (10-70 mg L⁻¹), and ozone dosage (0.2-1.5 mg min⁻¹) on captopril removal were investigated. The removal captopril of 99.4% was obtained in the optimum condition, including ZnO/Fe₂O₃ nanocomposite dosage of 2.0 g L⁻¹, solution pH of 5.0, initial captopril concentration of 40 mg L⁻¹, and ozone dosage of 0.5 mg min⁻¹. The ZnO/Fe₂O₃ nanocomposite as a catalyst was a critical component in the catalytic ozonation process. According to the obtained results, the catalytic ozonation process in the presence of ZnO/Fe₂O₃ nanocomposite has high efficiency in removing captopril from water sources.

1. Introduction

Recently, the attention of many researchers working in the field of water and wastewater treatment has focused on the removal of pharmaceutical compounds as a new group of emerging pollutants [1]. After humans and animals consume pharmaceutical compounds, part of them in their unmetabolized and metabolized form is excreted from the body and enters the environment [2]. Captopril is a commonly used

pharmaceutical compound prescribed to reduce high blood pressure, treat heart failure, protect the heart and blood vessels against damage and heart attack, and protect the kidneys in diabetic patients [3, 4]. Captopril is a potent, competitive inhibitor of the angiotensin-converting enzyme, the enzyme responsible for converting angiotensin I to angiotensin II. Angiotensin II is a potent mediator that causes the narrowing of blood vessels and retention of sodium and water in the body [5].

Captopril has been detected in various environments such as water and soil). The captopril concentration in the environment causes dizziness,

*Corresponding Author: Saeid Ahmadzadeh

Email: saeid.ahmadzadeh@kmu.ac.ir

<https://doi.org/10.24200/amecj.v5.i03.197>

cough, hyperkalemia, impotence, nocturnal enuresis, nausea, vomiting, diarrhea, insomnia, Stevens-Johnson syndrome, gynecomastia, thrombocytopenia, and angioedema. Considering the problems caused by the presence of captopril in the environment, removing captopril from the aquatic environment is essential [3, 4]. Although conventional processes in water and wastewater treatment can remove a part of pharmaceutical compounds during the treatment process, conventional treatment processes cannot thoroughly remove these compounds, so we finally need advanced oxidation processes to treat these pollutants [6].

Ozonation technique is one of the advanced oxidation processes in water and wastewater treatment. Ozonation is used in water and wastewater treatment for several purposes such as disinfection, removal and control of taste, odor, and color, oxidation of iron and manganese and other mineral contaminants, algae control, improving the coagulation process, and oxidation of persistent organic contaminants [7, 8].

As a strong oxidant, Ozone molecules break down recalcitrant and hazardous organic compounds into smaller molecules [9, 10]. The ozonation reaction is accomplished through two pathways (direct and indirect). In the direct method, the ozone molecule appears as an electron acceptor and thus oxidizes the organic pollutants. Nevertheless, in the indirect method, the ozone molecule is converted into a radical ($\cdot\text{OH}$) during chain reactions, which has a higher oxidation potential than ozone. The indirect method decomposes pollutants with incredible speed and power [11, 12]. Ozone presents a high reactivity mainly attributed to its electronic configuration. It is a selective molecule that attacks electron-rich functional groups like double bonds, amines, and activated aromatic rings [13, 14]. In recent years, heterogeneous catalytic ozonation has received much attention in water treatment due to its high oxidation potential. In the current work, the effect of main operational variables, including solution pH, catalyst dosage ($\text{ZnO}/\text{Fe}_2\text{O}_3$ nanocomposite), initial captopril concentration,

and reaction time was evaluated during the catalytic ozonation for removal of captopril from aqueous solution.

2. Material and methods

2.1. Chemical

Captopril ($\text{C}_9\text{H}_{15}\text{NO}_3\text{S}$, CAS N: 62571-86-2) was purchased from Darou Pakhsh Pharmaceutical Company. Sodium chloride (NaCl , CAS Number: 7647-14-5; Molecular Weight: 58.44), sodium hydroxide (NaOH , CAS 1310-73-2. Molecular Weight 40.00), hydrochloric acid (HCl , reagent, 37%; CAS Number: 7647-01-0; EC Number: 231-595-7), sodium thiosulfate ($\text{Na}_2\text{S}_2\text{O}_3$, CAS Number: 7772-98-7; Molecular Weight: 158.11), ferric chloride (FeCl_3 , CAS 7705-08-0, EC Number 231-729-4), zinc oxide (ZnO , CAS 1314-13-2, Molecular Weight 81.39), acetonitrile anhydrous (CAS Number: 75-05-8, Molecular Weight: 41.05), trifluoroacetic (TFA, CAS 76-05-1, Molecular Weight 114.02), and potassium iodide (KI , CAS 7681-11-0, Molecular Weight 166.00), were obtained from Sigma, Germany. All chemicals were of analytical reagent grade.

2.2. Instrumental

The determination of captopril concentration was analyzed using high-performance liquid chromatography (HPLC) system (HPLC 862 Bar, Knauer Smartline, Germany). This system consisted of a photodiode array (PDA) detector, set at 282 nm, and a C_{18} column (RP- C_{18} , 5 μm 4.6 \times 150 mm) kept at 30°C, with an injection flow rate of 1.2 mL min^{-1} . The mobile phase solution was applied using 15% acetonitrile and 85% trifluoroacetic/water acid (2% v/v) [16]. Digital PH meter (meterohm 827 pH lab, Switzerland) was used.

2.3. Preparation of the $\text{ZnO}/\text{Fe}_2\text{O}_3$ nanocomposite

In a theoretical procedure, 19.4 mg FeCl_3 and 200 mg ZnO particles were added to 50 mL of deionized water, and the mixture was dispersed at 100 °C for 12.0 h (Fig.1). After cooling to 20 °C, the nanoparticles were separated using centrifugation

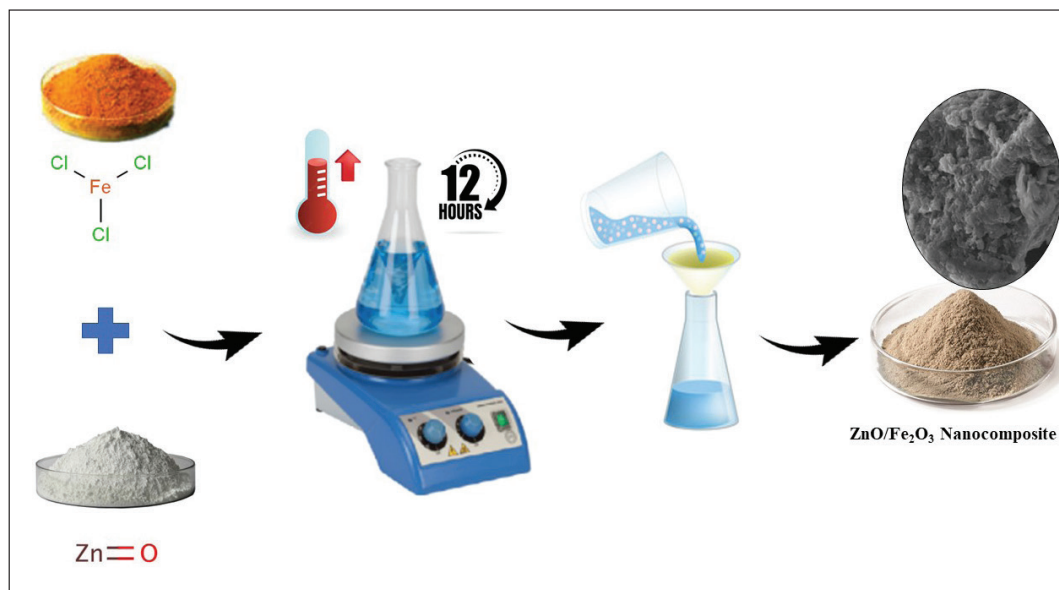


Fig.1. Procedure for Preparation of the ZnO/Fe₂O₃ nanocomposite

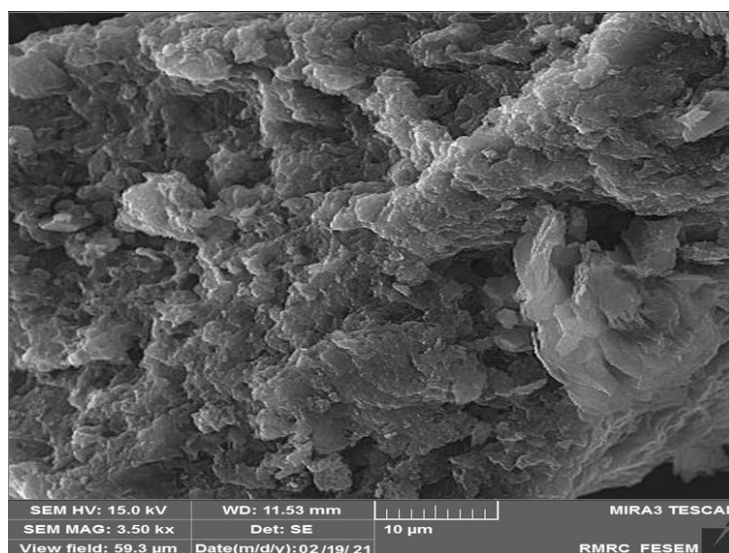


Fig.2. SEM images of the ZnO/Fe₂O₃ nanocomposite

and washed several times with ethanol and deionized water. The ZnO/Fe₂O₃ nanocomposite was dried at 100°C for 3.0 h and then was used as the catalyst in the ozonation process for the degradation of captopril [15]. FE-SEM of nanoparticles of ZnO/Fe₂O₃ nanocomposite showed in Figure 2.

2.4. Catalytic ozonation experiments

The catalytic ozonation of captopril was performed in a 500 mL Pyrex reactor with 8.0 cm diameter and 12 cm high and equipped with a magnetic stirrer at room temperature. Ozone was

generated from the air using an ozone generator (ARDA, Model MOG+10) with an input rate of 5 g h⁻¹. The reactor included an input/output port for the ozone gas stream. Ozone was introduced through a porous fritted diffuser that can produce reasonably fine bubbles. The excess ozone at the outlet was adsorbed by a sequential 2% potassium iodide solution. The solution pH was adjusted using NaOH or HCl in the catalytic ozonation process. After performing the reaction in each experimental run, 5 mL of sample was

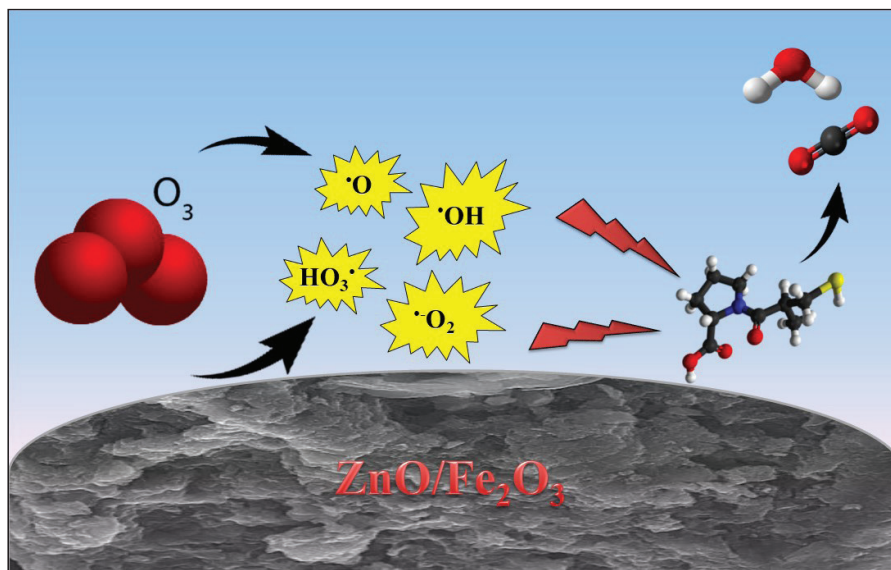


Fig.3. Mechanism of removal of captopril based on the catalytic ozonation and the $\text{ZnO/Fe}_2\text{O}_3$ nanocomposite

taken and filtered by PTFE filters to analyze for degradation efficiency of captopril using the catalytic ozonation process. Mechanism of removal of captopril based on the $\text{ZnO/Fe}_2\text{O}_3$ nanocomposite by the catalytic ozonation which was presented in Figure 3.

3. Results and discussion

3.1. Effect of solution pH

The effect of solution pH is one of the critical

parameters in the catalytic ozonation process for removing contaminants. Therefore, in the present study, the effect of solution pH was investigated in the range of 3.0 to 11.0 for removal of captopril from aqueous solution, in the constant condition, including initial captopril concentration of 30 mg L^{-1} , $\text{ZnO/Fe}_2\text{O}_3$ nanocomposite dosage of 1.0 g L^{-1} , and ozone dosage of 0.5 mg min^{-1} . The obtained results are shown in Figure 4. According to the achieved results, it was found that the removal

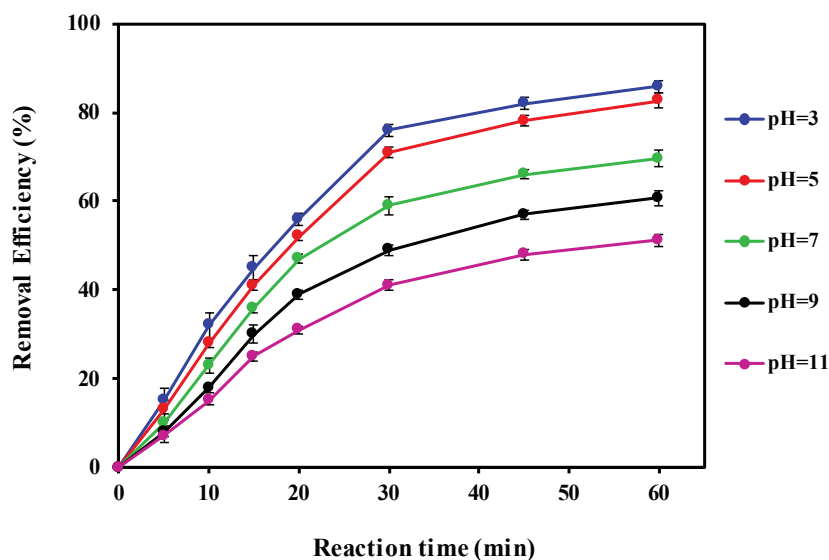


Fig. 4. Effect of solution pH and reaction time for removal captopril using catalytic ozonation. Experimental conditions: initial captopril concentration of 30 mg L^{-1} , $\text{ZnO/Fe}_2\text{O}_3$ nanocomposite dosage of 1.0 g L^{-1} , ozone dosage of 0.5 mg min^{-1} .

efficiency of captopril decreased with the increase of pH solution. As the pH value increased from 3 to 11, the removal efficiency of captopril decreased from 85.8% to 51.2% after 60 min. The removal efficiency in the acid conditions is better than in alkali conditions because high pH in the solution leads to the creation of more free radical scavengers derived from the mineralization of organic material, resulting in a decrease in the concentration of •OH. Generally, ozone oxidation pathways include direct oxidation by ozone molecules and radical oxidation by •OH. Direct oxidation is more selective and dominates under acidic conditions. While radical oxidation is less selective and predominates under primary conditions [17, 18]. Since the removal efficiency at a solution pH of 5 (82.6%) is very close to the removal efficiency at a solution pH of 3 (85.8%), due to the destructive effects of acidic conditions, a pH of 5 was chosen as the optimal solution pH in the catalytic ozonation process for removal of captopril.

3.2. Effect of ZnO/Fe₂O₃ nanocomposite dosage

The effect of catalyst dosage (ZnO/Fe₂O₃ nanocomposite) on captopril removal in the catalytic ozonation process was investigated in the range of 0.50–2.5 g L⁻¹. In the constant condition, including solution pH of 5, initial captopril concentration of 30 mg L⁻¹, and ozone dosage of

0.5 mg min⁻¹. According to the obtained results, the captopril removal efficiency increased with increasing ZnO/Fe₂O₃ nanocomposite dosage. As seen in Figure 5, the removal efficiency of captopril increased to 72.3%, 82.6%, 88.6%, 95.6%, and 98.2% when the catalyst dosage (ZnO/Fe₂O₃ nanocomposite) was increased to 0.50, 1.0, 1.5, 2.0, and 2.5 g L⁻¹, respectively. Nevertheless, the captopril removal efficiency at the catalyst (ZnO/Fe₂O₃ nanocomposite) dosage of 2.0 g L⁻¹ is very close to 2.5 g L⁻¹ (less than 3%). Therefore, a catalyst dosage of 2.0 g L⁻¹ was chosen as the optimum catalyst dosage. The obtained results illustrate that ZnO/Fe₂O₃ nanocomposites show high performance on catalytic oxidation removal of captopril. During catalytic ozonation, catalysts can promote the ozonation process and generate active free radicals. Consequently, enhancing the degradation and mineralization of organic contaminants [10, 14].

3.3. Effect of the initial captopril concentration

The effect of the initial concentration of captopril on the removal efficiency using the catalytic ozonation process was investigated in the range from 10 to 70 mg L⁻¹. In the stable condition, including solution pH of 5, ZnO/Fe₂O₃ nanocomposite dosage of 2.0 g L⁻¹, and ozone dosage of 0.5 mg min⁻¹. The results are displayed in Figure 6. The removal efficiency of

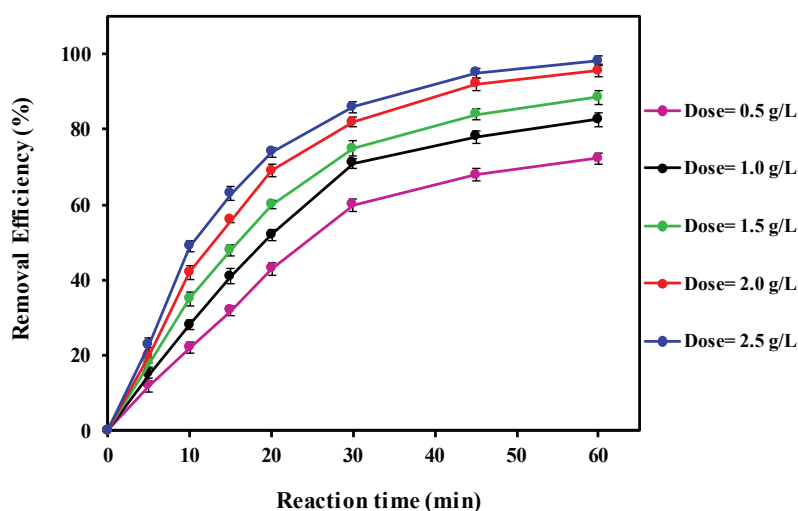


Fig. 5. Effect of ZnO/Fe₂O₃ nanocomposite dosage and reaction time for removal captopril using catalytic ozonation. Experimental conditions: initial captopril concentration of 30 mg L⁻¹, solution pH of 5.0, ozone dosage of 0.5 mg min⁻¹.

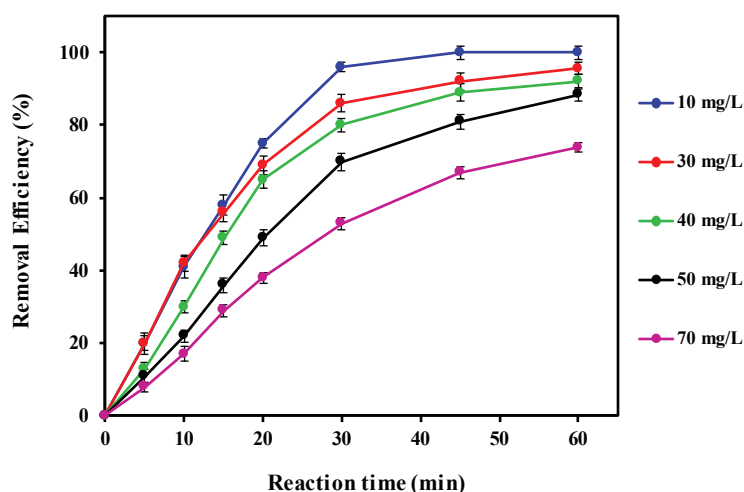


Fig. 6. Effect of initial captopril concentration and reaction time for removal captopril using catalytic ozonation. Experimental conditions: solution pH of 5.0, ZnO/Fe₂O₃ nanocomposite dosage of 1.0 g L⁻¹, ozone dosage of 0.5 mg min⁻¹.

captopril indeed decreased with the increase of the initial concentration. After 60 min of reaction time, when the initial concentration of captopril increased to 10, 30, 40, 50, and 70 mg L⁻¹ removal efficiency reached 100.0%, 95.6%, 92.1%, 88.4%, and 73.9%, respectively. This phenomenon can be due to, at constant conditions, the ozone concentration in the reactor being constant, so the amount of $\cdot\text{OH}$ in the reactor would be constant under the same conditions. The high concentration of captopril would consume more $\cdot\text{OH}$, so the removal

efficiency is reduced with the increase of the initial concentration of contaminants [19, 20]. Due to the captopril removal efficiency at a concentration of 40 mg L⁻¹ being a good performance (above 90%), a captopril concentration of 40 mg L⁻¹ was selected as the optimum concentration.

3.4. Effect of ozone dosage

Figure 7 shows the removal efficiency of captopril under different ozone dosages. Various levels of ozone dosage were set by adjusting the inlet gas

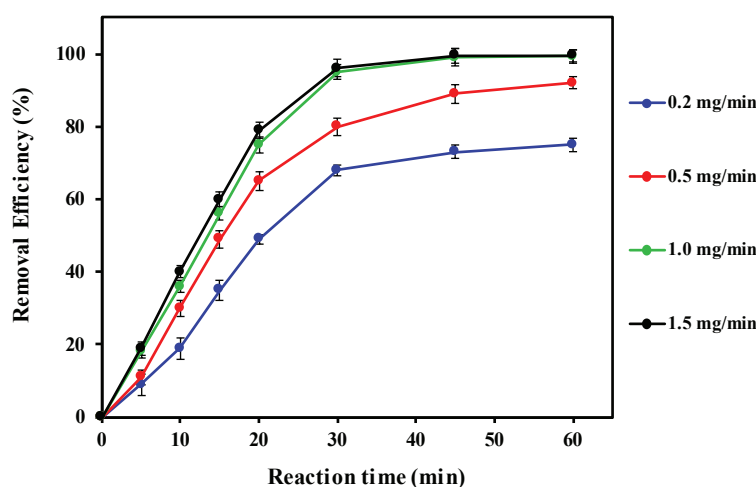


Fig. 7. Effect of ozone dosage and reaction time for removal captopril using catalytic ozonation. Experimental conditions: solution pH of 5.0, ZnO/Fe₂O₃ nanocomposite dosage of 2.0 g L⁻¹, initial captopril concentration of 40 mg L⁻¹.

concentration. The ozone dosage effect in the range of 0.2 to 1.5 mg min⁻¹ was investigated in constant conditions, including solution pH of 5, ZnO/Fe₂O₃ nanocomposite dosage of 1.0 g L⁻¹, and initial captopril concentration of 40 mg L⁻¹. The experimental results are presented in Figure 4. According to the results, the captopril removal efficiency increased to 75.0%, 92.1%, 99.4%, and 99.6% when the ozone dosage was increased to 0.2, 0.5, 1.0, and 1.5 mg min⁻¹, respectively. More than 99.4% of captopril is removed within 45 minutes when the ozone dosage is 1.0 mg min⁻¹.

Further increase of ozone dosage (≥ 1.0 mg min⁻¹) had no significant effect on the captopril removal efficiency. This result is probably because the ozone dosage of 1.0 mg min⁻¹ reached the maximum ozone utilization of the ZnO/Fe₂O₃ nanocomposite. Thus, the optimum ozone dosage was selected as 1.0 mg min⁻¹ [21, 22]. He *et al.* removed the metoprolol and ibuprofen using catalytic ozonation; their results showed that in optimal conditions, the catalyst dosage was 0.1 g L⁻¹ [21].

Bai *et al.* removed the sulfamethazine using a catalytic ozonation process (Ce_{0.1}Fe_{0.9}OOH as a catalyst), their results indicated that under optimal conditions including pH of 7.0, catalyst dosage of 0.2 g L⁻¹, ozone dosage of 15 mg min⁻¹, and sulfamethazine concentration of 20 mg L⁻¹, TOC removal efficiency was obtained of 44% at during 120 min [23]. In addition, Qi *et al.* removed the phenacetin using catalytic ozonation with CuFe₂O₄ and its precursor; their results showed that in optimal conditions (pH of 7.72, catalyst dosage of 2.0 g L⁻¹; ozone dosage of 0.36 mg min⁻¹, and phenacetin concentration of 0.2 mM), the TOC removal efficiency was obtained of 90% at during 180 min [24]. Moreover, Zhao *et al.* removed the phenol using catalytic ozonation with NiFe₂O₄ as a catalyst; their results showed that in optimal conditions (pH of 6.5, catalyst dosage of 1.0 g L⁻¹; ozone dosage of 0.75 mg min⁻¹, and phenol concentration of 300 mg L⁻¹), the phenol removal efficiency was obtained of 38.9% at during 60 min [25].

4. Conclusion

This current study aims to evaluate the removal efficiency of captopril using ZnO/Fe₂O₃ nanocomposite as a low-cost catalyst by a catalytic ozonation process. The maximum captopril removal efficiency was 99.4% under optimal conditions. During catalytic ozonation, catalysts can promote the ozonation process and generate active free radicals. It enhanced the degradation and mineralization of organic contaminants. Solution pH and initial captopril concentration had an inverse effect, and the catalyst and ozone dosage directly affected the removal efficiency of captopril. The catalytic ozonation process is an eco-friendly advanced oxidation process successfully applied to remove captopril from polluted water.

5. Acknowledgements

The authors would like to express their appreciation to the student research committee of Kerman University of Medical Sciences [Grant number 401000072] for supporting the current work.

Funding: This work received a grant from the Kerman University of Medical Sciences [Grant number 401000072].

Conflict of interest: The authors declare that they have no conflict of interest regarding the publication of the current paper.

Ethical approval: The Ethics Committee of Kerman University of Medical Sciences approved the study (IR.KMU.REC.1401.099).

6. References

- [1] P.A. Nishad, A. Bhaskarapillai, Antimony, a pollutant of emerging concern: A review on industrial sources and remediation technologies, *Chemosphere*, 277 (2021) 130252. <https://doi.org/10.1016/j.chemosphere.2021.130252>.
- [2] S. Ahmed, F.S.A. Khan, N.M. Mubarak, M. Khalid, Y.H. Tan, S.A. Mazari, R.R. Karri, E.C. Abdullah, Emerging pollutants and their removal using visible-light responsive photocatalysis—a comprehensive review,

- J. Environ. Chem. Eng., 9 (2021) 106643. <https://doi.org/10.1016/j.jece.2021.106643>.
- [3] M.R. Cunha, E.C. Lima, D.R. Lima, R.S. da Silva, P.S. Thue, M.K. Seliem, F. Sher, G.S. dos Reis, S.H. Larsson, Removal of captopril pharmaceutical from synthetic pharmaceutical-industry wastewaters: Use of activated carbon derived from *Butia catarinensis*, J. Environ. Chem. Eng., 8 (2020) 104506. <https://doi.org/10.1016/j.jece.2020.104506>.
- [4] F.M. Kasperiski, E.C. Lima, C.S. Umpierrez, G.S. dos Reis, P.S. Thue, D.R. Lima, S.L. Dias, C. Saucier, J.B. da Costa, Production of porous activated carbons from *Caesalpinia ferrea* seed pod wastes: Highly efficient removal of captopril from aqueous solutions, J. Clean. Prod., 197 (2018) 919-929. <https://doi.org/10.1016/j.jclepro.2018.06.146>.
- [5] L. Zhang, D. Edwards, K. Berecek, Effects of early captopril treatment and its removal on plasma angiotensin converting enzyme (ACE) activity and arginine vasopressin in hypertensive rats (SHR) and normotensive rats (WKY), Clin. Exp. Hypertens., 18 (1996) 201-226. <https://doi.org/10.3109/10641969609081765>.
- [6] S. Hena, L. Gutierrez, J.-P. Croué, Removal of pharmaceutical and personal care products (PPCPs) from wastewater using microalgae: A review, J. Hazard. Mater., 403 (2021) 124041. <https://doi.org/10.1016/j.jhazmat.2020.124041>.
- [7] B. Wang, H. Zhang, F. Wang, X. Xiong, K. Tian, Y. Sun, T. Yu, Application of heterogeneous catalytic ozonation for refractory organics in wastewater, Catal., 9 (2019) 241. <https://doi.org/10.3390/catal9030241>.
- [8] E. Issaka, J.N.-O. Amu-Darko, S. Yakubu, F.O. Fapohunda, N. Ali, M. Bilal, Advanced catalytic ozonation for degradation of pharmaceutical pollutants—A review, Chemosphere, 289 (2022) 133208. <https://doi.org/10.1016/j.chemosphere.2021.133208>.
- [9] J. Wang, Z. Bai, Fe-based catalysts for heterogeneous catalytic ozonation of emerging contaminants in water and wastewater, Chem. Eng. J., 312 (2017) 79-98. <https://doi.org/10.1016/j.cej.2016.11.118>.
- [10] S. Psaltou, K. Sioumpoura, E. Kaprara, M. Mitrakas, A. Zouboulis, Transition metal ions as ozonation catalysts: an alternative process of heterogeneous catalytic ozonation, Catal., 11 (2021) 1091. <https://doi.org/10.3390/catal11091091>.
- [11] A.N. Gounden, S.B. Jonnalagadda, Advances in treatment of brominated hydrocarbons by heterogeneous catalytic ozonation and bromate minimization, Molecules, 24 (2019) 3450. <https://doi.org/10.3390/molecules24193450>.
- [12] S. Yuan, M. Wang, J. Liu, B. Guo, Recent advances of SBA-15-based composites as the heterogeneous catalysts in water decontamination: a mini-review, J. Environ. Manage., 254 (2020) 109787. <https://doi.org/10.1016/j.jenvman.2019.109787>.
- [13] Z. Yang, H. Yang, Y. Liu, C. Hu, H. Jing, H. Li, Heterogeneous catalytic ozonation for water treatment: preparation and application of catalyst, Ozone: Sci. Eng., (2022) 1-27. <https://doi.org/10.1080/01919512.2022.2050183>.
- [14] N. Hien, L.H. Nguyen, H.T. Van, T.D. Nguyen, T.H.V. Nguyen, T.H.H. Chu, T.V. Nguyen, X.H. Vu, K.H.H. Aziz, Heterogeneous catalyst ozonation of Direct Black 22 from aqueous solution in the presence of metal slags originating from industrial solid wastes, Sep. Purif. Technol., 233 (2020) 115961. <https://doi.org/10.1016/j.seppur.2019.115961>.
- [15] F. Achouri, S. Corbel, A. Aboulaich, L. Balan, A. Ghrabi, M.B. Said, R. Schneider, Aqueous synthesis and enhanced photocatalytic activity of ZnO/Fe₂O₃ heterostructures, J. Phys. Chem. Solids, 75 (2014) 1081-1087. <https://doi.org/10.1016/j.jpcs.2014.05.013>.
- [16] T. Huang, Z. He, B. Yang, L. Shao, X. Zheng, G. Duan, Simultaneous determination of captopril and hydrochlorothiazide in human

- plasma by reverse-phase HPLC from linear gradient elution, *J. Pharm. Biomed. Anal.*, 41 (2006) 644-648. <https://doi.org/10.1016/j.jpba.2005.12.007>.
- [17] Y. Huang, Y. Sun, Z. Xu, M. Luo, C. Zhu, L. Li, Removal of aqueous oxalic acid by heterogeneous catalytic ozonation with MnOx/sewage sludge-derived activated carbon as catalysts, *Sci. Total Environ.*, 575 (2017) 50-57. <https://doi.org/10.1016/j.scitotenv.2016.10.026>.
- [18] J. Liu, J. Li, S. He, L. Sun, X. Yuan, D. Xia, Heterogeneous catalytic ozonation of oxalic acid with an effective catalyst based on copper oxide modified g-C₃N₄, *Sep. Purif. Technol.*, 234 (2020) 116120. <https://doi.org/10.1016/j.seppur.2019.116120>.
- [19] X. Wei, S. Shao, X. Ding, W. Jiao, Y. Liu, Degradation of phenol with heterogeneous catalytic ozonation enhanced by high gravity technology, *J. Clean. Prod.*, 248 (2020) 119179. <https://doi.org/10.1016/j.jclepro.2019.119179>.
- [20] Y. Huang, C. Cui, D. Zhang, L. Li, D. Pan, Heterogeneous catalytic ozonation of dibutyl phthalate in aqueous solution in the presence of iron-loaded activated carbon, *Chemosphere*, 119 (2015) 295-301. <https://doi.org/10.1016/j.chemosphere.2014.06.060>.
- [21] Y. He, L. Wang, Z. Chen, B. Shen, J. Wei, P. Zeng, X. Wen, Catalytic ozonation for metoprolol and ibuprofen removal over different MnO₂ nanocrystals: Efficiency, transformation and mechanism, *Sci. Total Environ.*, 785 (2021) 147328. <https://doi.org/10.1016/j.scitotenv.2021.147328>.
- [22] S.-Q. Tian, J.-Y. Qi, Y.-P. Wang, Y.-L. Liu, L. Wang, J. Ma, Heterogeneous catalytic ozonation of atrazine with Mn-loaded and Fe-loaded biochar, *Water Res.*, 193 (2021) 116860. <https://doi.org/10.1016/j.watres.2021.116860>.
- [23] Z. Bai, Q. Yang, J. Wang, Catalytic ozonation of sulfamethazine using CeO₂/FeO. 9OOH as catalyst: Mineralization and catalytic mechanisms, *Chem. Eng. J.*, 300 (2016) 169-176. <https://doi.org/10.1016/j.cej.2016.04.129>.
- [24] F. Qi, W. Chu, B. Xu, Comparison of phenacetin degradation in aqueous solutions by catalytic ozonation with CuFe₂O₄ and its precursor: surface properties, intermediates and reaction mechanisms, *Chem. Eng. J.*, 284 (2016) 28-36. <https://doi.org/10.1016/j.cej.2015.07.095>.
- [25] H. Zhao, Y. Dong, G. Wang, P. Jiang, J. Zhang, L. Wu, K. Li, Novel magnetically separable nanomaterials for heterogeneous catalytic ozonation of phenol pollutant: NiFe₂O₄ and their performances, *Chem. Eng. J.*, 219 (2013) 295-302. <https://doi.org/10.1016/j.cej.2013.01.019>.



An efficient cheap source of activated carbon as solid phases for extraction and removal of Congo Red from aqueous solutions

Tahrer N. Majid ^a and Ali A. Abdulwahid ^{a,*}

^aUniversity of Basra, College of Science, Chemistry Department, PO Box 49, Basra, Iraq,

ARTICLE INFO:

Received 17 May 2022

Revised form 28 Jul 2022

Accepted 19 Aug 2022

Available online 29 Sep 2022

Keywords:

Solid phase extraction,

Active carbon,

Congo Red,

Enrichment factor,

UV-Vis technology

ABSTRACT

The present study reported the preparation of solid phases from various available and cheap natural sources represented by activated carbon to remove the polluting dye Congo Red (CR). Activated carbon derived from the leaves of the Consocarpus plant (C/AC) and Ziziphus Spina-Christi plant (Z/AC) and Myrtus plant (M/AC) by chemical activation. The prepared solid phases were diagnosed and examined using FTIR, FESE, and XRD. The results of the study indicated that the best amount for the solid phase was 0.25 g for the three solid phases used against dye, the optimal concentration of the CR was 100 mg L⁻¹, and the optimum acidity function was equal to 5 with a volume of 25 mL, as the optimization experiments indicated that the best flow rate of the eluting solution was equal to 0.5 ml min⁻¹. The elution processes were carried out using several solvents different in polarity and it was found that 8 mL of DMSO achieved the best percentage of recovery (%R). Also, this study included calculating adsorption capacity based on the optimal conditions that were obtained by applying Langmuir and Freundlich isotherm models, and q_{max} , according to the Langmuir model, was (21.74, 23.53, 22.17) mg g⁻¹ for (Z/AC), (C/AC), and (M/AC) adsorbents, respectively.

1. Introduction

In recent years, human pollution of natural waters has led to a significant reduction in operational freshwater resources on Earth [1]. These pollutants from multiple sources have caused significant environmental and health problems that threaten society and living organisms [2, 3]. Many contaminants such as toxic heavy metals, and organic contaminants, such as dyes, pesticides, drugs, degraded organic matter, and so on, are present in polluted waters [4]. Among these pollutants are dyed [5]. A dye is a coloring substance that can be natural, semi-synthetic, or fully synthetic and blend with the substrate to

which it is applied. Natural dyes can be non-toxic compared to synthetic dyes due to their natural origin. The primary sources of pollution of synthetic dyes are the textile, rubber, paper, plastic, printing, paint, and leather industries [6]. It is estimated that about 10,000 types of artificial and natural dyes are produced annually worldwide, with a significant number of dyes being wasted during manufacturing and application processes [7]. The main reason is the incomplete adhesion of the paints to the layers when painting. The amount of unstable dyes in textile effluents is higher than that of effluents discharged by other industries [8]. Many chemicals and dyes remain unused during the dyeing process of textiles, releasing excess liquid dye into the environment. It is estimated that textiles subject

*Corresponding Author: Ali A. Abdulwahid

Email: ali.abdulwahid@uobasrah.edu.iq

<https://doi.org/10.24200/amecj.v5.i03.205>

to dyeing can absorb about 80% of dye liquor due to their limited adsorption capacity [9]. Of all the colors, "azo" colors are most often used to dye different substrates. They are complex in nature and are potentially carcinogenic. Due to the larger molecular structures, their decomposition products are also toxic [10]. If azo dyes are absorbed into the soil from the water, they can alter the chemical and physical properties of the soil. This can lead to the destruction of the vegetation in the environment; if the toxic chemical dyes remain in the soil for a long time, they also kill beneficial microorganisms in the soil, significantly affecting agricultural fertility [11]. Therefore, these toxic dyes should be disposed of from wastewater as much as possible before they are released into terrestrial or aquatic resources in an environmentally sound manner [12]. The search for efficient and safe technologies for removing organic paints from aquatic systems is of great interest for environmental protection. The best water treatment methods chosen depend on several factors, including the nature, quantity and quality of the paint materials in the systems analyzed [13]. Great attention has been paid to technologies for removing paint from wastewater, and many chemical, biological and physical methods have been developed for this purpose [14,15], including adsorption, chemical oxidation, photocatalysis, electrochemical oxidation, biodegradation, ion-exchange filtration, coagulation/flocculation, membrane filtration, catalytic degradation and so on. Most conventional methods have major drawbacks of low selectivity, high power consumption, and low color degradation [16]. Many attempts have been made today to develop

new selective and sensitive techniques for the purification of samples and separation of selected materials, and solid phase extraction (SPE) is the most widely used method [17]. As SPE for sample pretreatment offers several advantages, including fast separation, low cost, low solvent consumption, high enrichment efficiency and recovery rates, short processing times, no emulsion formation, and the ability to combine with many advanced detection methods [18], simple composition, high recovery and high enrichment factor. The basic principle of the elements/species of particular interest is to transfer the target elements/species from the sample matrix to the active site of the SPE adsorbent. The sorbent is the main factor that determines the selectivity, sensitivity, and extraction/absorption dynamics of the relevant method [19]. In this study, three natural materials were selected to convert them into activated carbon and use the products as a solid phase in the study of the solid phase extraction technology (SPE), where *Ziziphus Spina-Christi* leaves, *Consocarpus* leaves and *Myrtus Communis* leaves were used. Materials in the preparation of solid phases (Z/AC), (C/AC) and (M/AC) respectively to remove Congo red (CR) in aqueous solutions using SPE under optimal conditions.

This paper aims to investigate the applicability of activated carbon prepared from cheap and available natural sources as a solid phase in SPE for the purify water contaminated with organic Congo red (CR) dye, [1-naphthalene sulfonic acid, 3, 30-(4, 40-biphenylenebis (azo)) bis (4-amino-) disodium salt] (Fig. 1).

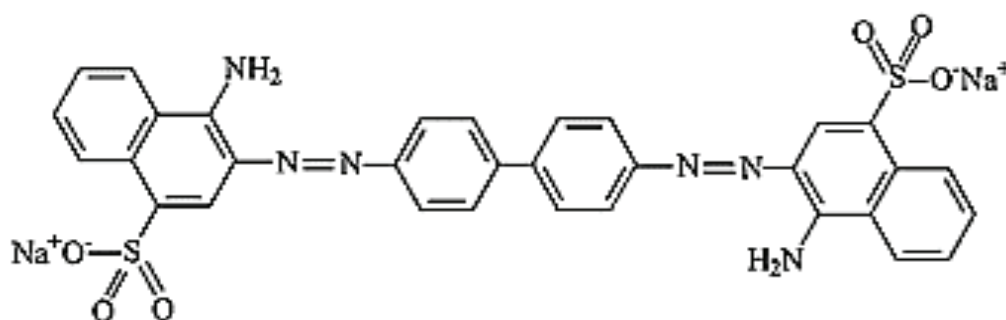


Fig. 1. Chemical structure of Congo red

2. Experimental

2.1. Chemicals and Materials

Chemical reagents including Congo Red (CR), 85% dye content ($C_{32}H_{22}N_6Na_2O_6S_2$, Mw: 696.665 g mol⁻¹) purchased from (Pub Chem). A stock solution (100 mg.L⁻¹) of (CR) was prepared by dissolving the required amount of dye in distilled water. The pH was adjusted with 0.1 mol L⁻¹ of NaOH (Univar) and 0.1 mol.L⁻¹ HCl (AnalaR) and measured with a pH meter (model SD 300, Germany). The potassium hydroxide (KOH), (Sigma-Aldrich) was used to activate the carbon that was prepared from multiple natural sources (Ziziphus Spina-Christi leaves, Consocarpus leaves, and Myrtus communis leave). The ethanol, methanol, dimethyl sulfoxide (DMSO), n-Hexane, and toluene (Sigma-Aldrich) were used in the solid phase elution to recover the dye. Distilled water was used throughout this study. AC was distinguished by FT-IR, XRD, TEM and SEM technologies. The absorbance of the CR dye solution was measured at the wavelength of 494 nm, using a UV-visible spectrophotometer (PG Instrument T80 + UV/VIS model). The percentage of dye removal efficiency, R and the amount of CR dye adsorbed per unit weight of adsorbent at time t, qt (mg g⁻¹) was calculated as Equation 1 and 2:

$$\%Recovery = \frac{\text{concentration of dye recoverd on extraction}}{\text{original concentration of dye}} \times 100\% \quad (\text{Eq.1})$$

$$q = \frac{(C_o - C_e)V}{M} \quad (\text{Eq.2})$$

Where C_e is the concentration of CR at time t, C_o is the initial dye concentration (mg L⁻¹), M is the mass of adsorbent (g) and V is the volume of solution (L).

2.2. Activated carbon preparation

Three categories of activated carbon were produced from Ziziphus Spina Christi leaves, Consocarpus leaves and Myrtus communis leaves, and were denoted by (Z/AC), (C/AC) and (M/AC) respectively. The

leaves of the plants were collected and washed well with distilled water; then each substance was boiled in two liters of water for two hours, to remove other water-soluble organic and phenolic compounds, then dried at 70°C in Oven for 8 hours. Subsequently, they were crushed and sieved (40–60 mesh). Afterward, 125 g of each type of dried plant leaf powder was used as the initial amount to produce every kind of activated carbon and impregnation of the plant leaves in a potassium hydroxide KOH (25%) by using a solution (KOH) to solid (plant leaves powder) ratio of 3:1 for 24 h, and then rinsed with distilled water several to reach the pH of the washing liquid. Then, the washed solid samples were dried at 100 °C; then pyrolyzed in a muffle furnace at 500 °C carbonization temperature for 1 hour. After that, the samples were washed with deionized water many times until the pH of the solution was equal to the pH of the distilled water. The resulting activated carbon was dried up at 100 °C and kept dry till usage in the experiment [20,21].

2.3. Solid phase extraction

The solid phase extraction method includes three basic stages, column preparation, loading, and elution [22,23]. The column of the polypropylene cartridge was prepared (Fig. 2). The column was filled with a permeable polypropylene film (disc) with a thickness of 1 mm. Four layers of glass paper were placed glass filter paper; then the column was filled with a fixed weight (0.5 gm) of the solid phase, which is the activated carbon prepared in this study from different natural sources (Z/AC), (C/AC), (M/AC). The steel was homogeneous, so, that it was free of voids and of equal height from the top, then a layer of glass paper was placed over the solid phase. The CR dye solution was passed at the pH_{pzc}, where the dye is bound at this stage to the solid phase pre-packed in the column and the unbound part of the dye passes from the column as well as the rest of the original components and at a running rate depends on gravity. As for the rinsing stage, it included passing the elution solution through the separation column, which breaks the link between the dye and the solid phase, and then transfers the solution to measurement using UV-

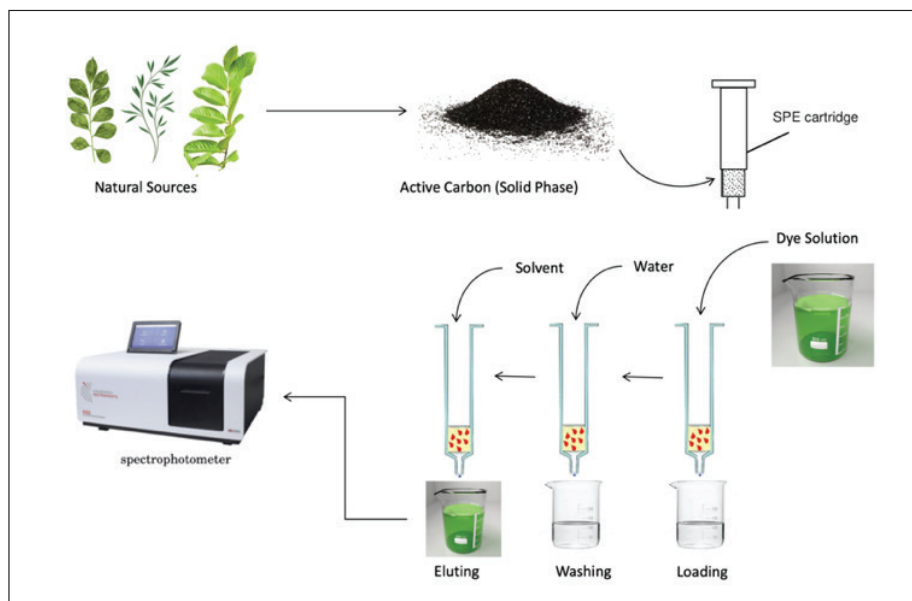


Fig. 2. Summary of preparation of activated carbon and extraction procedure

visible technology to know the concentration extracted from the dye. The ratio can be calculated as the percentage of recovery % through Equation 3, and this study included finding the ideal conditions for the optimization of the extraction process as shown below.

$$\% \text{Recovery} = \frac{\text{concentration of dye recovered on extraction}}{\text{original concentration of dye}} \times 100\% \quad (\text{Eq.3})$$

2.4. Characterization Methods

To investigate the surface characteristic of (Z/AC), (C/AC), and (M/AC), FT IR, XRD, and SEM spectra were studied. FT-IR spectroscopy was carried out to determine the type and nature of the functional groups present in the activated carbon. The presence of these functional groups increases heterogeneity and, thereby the extraction. The

spectra of (Z/AC), (C/AC), and (M/AC) samples are shown in Table 1. To explore the crystal lattice structure of activated carbon, an X-ray diffraction pattern was carried out; Figure 3 shows the XRD configuration of the three AC types (Z/AC), (C/AC) and (M/AC). In this pattern, several peaks were found corresponding to their semi-crystalline nature. XRD spectra of the fitted conditioners revealed a sharp diffraction peak of 29.5° for all solutions that (Z/AC), (C/AC), and (M/AC) and this is evidence for the possible presence of potassium compounds with high crystallinity after activation with KOH. The SEM is a tool for characterizing the surface morphology and physical properties of the adsorbent surface. It helps determine the particle shape, appropriate size distribution of the adsorbent and porosity. The surface morphology of the (Z/AC), (C/AC) and (M/AC) adsorbents are shown in Figure 4a-c.

Table 1. FT-IR analysis (Z/AC), (C/AC) and (M/AC)

	M\AC	C\AC	Z\AC
O-H	3422.06	3754.73	3438.46
\equiv CH	3302.5	-	3374.82
CH=	3267.79	-	3225.36
\equiv CH	2360.44	-	2369.12
CH-	2900.41	-	2948.63
C-O	1435.74	1432.85	1445.39
C=C	-	1609.13	-

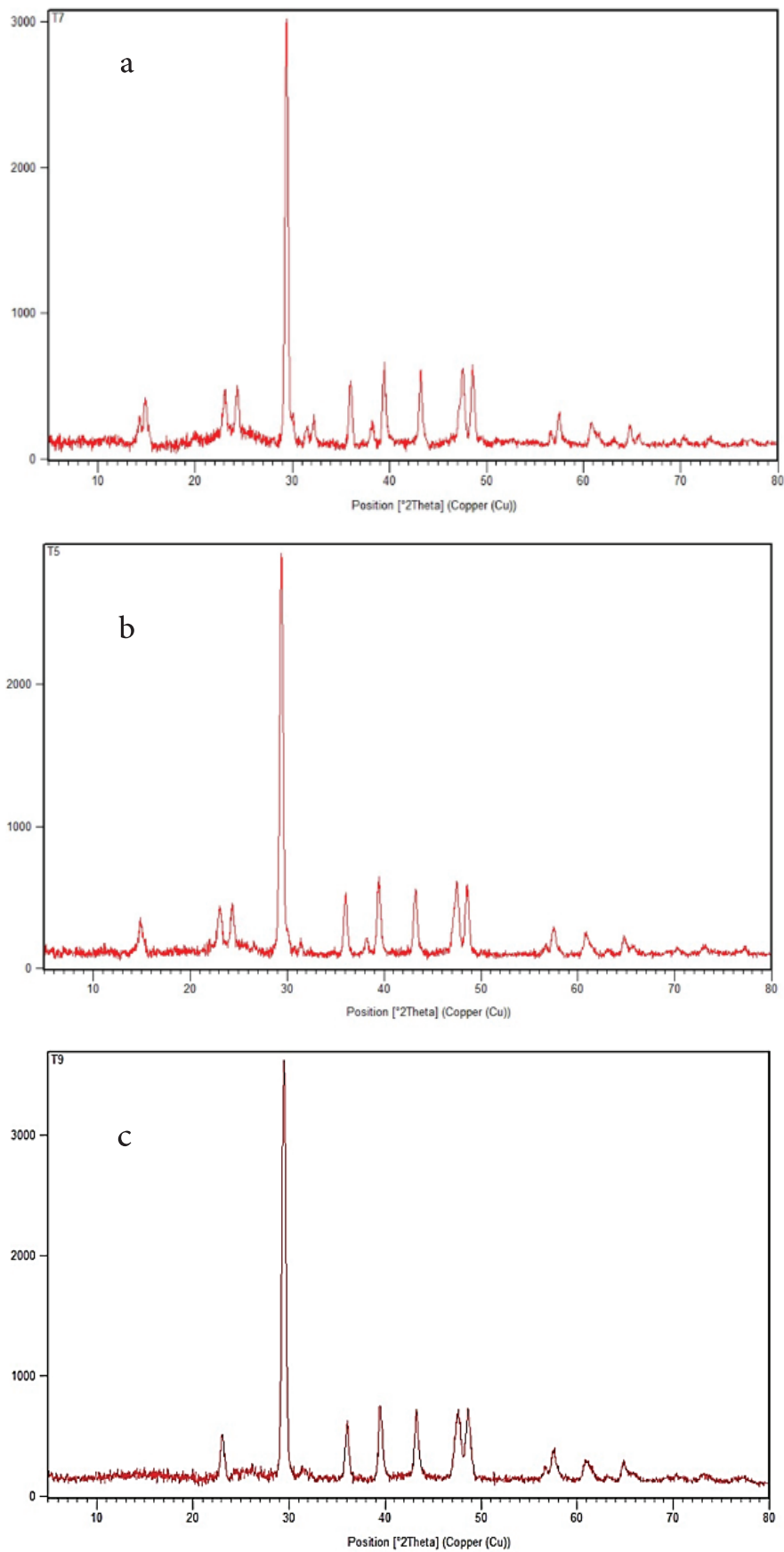


Fig. 3. XRD pattern of a: (Z/AC), b: (C/AC) and c: (M/AC)

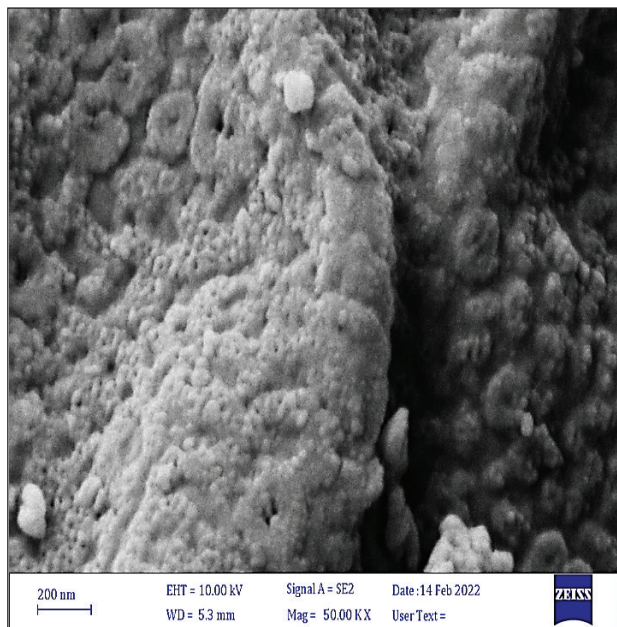


Fig. 4a. SEM of Ziziphus spina-christi (Z/AC)

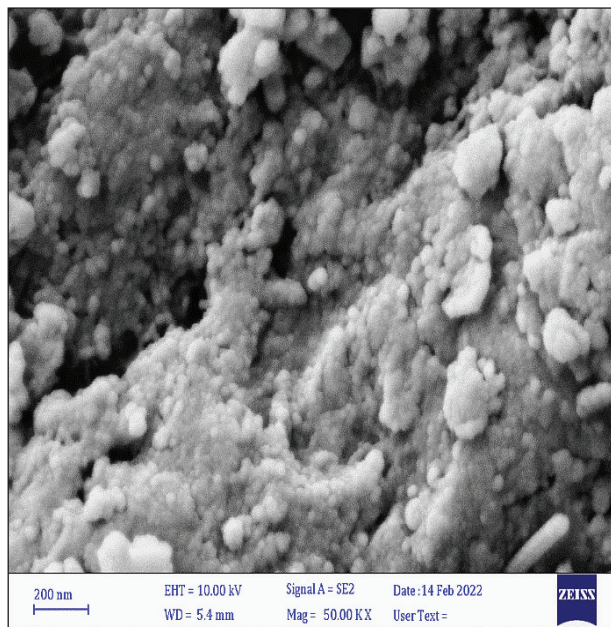


Fig. 4b. SEM of Consocarpus plant (C/AC)

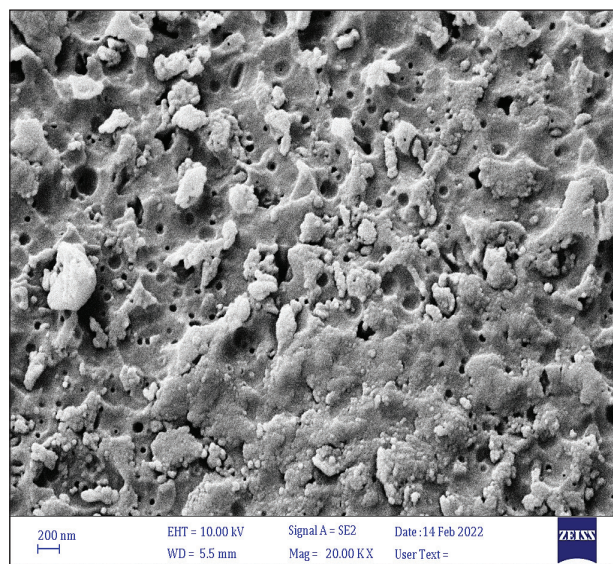


Fig. 4c. SEM image of Myrtus plant (M/AC)

3. Results and Discussion

3.1. Optimization of the extraction procedure

The study of finding the optimal conditions for any analytical method includes the process of changing one of the conditions of the experiment and fixing the rest of the other conditions that control the efficiency of the experiment. Adjusting the method to all the optimal values for all factors, and to find the ideal conditions and obtain the maximum efficiency of the process of extraction and removal of the dye, several experiments were conducted as follows:

3.2. Amount of solid phase

The effect of the weight of the packed solid phase in the separating column was studied, and the results proved that the percentage of retrieval varies according to the amount of the solid phase. Figure 5 shows an apparent behavior in increasing the retrieval percentage with increasing phase weight for the weights range (0.05-5.0) g, where the recovery percentage reaches the maximum value when using the weight of 0.25 g. Then the recovery percentages stabilize in the largest weights down to 0.5 g. This behavior was for all solid phases when studying the CR dye, which leads to the weight of 0.25 g of the solid phase being selected as a constant weight for all phases in all subsequent experiments.

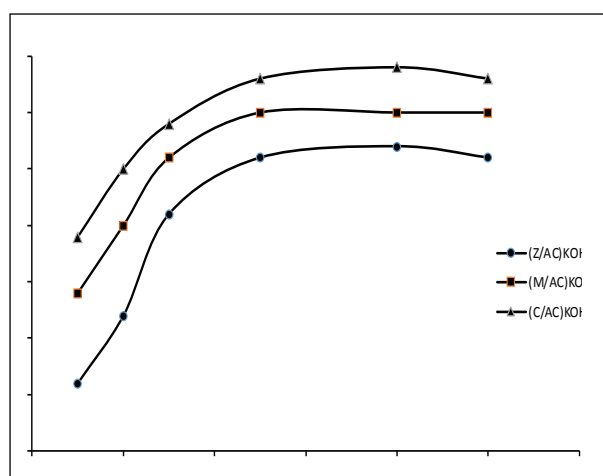


Fig. 5. Effect of the solid phase amount on the recovery of Congo Red

3.3. Effect of Dye concentration

The effect of the concentration of the CR solution was studied after packing the extraction column with 0.25 g of activated carbon and loading CR with a range of concentrations which is (50-400) mg L⁻¹ with the stabilization of the acidity function, the volume of the dye solution, the flow rate, the type and volume of the rinse solution, where a concentration of 100 mg L⁻¹ was chosen for the CR dye towards the corresponding solid phases, where this concentration achieves a recovery percentage ranging from 60-65% for the dyes. This ratio is necessary because the recovery efficiency was not at this stage at its maximum, and it is expected to increase it when conducting experiments on other factors affecting extraction. Due to Figure 6, the effect of the concentration of the CR solutions was shown.

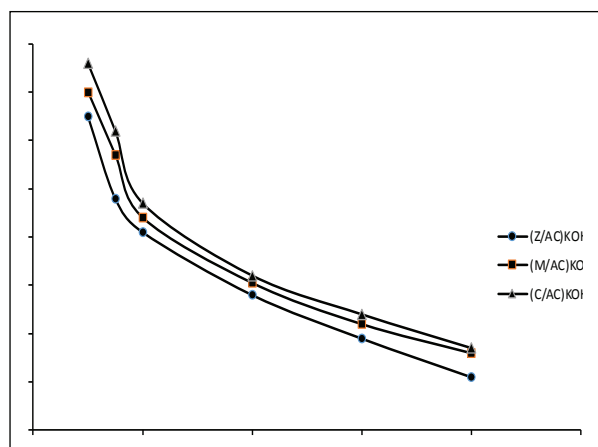


Fig. 6. Effect of Congo Red concentration on the recovery percentage

3.4. Effect of pH

The pH function is one of the critical factors in the study of extraction, which affects the surface charge of the solid phase and the composition of the dye [38]. The effect of acid functions on the solid phase extraction process with a range of (2-12) was studied. Figure 7 represents the effect of the acidity function on the percentage of recovery of CR (anionic) dye when extracted by (Z/AC) and (C/AC) and (M/AC) phases, as we notice that the %R values increase directly for the range of the acidity function (2-5) and then reach the optimal

acidity function $\text{pH} = 5$ and this increase in the %R values is attributed to the hydrostatic interactions between the solid phases and dyes, as for the acid functions that follow the optimum value and within the range (6-12), we notice a decrease in the values of %R, and this can be attributed to the fact that the hydroxyl radical OH^- whose concentration increases with the increase of the acidic function competes with the dye molecules towards the solid phases. The value of the optimal pH function in extracting or removing the CR dye is equal to 5 and was identical to the results of previous studies [24,25].

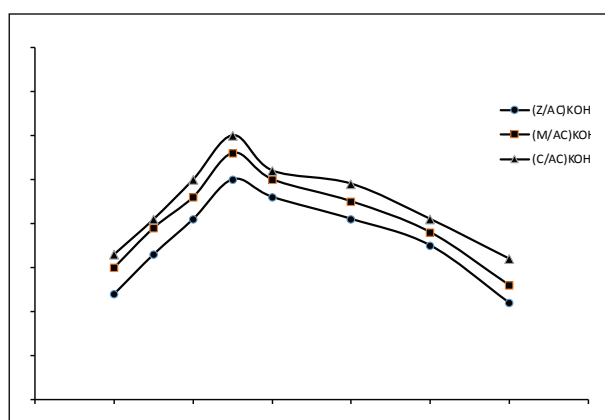


Fig. 7. Effect of pH on the recovery of Congo Red

3.5. Effect of dyes volume

Studying the effect of the target material solution's volume is essential in determining the optimal conditions for the solid phase extraction method [26,27]. Figure 8 showed that the percentages of recovery of CR dye were close to 100% for volumes less than 100 mL within the range of volumes (100-400) mL, the percentages of recovery gradually decreased. This behavior was very logical because the efficiency of the extraction decreases with the increase in the volume of the solution, as the concentration of the dye decreases with the increase in the volume of the solution, and therefore the remaining dye during the extraction process is more diluted the more the volume of the solution was more significant the extraction efficiency decreased. So, the volume of 25 mL is considered to be the optimum volume of the CR dye.

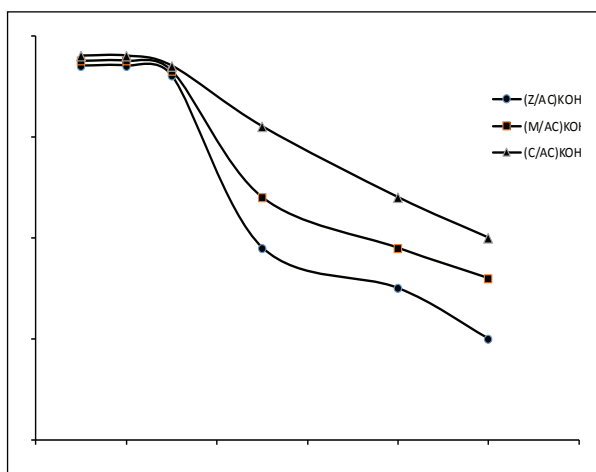


Fig. 8. Effect of Congo Red solution volume on the recovery percentage

3.6. Effect of flow rate

The effect of the flow rate of the dye solution is one of the critical factors affecting the efficiency of extraction in the solid phase. A balance in the flow rate is necessary in the sense that low flow rates do not achieve high rates of recovery of the target material due to the possibility of disengagement between the solid phase and the target material during the passage of the solution. Thus, the extraction efficiency decreases, and high flow rates are considered undesirable because they do not provide sufficient time for the connection between the solid phase and the material to be extracted. Figure 9 shows a graphic relationship between the percentages of dye recovery versus the rate of the flow rate of the CR solution. We found that the maximum flow rate was equal to 0.5 mL min.

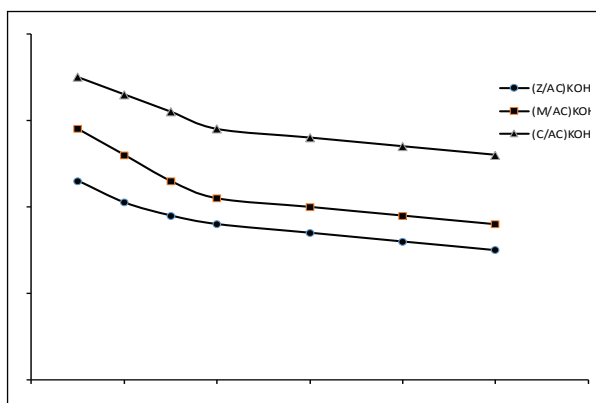


Fig.9. Effect of flow rate on the recovery of Congo Red

3.7. Effect of type and volume of eluting solution

Table 2 shows the solvents used as eluent solutions and their polarity index values, where the polarity coefficient represents the ability of the solvent to interfere with the solute[28], and Figure 10 shows the effect of the type of the solvent on the percentages of recovery of the two dyes. We note that the highest rate of recovery was achieved when the elution solution was DMSO with a polarity coefficient of 7.2 and the highest polarity among the solvents. It may be attributed to the great affinity of CR dyes towards the DMSO solvent because it is a polar dye. It makes the dye leave as a solid phase and moves with the more polar rinsing solution (Figure 10). we note that the percentages of recovery decrease with the decreasing polarity of the eluting solution. The study also included finding the optimum volume of the rinse solution; when observing in Figure 11, which represents the graphic relationship between the percentage of recovery of the CR dye and the volume of the rinse solution, we find that the volume that achieves the highest rate of recovery was equal to 8 mL. Finding the optimal volume of the rinsing solution leads us to calculate the enrichment factor, which evaluates

the extraction process, which can be calculated from Equation 4 [29].

$$\text{Enrichment Factor (EF)} = \frac{\text{Original Dye Volume}}{\text{Elution Solution Volume}} \quad (\text{Eq.4})$$

The enrichment coefficient can be calculated depending on the initial dye volume and the volume of the rinsing solution (Equation 4). Table 3 shows the values of the calculated enrichment coefficients for the extraction systems under study.

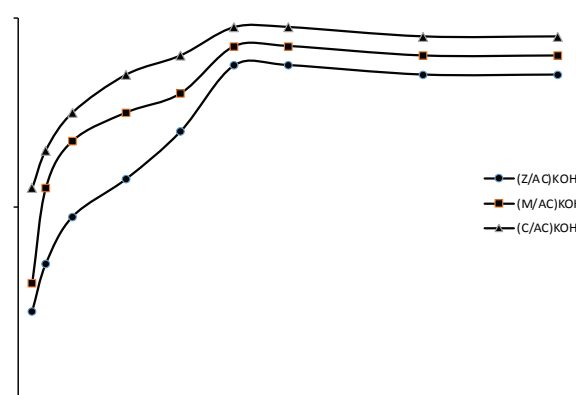


Fig. 11. Effect of DMSO volume on the recovery of Congo Red

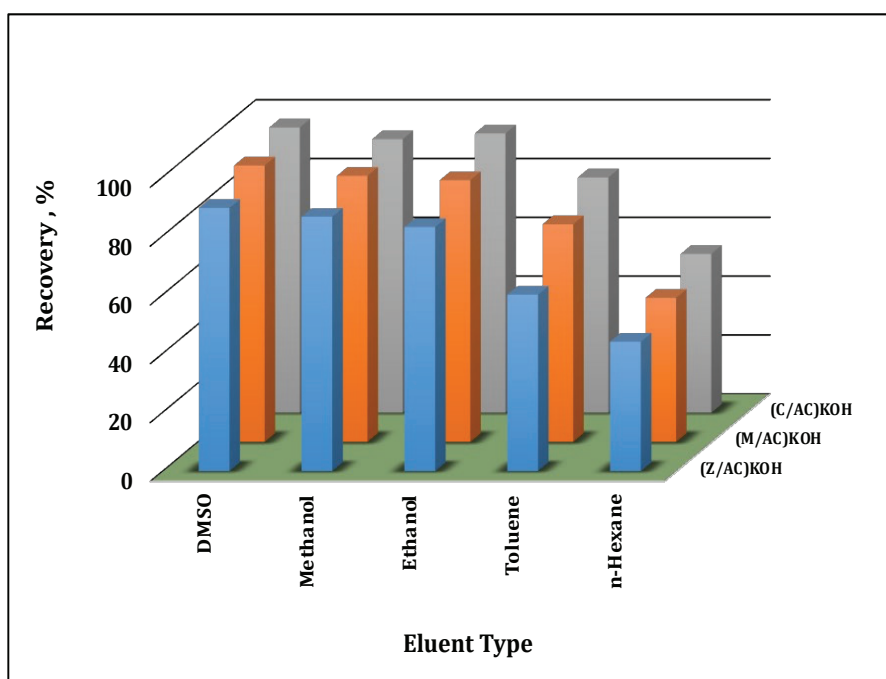


Fig. 10. Effect of elution type on the recovery of Congo Red

Table 2. Solvents used as elution solution and their polarity index

Solvent	Polarity index
DMSO	7.2
Methanol	5.1
Ethanol	4.3
Toluene	2.4
n-hexane	0.1

Table 3. Enrichment factors for extraction of CR

Solid Phase	Enrichment factor
(Z/AC)	3.125
(M/AC)	3.125
(C/AC)	3.125

3.8. Isotherm study

One of the most important benefits of the SPE extraction process is the removal of the target substance from its origin in which it is located [30]. Therefore, the results obtained in the extraction experiments can be employed in favor of the removal operations of CR from its aqueous solution. The residual concentration of the solutions of the CR dye was calculated and thus the weight adsorption capacity q (mg g^{-1}) was calculated based on Equation 5 [31, 32].

$$q = \frac{(C_o - C_e)V}{M} \quad (\text{Eq.5})$$

Through the study of the isotherm, it is possible to clarify the relationship between the solid phases and dye, and to suggest the mechanisms of interaction [33]. The study of the isotherm includes the application of many models, and the Langmuir and Freundlich models were chosen in this study.

3.9. Langmuir isotherm model

The Langmuir equation [34] which was developed in 1916 applies to monolayer or single-molecular adsorption of the target material on the surface of the adsorbent material or the solid phase (Equation 6), where this equation assumes the existence of homogeneous adsorption sites [35].

$$\frac{C_e}{q_e} = \frac{1}{(q_{max} \times K_L)} + \frac{C_e}{q_{max}} \quad (\text{Eq.6})$$

Figure 12 represents the Langmuir model for CR. Table 4 also shows the results obtained from this model. The values of the maximum adsorption capacity q_{max} , Langmuir constant K_L and correlation coefficient R^2 were calculated by plotting the graphical relationship of the Langmuir equation between C_e/q_e on the Y-axis and C_e on the X-axis as in Figure 12, where the slope of the straight line represents $(1/q_{max})$ and the cutoff represents $(1/q_{max} \cdot K_L)$ and by noting the Table 4, we find that the maximum adsorption capacity of CR dye by the solid phase (C/AC) is the highest in comparison with the other two phases. This may be due to the nature of the interaction between this dye and the prepared solid phases, which certainly had the advantage compared to the nature of the association with CR dye, and also through Table 4 we find that the values of Langmuir constant rise in the same pattern, which indicates the extent of the strong interaction between the active sites in the dye and between the solid phase. It is also noted the values of the correlation coefficient very close to the right one, which indicates the relative applicability of the studied adsorption systems on the Langmuir model.

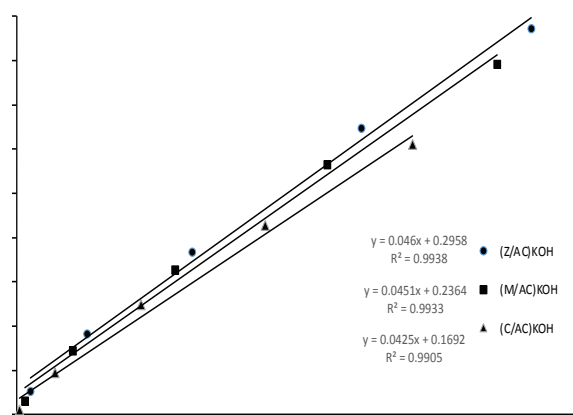


Fig. 12. Langmuir isotherm of adsorption of Congo Red

Table 4. Langmuir isotherm parameters for the adsorption of CR dye at 25 °C

Solid Phase	q_{\max} (mg. g ⁻¹)	K_L	R^2
(Z/AC)	21.7391	0.9938	1.5551
(M/AC)	22.1729	0.9933	1.90778
(C/AC)	23.5294	0.9905	2.51182

3.10. Freundlich isotherm model

As Equation 7, the Freundlich equation developed in 1926 [36] It explains the processes of interference and adsorption that occur on heterogeneous surfaces and assumes that adsorption occurs at sites of varying adsorption energy [37].

$$\ln q_e = \ln K_F + \frac{1}{n} \ln C_e$$

(Eq.7)

The Figure 13 represent Freundlich model for CR. Table 5 also shows the results obtained from this model. The values of Freundlich constant K_F and correlation coefficient R^2 were calculated by plotting the graph of Freundlich equation between $\ln q_e$ on the Y-axis and $\ln C_e$ on the X-axis as in Figure 13, where the slope of the straight line represents $(1/n)$ and the cut off represents $(\ln K_F)$. By noting the Table 5, we find that the highest value of K_F , which represents the adsorption energy between the solid phase and the dye [38] is for the adsorption system of the solid phase (C/AC) and this result is

in agreement with the q_{\max} values calculated from the Langmuir model. The values of $1/n$ give an indication that the adsorption process is preferred or unfavorable, as if the values of $1/n = 0$, this means that the adsorption is irreversible, but when it is $0 < 1/n < 1$, this indicates that the adsorption between the solid phase and target material is a preferred process, and adsorption may not be favorable when $1/n > 1$ [39]. When observing the values of $1/n$ from Table 5, we find that they are greater than zero and less than one for all solid phases. Thus, could be concluded that the adsorption systems in this study are preferred. After reviewing Tables 4 and 5, we find that the R^2 values of the Freundlich model for all systems are higher than the corresponding values in the Langmuir model leading to suggest a physisorption mechanism.

4. Conclusion

In conclusion, the efficient removal of the dyes CR from aqueous solutions was observed when using the active carbon (Z/AC), (C/AC) and (M/AC) as solid phases. The optimization approach

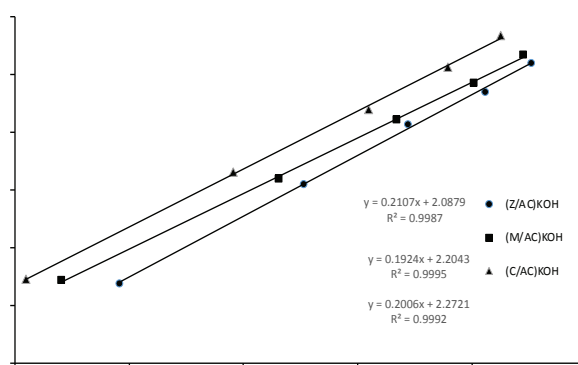


Fig. 13. Freundlich isotherm of adsorption of Congo Red

Table 5. Freundlich isotherm parameters for the adsorption of CR dye at 25 °C

Solid Phase	K_F	$1/n$	R^2
(Z/AC)	8.06795	0.2107	0.9987
(M/AC)	9.0639	0.1924	0.9995
(C/AC)	9.69975	0.2006	0.9992

for the extraction of CR observed that the optimum amount of solid phases was 0.25 g, the initial concentration of dye solution was 100 mg L⁻¹, the optimum pH was 5, the volume of dye solution was 25.0 mL with a flow rate equal to 0.5 mL min⁻¹, and the optimum elution solution was DMSO with a volume equal to 2.0 mL, from the linearized form (from the calculation of the Langmuir equation, q_{max}), values for the CR dye were (21.74, 23.53, 22.17) mg g⁻¹ for (Z/AC), (C/AC), and (M/AC), respectively.

5. References

- [1] X. Li, W. Bo, C. Yuhua, Z. Shuang, W. Hang, F. Xiao, Z. Junwen, M. Xiaojie, Water contaminant elimination based on metal-organic frameworks and perspective on their industrial applications, *ACS Sustain. Chem. Eng.*, 7 (2019). 4548–4563. <https://doi.org/10.1021/acssuschemeng.8b05751>.
- [2] N. Masoudian, M. Rajabi, M. Ghaedi, Titanium oxide nanoparticles loaded onto activated carbon prepared from bio-waste watermelon rind for the efficient ultrasonic-assisted adsorption of congo red and phenol red dyes from wastewaters, *Polyhedron*, 173 (2019) 114105. <https://doi.org/10.1016/j.poly.2019.114105>.
- [3] K. Hossienzadeh, A. Maleki, H. Daraei, M. Safari, R. Pawar, S. M. Lee, Sonocatalytic and photocatalytic efficiency of transition metal-doped ZnO nanoparticles in the removal of organic dyes from aquatic environments, *Korean J. Chem. Eng.*, 36 (2019) 1360–1370. <https://doi.org/10.1007/s11814-019-0299-6>.
- [4] J. C. G. Sousa, A. R. Ribeiro, M. O. Barbosa, M. F. R. Pereira, A. M. T. Silva, A review on environmental monitoring of water organic pollutants identified by EU guidelines, *J. Hazard. Mater.*, 344 (2018) 146–162. <https://doi.org/10.1016/j.jhazmat.2017.09.058>.
- [5] M. A. Hassaan, A. El Nemr, Health and environmental impacts of dyes: Mini review, *Am. J. Environ. Sci. Eng.*, 1

- (2017) 64-67. [https://doi: 10.11648/j.ajese.20170103.11](https://doi.org/10.11648/j.ajese.20170103.11).
- [6] K. Singh, S. Arora, Removal of synthetic textile dyes from wastewaters: A critical review on present treatment technologies, *Crit. Rev. Environ. Sci. Technol.*, 41 (2011) 807–878. [https://doi: 10.1080/10643380903218376](https://doi.org/10.1080/10643380903218376).
- [7] E. Errais, Efficient anionic dye adsorption on natural untreated clay: Kinetic study and thermodynamic parameters, *Desalination*, 275 (2011) 74–81. <https://doi.org/10.1016/j.desal.2011.02.031>.
- [8] E. Zabłocka-Godlewska, W. Przystaś, E. Grabińska-Sota, Possibilities of obtaining from highly polluted environments: new bacterial strains with a significant decolorization potential of different synthetic dyes, *Water Air Soil Pollut.*, 229 (2018)176. [https://doi: 10.1007/s11270-018-3829-7](https://doi.org/10.1007/s11270-018-3829-7).
- [9] M. S. El-Geundi, H. M. Ismail, K. M. E. Attyia, Activated clay as an adsorbent for cationic dyestuffs, *Adsorpt. Sci. Technol.*, 12 (1995) 109–117. [https://doi: 10.1177/026361749501200203](https://doi.org/10.1177/026361749501200203).
- [10] S. A. Jadhav, Recent advancements in silica nanoparticles based technologies for removal of dyes from water, *Colloid Interface Sci. Commun.*, 30 (2019) 100181. <https://doi.org/10.1016/j.colcom.2019.100181>.
- [11] X. Meng, Synthesis, characterization, and utilization of a lignin-based adsorbent for effective removal of azo dye from aqueous solution, *ACS omega*, 5 (2020) 2865–2877. [https://doi: 10.1021/acsomega.9b03717](https://doi.org/10.1021/acsomega.9b03717).
- [12] T. M. Budnyak, Methylene Blue dye sorption by hybrid materials from technical lignins, *J. Environ. Chem. Eng.*, 6 (2018) 4997–5007. [https://doi: 10.1016/j.jece.2018.07.041](https://doi.org/10.1016/j.jece.2018.07.041).
- [13] S. Banerjee, M. C. Chattopadhyaya, Adsorption characteristics for the removal of a toxic dye, tartrazine from aqueous solutions by a low cost agricultural by-product, *Arab. J. Chem.*, 10 (2017) S1629–S1638. [https://doi: https://doi.org/10.1016/j.arabj.2013.06.005](https://doi.org/10.1016/j.arabj.2013.06.005).
- [14] M. B. Ahmed, J. L. Zhou, H. H. Ngo, W. Guo, N. S. Thomaidis, J. Xu, Progress in the biological and chemical treatment technologies for emerging contaminant removal from wastewater: A critical review, *J. Hazard. Mater.*, 323 (2017) 274–298. <https://doi.org/10.1016/j.jhazmat.2016.04.045>.
- [15] Y. Zhou, J. Lu, Y. Zhou, Y. Liu, Recent advances for dyes removal using novel adsorbents: A review, *Environ. Pollut.*, 252 (2019) 352–365. [https://doi: 10.1016/j.envpol.2019.05.072](https://doi.org/10.1016/j.envpol.2019.05.072).
- [16] J. Wang, Two new uncommon 3D cobalt-based metal organic frameworks: Temperature induced syntheses and enhanced photocatalytic properties against aromatic dyes, *Dye. Pigment.*, 187 (2021), 109068. <https://doi.org/10.1016/j.dyepig.2020.109068>.
- [17] E. Dziurkowska, M. Wesolowski, Solid phase extraction purification of saliva samples for antipsychotic drug quantitation, *Molecules*, 23 (2018) 2946. [https://doi: 10.3390/molecules23112946](https://doi.org/10.3390/molecules23112946).
- [18] W. Jing, J. Wang, B. Kuipers, W. Bi, D. D. Y. Chen, Recent applications of graphene and graphene-based materials as sorbents in trace analysis, *TrAC Trends Anal. Chem.*, 137 (2021) 116212. [https://doi: https://doi.org/10.1016/j.trac.2021.116212](https://doi.org/10.1016/j.trac.2021.116212).
- [19] M. He, L. Huang, B. Zhao, B. Chen, B. Hu, Advanced functional materials in solid phase extraction for ICP-MS determination of trace elements and their species - A review, *Anal. Chim. Acta*, 973 (2017) 1–24. [https://doi: 10.1016/j.aca.2017.03.047](https://doi.org/10.1016/j.aca.2017.03.047).
- [20] M. H. Abdel-Aziz, DFT and experimental study on adsorption of dyes on activated carbon prepared from apple leaves,

- Carbon Lett., 31 (2021) 863–878. [https://doi: 10.1007/s42823-020-00187-1](https://doi.org/10.1007/s42823-020-00187-1).
- [21] H. Javadian, Using fuzzy inference system to predict Pb (II) removal from aqueous solutions by magnetic Fe₃O₄/H₂SO₄-activated Myrtus Communis leaves carbon nanocomposite, J. Taiwan Inst. Chem. Eng., 91 (2018) 186–199. [https://doi: 10.1016/j.jtice.2018.06.021](https://doi.org/10.1016/j.jtice.2018.06.021).
- [22] S. Farrokhzadeh, H. Razmi, B. Jannat, Application of marble powder as a potential green adsorbent for miniaturized solid phase extraction of polycyclic aromatic hydrocarbons from water samples, Sep. Sci. Technol., 55 (2020) 2737–2745. [https://doi: 10.1080/01496395.2019.1655054](https://doi.org/10.1080/01496395.2019.1655054).
- [23] J. Dai, Fabrication of novel ZIF-67 composite microspheres for effective adsorption and solid-phase extraction of dyes from water, Chem. Select, 3 (2018) 5833–5842. [https://doi: https://doi.org/10.1002/slct.201800778](https://doi.org/10.1002/slct.201800778).
- [24] H. S. Al-Niaeem, A. A. Abdulwahid, W. S. Hanoosh, Removal of carcinogenic dyes congo red (CR) and Bismarck brown Y (BBY) by adsorption onto reusable hydrogels derived from acrylamide, J. Phys. Conf. Ser., 2063 (2021) 012011. [https://doi: 10.1088/1742-6596/2063/1/012011](https://doi.org/10.1088/1742-6596/2063/1/012011).
- [25] A. A. Mizhir, A. A. Abdulwahid, H. S. Al-Lami, Adsorption of carcinogenic dye congo red onto prepared graphene oxide-based composites, Desalin. Water Treat., 202 (2020) 381–395. [https://doi: 10.5004/dwt.2020.26141](https://doi.org/10.5004/dwt.2020.26141).
- [26] A. A. Gouda, W. A. Zordok, Solid-phase extraction method for preconcentration of cadmium and lead in environmental samples using multiwalled carbon nanotubes, Turkish J. Chem., 42 (2018) 1018–1031. [https://doi:10.3906/kim-1711-90](https://doi.org/10.3906/kim-1711-90).
- [27] K. Hossein, Mahdi and Dalali, Nasser, Karimi, Ali and Dastanra, Solid phase extraction of copper, nickel, and cobalt in water samples after extraction using surfactant coated alumina modified with indane-1,2,3-trione 1,2-dioxime and determination by flame atomic absorption spectrometry, Turk. J. Chem., (2010), 805–814. <https://doi.org/10.3906/sag-1203-108>.
- [28] L. R. Snyder, Classification off the solvent properties of common liquids, J. Chromatogr. Sci., 16 (1978) 223–234. [https://doi: 10.1093/chromsci/16.6.223](https://doi.org/10.1093/chromsci/16.6.223).
- [29] Y. Li, W. Zhang, R.-G. Wang, P.-L. Wang, X.-O. Su, Development of a efficient and sensitive dispersive liquid–liquid microextraction technique for extraction and preconcentration of 10 β₂-agonists in animal urine, PLOS One, 10 (2015) 1–16. [https://doi: 10.1371/journal.pone.0137194](https://doi.org/10.1371/journal.pone.0137194).
- [30] R. Amer, H. Hadi, Application of CTAB-coated magnetic nanoparticles for solid-phase extraction of thiamine hydrochloride from pharmaceutical formulations and urine samples, Arab. J. Sci. Eng., 47 (2022) 429–440. [https://doi: 10.1007/s13369-021-05671-y](https://doi.org/10.1007/s13369-021-05671-y).
- [31] E. Yilmaz, G. Guzel Kaya, H. Deveci, Removal of methylene blue dye from aqueous solution by semi-interpenetrating polymer network hybrid hydrogel: Optimization through Taguchi method, J. Polym. Sci. Part A Polym. Chem., 57 (2019) 1070–1078. [https://doi: https://doi.org/10.1002/pola.29361](https://doi.org/10.1002/pola.29361).
- [32] M. T. Nakhjiri, G. Bagheri Marandi, M. Kurdtabar, Adsorption of methylene blue, brilliant green and rhodamine B from aqueous solution using collagen-g-p(AA-co-NVP)/Fe₃O₄@SiO₂ nanocomposite hydrogel, J. Polym. Environ., 27 (2019) 581–599. [https://doi: DOI:101007/s10924-019-01372-8](https://doi.org/10.1007/s10924-019-01372-8).
- [33] Y. Kuang, X. Zhang, S. Zhou, Adsorption of methylene blue in water onto activated carbon by surfactant modification, Water, 12 (2020) 587. [https://doi: 10.3390/w12020587](https://doi.org/10.3390/w12020587).
- [34] I. Langmuir, The constitution and fundamental properties of solids and

- liquids part 1 solids, *J. Am. Chem. Soc.*, 38 (1916) 2221–2295. <https://doi: 10.1021/ja02268a002>.
- [35] A. A. Mizhir, A. A. Abdulwahid, H. S. Al-Lami, Chemical functionalization graphene oxide for the adsorption behavior of bismarck brown dye from aqueous solutions, *Egypt. J. Chem.*, 63 (2020) 1679–1696. <https://doi: 10.21608/ejchem.2020.21260.2271>.
- [36] Wi. B. Meldrum, Experiments in physical chemistry, *J. Chem. Educ.*, 28 (1951) 174. <https://doi: 10.1021/ed028p174.3>.
- [37] I. Crisan, R. Vidican, Phytoremediation Potential of *Iris spp*, *Bull. Univ. Agric. Sci. Vet. Med. Cluj-Napoca. Agric.*, 78 (2021) 1–10. <https://doi: 10.15835/buasvmcn-agr:2020.0046>.
- [38] P. Luo, B. Zhang, Y. Zhao, J. Wang, H. Zhang, J. Liu, Removal of methylene blue from aqueous solutions by adsorption onto chemically activated halloysite nanotubes, *Korean J. Chem. Eng.*, 28 (2011) 800–807. <https://doi: 10.1007/s11814-010-0426-x>.
- [39] A. S. Muhammad, M. A. Abdurrahman, Adsorption of methylene blue onto modified agricultural waste, *Moroccan J. Chem.*, 8 (2020) 412–427. <https://doi.org/10.48317/IMIST.PRSM/morjchem-v8i2.16692>.



Optimization and effect of varying catalyst concentration and trans-esterification temperature on the yield of biodiesel production from palm kernel oil and groundnut oil

Obidike Blessing Magarette^a, Okwara Nelson Onyekachi^b, Andrew Wirnkor Verla^c,
Christian Ebere Enyoh^{d,*} and Mbagwu JohnPaul^e

^aDepartment of Chemical Sciences, Akwa-Ibom State Polytechnic Ikot-Osuruwa, Ikot-Ekpen Nigeria.

^bEunisell Globals Limited, Victoria Island, Lagos State Nigeria.

^cDepartment of Chemistry, Imo State University Owerri, Nigeria.

^{d,*} Graduate School of Science and Technology, Saitama University, Saitama, Japan

^eDepartment of Physics and Astronomy, University of Kansas, USA

ARTICLE INFO:

Received 8 May 2022

Revised form 16 Jul 2022

Accepted 11 Aug 2022

Available online 30 Sep 2022

Keywords:

Biodiesel,
Trans-Esterification,
Mineral diesel,
Palm kernel oil,
Groundnut oil,
Optimization

ABSTRACT

The negative environmental impact generated by fossil fuel has resulted in the demand to search for alternative routes of renewable sources of energy, such as biodiesel, that have unlimited duration while having little or no hazardous impact. In this study, trans-esterification of palm kernel oil and groundnut oil was carried out using sodium methoxide (CH_3ONa) as a catalyst. The effect of varying Sodium Methoxide (CH_3ONa) catalyst concentrations of (0.25, 0.5, 1.0, 1.5, and 2.0) % w/v at trans-esterification temperatures of (50, 55, and 60) °C on the yield of biodiesel from groundnut oil and palm kernel oil was determined. This was to identify the catalyst concentration and trans-esterification temperature with optimal process yield. The process gave optimum biodiesel yields of 98% and 84% by volume of groundnut oil and palm kernel oil at reaction conditions of 0.5%w/v CH_3ONa as catalyst, trans-esterification temperature of 55°C, 360 rpm mixing rate and a reaction time of 90 minutes. The biodiesel produced was analyzed for fuel properties using the American Society of Testing and Materials (ASTM) standard, and the results obtained were as follows; specific gravity (0.8835, 0.8815 at 15°C), flash point (98, 124) °C, viscosity (5.2, 7.6) mm^2S^{-1} at 40°C, pour point (9, -1)°C, iodine value (8.04, 17.11) /100, acid value (0.67, 0.48) mg/KOH/g, peroxide value (28, 60) mg Kg^{-1} , fire point (108,136)°C for palm kernel oil and groundnut oil respectively.

1. Introduction

Considering the rapid increase in the global population in the world today, the long-term strength of a complex environment is tested by the demand for a higher standard of living. This involves meeting the energy and food requirements of over 9 billion people [1]. A

recent statement by BP's Energy Outlook to 2035 proposed that the average world energy usage is expected to increase by 34% between 2014 and 2035 [2]. However, the use of petroleum is a suitable means of harnessing energy for global consumption. But its drastic increase in price, non-ecofriendly nature, and great addition to pollution of the atmosphere have led to the need to develop alternative routes of renewable sources of energy that have unlimited duration

*Corresponding Author: [Christian Ebere Enyoh](mailto:Christian.Ebere.Enyoh@ gmail.com)

Email: cenyoh@gmail.com

<https://doi.org/10.24200/amecj.v5.i03.203>

while having little or no hazardous impact on the environment [3]. Several alternative means, such as bio-ethanol from the ebullition of starch, biomass gasification, and biodiesel, have been harnessed over the years [4]. However, the use of biodiesel remains the best. It covers an estimated 82% of the total biofuel production as stated by the EU. It has also shown a substantial contribution to future energy demands of both domestic and industrial sectors [5,6]. In comparison with petroleum-based derived diesel, it is non-toxic, biodegradable, and a cleaner source of energy [2]. Vehicles using biodiesel emit less harmful greenhouse gases of carbon monoxide and sulfur dioxide [7]. Biodiesel could reduce the emission of particulate matter (PM) and act as a good lubricant for diesel engines, thus prolonging the shelf-life of the engine. In addition, biodiesel has a higher flash point, making it safer to handle than mineral diesel [8]. Other profitable characteristics of biodiesel that make it an effective alternative to mineral-derived-diesel oil are liquid nature portability, sustainability, ignition performance, and higher octane number [9]. Biodiesel, also known as fatty acids methyl esters (FAME) is a domestic and renewable biomass fuel for diesel engines obtained from vegetable oils or animal fats, designated B100. It must meet the requirements of ASTM D6751 [8]. Feedstocks used in biodiesel production are available and could always be re-planted or grown [8]. Biodiesel is produced through chemical processes such as transesterification or esterification reactions [10]. Trans-esterification is the reaction between an alcohol and an ester [11], while esterification is the reaction between a carboxylic acid and alcohol. During the process of trans-esterification, the alcohol functional group is deprotonated by the action of the base which compels it into a stronger nucleophile [12]. The most frequently employed alcohols in this process are ethanol or methanol. Under standard conditions, the trans-esterification reaction proceeds at a very slow rate or not at all, so, heats and catalysts (acid and/or base) are used to increase the reaction rate.

[13]. It is vital to know that catalysts are not absorbed during trans-esterification reactions [11]. Heterogeneous, homogeneous, Nano, and super-critical fluid catalysts have all been utilized to activate trans-esterification reactions [14]. But in this study, the homogenous catalyst is used for the trans-esterification process. This is because it permits a higher degree of interaction with the reaction mixture, and allows the complete conversion of feedstock to biodiesel [6]. More often in the presence of a base catalyst, an undesirable saponification reaction could occur if the feedstock contains free fatty acids. Therefore, feedstock containing less than 0.5wt% free fatty acid is employed during the trans-esterification process to avoid soap formation [15]. The feedstock composition controls the chemical pathway and dictates the type of catalyst to be utilized in the production of biodiesel [2]. The feedstock used for biodiesel production is Fats and oils from plants and animals; they comprise triglycerides which are esters that contain three fatty acids, trihydric alcohol, and glycerol. The feedstock includes a range of edible vegetable oil, non-edible oils, waste or recycled oils, and animal fats [7, 9 -10]. Edible oils are connected to edible biomass, examples are; soybean, rapeseed, sunflower, palm, coconut and linseed while the non-edible biofuels are biomass fuel, ranging from lignocellulose feedstock to municipal solid wastes [16]. From literature reviews various types of oil have been used, but in this study the use of edible oils like unrefined groundnut oil and palm kernel oil is selected owing to their unique properties. Groundnut oil is mild-tasting vegetable oil with a high smoke point compared to several cooking oils [17]. The oil is obtainable in purified, unrefined, cold pressed, and roasted variations have a strong peanut flavor and aroma [15]. Palm kernel oil is edible plant oil derived from the kernel of the oil palm [12]. Palm kernel oil is among one of the essential oils that contain saturated vegetable fats, this is because it is composed of 16-carbon saturated fatty acid and excessive palmitic acid [13]. Palm

Table 1. Literatures reviews of some studies conducted on the effect of varying catalyst concentration and Trans-esterification temperature on the yield of biodiesel in Nigeria

N	Feed Stock	Catalyst Type	T	Catalyst Concentration	RT	Biodiesel Yield	Ref.
1.	Palm kernel oil	Homogeneous	60°C	,1.5 ,1.25 ,1.0 ,0.75 ,0.5) and 2.0)%w/v of KOH 1.75	120	,85.2 ,95.8 ,95.0 ,90.5) % (71.3 ,71.1 ,73.3	[19]
2.	Milk Bush seed oil	Heterogeneous Homogeneous	65°C	wt. % of CSS and KOH 3.0	120	and 94.33% 81%	[20]
3.	False Shea seed oil	Homogeneous	50°C	0.3mol/dm ³ of NaOH	120	85.0%	[21]
4.	Water Melon Seed oil	Homogeneous	60°C	g of NaOH(0.18 ,0.15 ,0.13)	(150 ,120 ,90)	%(49 ,53 ,70)	[22]
5.	Jatropha curcas oil	Homogeneous	48°C	0.88M of KOH	240	84.70%	[23]
6.	Palm kernel oil	Homogeneous	60°C	w/v of KOH 1.0%	,90 ,75 ,60 ,45 ,30) (120 ,105	,94.2 ,92.5 ,90.1 ,87.4) % (96.0 ,96.0 ,96.0	[24]
7.	PKO-GO	Homogeneous	55°C	w/v of NaOH 0.7%	-----	91.98 ,90.53	[25]

RT: Reaction time (mins) T:Temperature PKO-GO: Palm kernel oil and groundnut oil

kernel oil is semi-solid at room temperature, stable at high cooking temperatures and has extended storage capacity [18]. Several studies have conducted experiments on biodiesel production using different catalyst types and feedstock to varying temperatures as summarized in Table 1. In this study, biodiesel will be produced from palm kernel oil and groundnut oil through different trans-esterification temperatures by varying catalyst concentrations of sodium methoxide. The result from this study will be a basis for determining the optimal reaction conditions for the production of biodiesel production.

2. Experimental

The data generated from the experimental results were modelled using linear, interaction, pure quadratic, quadratic, 3rd order polynomial, and 4th order polynomial. From the result obtained, the 4th-order polynomial showed a good correlation with the experimental results; demonstrating that the model was useful for optimization. Newton Raphson's multivariable optimization technique and Response Surface Methodology (RSM) were further used to enhance the process parameters of the trans-esterification reaction. Newton Raphson's

multivariable optimization technique gave an optimal yield of 100.5 mL and 90.7 mL for groundnut oil and PKO FAME with a corresponding catalyst concentration and trans-esterification temperatures of (0.25%, 0.48%) and (51.3 °C, 50 °C). Whereas the surface plots gave optimal yields of 104.8 mL and 89.8 mL with the catalyst concentration and trans-esterification temperatures of (0.6%, 0.425%) and (58°C, 50°C) for groundnut oil and Palm kernel Oil (PKO) based Fatty Acid Methyl Esters (FAME). The findings from this study were in good correlation with ASTM standards for fuel. Therefore, it can be used as an excellent alternative fuel for diesel engines.

2.1. Materials

The reagents used were distilled H₂O, Concentrated Sulphuric acid (H₂SO₄), Methanol (CH₃OH), Sodium hydroxide (NaOH), and two different oils, namely groundnut and palm kernel. Reagent like NaOH was properly reserved in an airtight plastic container to prevent them from absorbing moisture from the atmosphere since it is deliquescent in nature. Methanol was reserved in an airtight brown bottle to prevent evaporation as methanol is a volatile liquid.



Fig. 1a. Low FFA oil after acid-catalyzed esterification

2.2. Sampling

Groundnut oil and Palm kernel oil were procured from a commercial shop in Ogbete main market Enugu state, Nigeria. The experiment was conducted in laboratory 3 of the materials and Energy Technology (MET) department of the Project Development Institute (PRODA), Enugu state Nigeria.

2.3. Acid-catalyzed esterification

Delving directly into base-catalyzed transesterification may result in soap production instead of biodiesel due to the high FFA content of the unrefined groundnut oil and palm kernel oil. In order to eradicate the possibility of this side reaction (i.e., saponification), the FFA content of the unrefined sample is reduced to the barest minimum by acid-catalyzed esterification reaction using conc. Sulfuric acid (conc. H_2SO_4) as catalyst [8]. The diagrammatic setup is shown in Figure 1a and 1b.

2.3.1. Experimental procedure of the acid-catalyzed esterification

Unrefined groundnut oil and palm kernel oil were poured into a conical flask and heated to a temperature of $60^\circ C$ for 10 minutes. The temperature was monitored using mercury in a glass thermometer fitted with a ca lamp in the retort stand. Methanol (60% weight of the sample) was introduced into the beakers containing the preheated



Fig. 1b. High FFA oil before acid catalyzed esterification

oil samples. Concentrated sulfuric acid (H_2SO_4) of 1.2% weight of the sample was added to the mixture. The mixture was stirred using a magnetic hot plate at $50^\circ C$ in an open system for an hour. The mixture was transferred into a separating funnel and allowed to separate overnight. The mixture is divided into three phases: the lower phases (impurities), the middle phase (the preheated sample) and the upper layer (the methanol-water phase).

2.4. Base catalyzed transesterification experimental procedure

9.65g of NaOH pellets were weighed and introduced into a round bottom flask containing 200mL of $CH_3OH(aq)$. It was stirred and allowed to dissolve completely by shaking vigorously until a solution of sodium-methoxide (CH_3ONa) was formed in the process. The CH_3ONa solution was added to 100mL of groundnut oil and palm kernel oil from the acid catalyzed esterification process into the different conical flasks. The mixture was then heated to a preferred trans-esterification temperature of $60^\circ C$ using the magnetic hot plate. At this point, the stirrer was introduced into the solution. Stirring was done at a constant speed (e.g., 360 revolutions per minute). It was continued until a given time of 90 minutes was attained. While heating and stirring simultaneously, the solution was made air-tight using a masking foil to prevent CH_3ONa from evaporating. After

the given time, the solution was removed from heat and poured into a separating funnel. It was left overnight for the separation to take place. Glycerin settled below, while the biodiesel (ethyl esters) which was the supernatant settled above. The glycerin was discarded and the biodiesel was washed with distilled water until the impurities were completely removed. These impurities were in the form of a foamy solution that settled. The biodiesel was again washed with hot water to remove further impurities. Measurements were also taken before and after the washing of biodiesel. The waste product removed with water was tested using phenolphthalein, which turned pink on the addition of phenolphthalein, confirming that sodium hydroxide was still present. So, in order to get purer biodiesel, continued washing with water was done until the product was removed as waste does not turn pink using the phenolphthalein Indicator. To neutralize the presence of NaOH(aq) ultimately, 1mL H₂SO₄(aq) was added after every negative phenolphthalein test because acids have no negative effect on biodiesel. The already washed biodiesel was collected and heated gradually at about 100 to give off the leftover water after washing, then was allowed to cool. A viscous solution with pale gold color was obtained and that was the biodiesel. The procedure was repeated using the same catalyst concentrations of 0.25%w/v at the trans-esterification temperature of 55°C and 50°C, respectively.

2.5. Physicochemical Characterization of Biodiesel

2.5.1. Determination of specific gravity at 55°C and viscosity at 40°C

empty S.G. bottle was weighed and filled with distilled water, and the reading was noted. An S.G bottle was filled with biodiesel and weighed again. The S.G. was calculated using Equation 1.

$$SG = \frac{\text{weight of the biodiesel}}{\text{weight of distilled water}} \quad (\text{Eq.1})$$

The viscosity of the biodiesel was determined using “Ostwald’s Viscometer”. This was done by filling the viscometer to the mark; sucking it up into the other side of the fuse, and setting a stop-clock or stop-watch to time when the oil flows back to the first tube with which the oil was first filled. The viscosity was then calculated as Equation 2.

$$\text{Viscosity} = \frac{4.39 \times t}{8} \quad (\text{Eq.2})$$

Where; 4.39 = centistokes constant, 8 = sugar or glucose constant, t = time taken to move in the viscometer.

2.5.2. Free fatty acid (FFA) or acid value

The acid number test was conducted using ASTM D-664 Test Method. 5g of the biodiesel sample was measured into a conical flask, and three drops of phenolphthalein indicator and 20 ml of ethanol were added. It was titrated with 0.1 M NaOH solutions and a pink coloration was observed. The FFA was calculated by Equation 3.

$$FFA = \frac{T.V \times N \times 5.61}{W} \quad (\text{Eq.3})$$

Where; T.V = Titre value, N = Normality of titrate, 5.61 = Acid constant, W = Weight of the sample

2.5.3. Saponification Value (SV)

The saponification value test for biodiesel in this present study was conducted in accordance to ASTM D5558 standard testing method. 5g of the biodiesel was measured into a conical flask, 0.5M of ethanolic KOH was added and refluxed (heat) in a round bottom flask, then allowed to stand for 3 minutes. The essence of refluxing was to get a perfect dissolution of biodiesel in the ethanolic potassium hydroxide. Three drops of phenolphthalein indicator were added and titrated with 0.5M hydrochloric acid. A blank

titration was also run; the saponification value was calculated using Equation 4.

$$SV = \frac{56.1 \times 0.5 \times (v_2 - v_1)}{\text{weight of biodiesel used}} \quad (\text{Eq.4})$$

Where; V_2 = Titer of blank, V_1 = Titer of sample, 56.1 = MW of KOH, 0.5 = Normality of KOH.

2.5.4. Determination of iodine value using EN 14112 test method

5.0 g of biodiesel was measured into a conical flask; 15mL of chloroform and 25mL of Wijis (iodine monochloride) solution were added and mixed together. The mixture was tightly covered and placed in the dark for 30 minutes. 20mL of 10% KI (Potassium iodide) and 50mL of distilled water were added and the resulting solution turned to red. The reddish solution was titrated with 0.1M Sodium Thiosulphate, 5.0 mL of 1% starch indicator was added and the color turned blue-black. It was later titrated with 0.1M Sodium Thiosulphate and turned colorless. Blank was also titrated and the iodine value was calculated by Equation 5.

$$IV = \frac{12.69 \times (v_2 - v_1) \times N}{\text{weight of biodiesel used}} \quad (\text{Eq.5})$$

Where; 12.69 = Constant for iodine value, N = Normality of Titrant, V_2 = Titer of blank, V_1 = Titer of sample.

2.5.5. Determination of peroxide value using ASTM D37031-13 methodology

5g of biodiesel was measured into a 100 mL beaker, 25 mL of acetic acid and chloroform solution in the ratio of 2:1 was added. 1mL of 10% Potassium Iodide was later added and shaken vigorously. The mixture was covered and kept in the dark place for 1 minute. 35 mL of the starch indicator was added and Titrated with 0.02M Sodium Thiosulphate $\text{Na}_2\text{S}_2\text{O}_3$ and a white color

was observed. A blank titration was also prepared in the same way as described excluding the step of addition of biodiesel. The peroxide value was calculated as Equation 6.

$$PV = \frac{100(v_1 - v_2) \times N}{\text{volume of biodiesel used}} \quad (\text{Eq.6})$$

Where; N = Normality $\text{Na}_2\text{S}_2\text{O}_3$, V_1 = Titer of sample, V_2 = Titer of blank, 100 = Peroxide value constant.

2.5.6. Determination of pour and flash point

This is the minimum temperature at which the oil can pour down. This test was done in accordance to the ASTM D97 Test method. The biodiesel was brought out at room temperature, it was allowed to melt gradually and the temperature at which the biodiesel became a complete liquid was recorded as the pour point.

The flash point of an oil is the lowest temperature at which vapour from biodiesel will ignite when a small flame is applied under standard test conditions. The test was carried out using the D93 test method. A source of the fire was placed at a distance away from the smoking biodiesel in a closed cup and the temperature at which the biodiesel catches fire was noted.

2.6. Model methodology

The yields of biodiesel obtained from both samples (i.e., groundnut oil and palm kernel oil) in this study were modeled concerning two independent variables (catalyst concentration and trans-esterification temperature) using Several models such as linear, interaction, pure quadratic, quadratic, 3rd order polynomial and 4th order polynomials.

2.7. Optimization methodology

Data obtained were optimized using MATLAB optimization tool box and Response Surface Methodology (RSM) as described by [40].

3. Results and discussion

3.1. *Experimental result on the yield of biodiesel obtained from groundnut oil and palm kernel oil by varying catalyst concentration and transesterification temperature*

The results obtained by varying transesterification temperature from 50-60°C at catalysts concentration of 0.25-2.0% w/v of CH_3ONa is presented in Table 2 and 3. From the result it can be deduce that biodiesel yield increases gradually with an increase in catalysts concentrations and trans-esterification temperature, but with an additional increase in catalyst concentration of 1%w/v resulted to a decrease in biodiesel yield. Hence, the maximum output of biodiesel was at 0.5 % w/v of CH_3ONa catalyst and a trans-esterification temperature of 55°C. This implies that, at that temperature and concentrations equilibrium is attained and this can be further explained by trans-esterification reversible reaction. The discovery from this research was in close proximity to the works of [26] who reported that catalysts concentrations above 1% w/v favored backward reaction, thereby shifting the equilibrium to the left as well as resulting in the loss of sodium methoxide and a reduction in the yield of biodiesel.

3.2. *Physicochemical characterization of the biodiesel*

The result for the physicochemical characterization of the biodiesel is presented in Table 4. The physiochemical characterization of biodiesel obtained from PKO and groundnut oil in this present study showed a good conformity to that of ASTM standard values for mineral diesel. Hence, it can be utilized as a better alternative for petroleum diesel. The density of the oil is a very vital factor to be considered because the fuel injection system works with volume metering approach. The density of biodiesel provides required details on the weight of the oil at specific temperatures. From this present study the specific gravities of biodiesel harnessed from palm kernel oil and groundnut oil were 0.8835 and 0.8815 respectively. These values are within the limits of 0.8833 of biodiesel specified by ASTM [27] and

were also in close proximity with various scientific studies carried out by [28] who reported specific gravities of 0.881, 0.865, and 0.887 for biodiesel from Mango seed oil, Palm kernel oil and Shea butter oil. Viscosity is one of the basic criteria to be considered when evaluating the quality of biodiesel. It is a key property which measures the resistance flow of fluids under the effect of gravity [29]. The viscosity value obtained from biodiesel of PKO and groundnut oil conducted in this experiment are $5.2 \text{ mm}^2 \text{ S}^{-1}$ and $7.6 \text{ mm}^2 \text{ S}^{-1}$ respectively. These values were within the limits of $4.0 - 6.0 \text{ mm}^2 \text{ S}^{-1}$ specified by ASTM, but the biodiesel from groundnut oil was a bit higher than ASTM required limit. The viscosity of biodiesel explains the effective lubricity of fuel; it shows that the biodiesel analyzed in this present study may protect diesel fuel pumps and engines from wear and seepage. Thus enhances the atomicity and combustion as well as reducing emissions of fumes from exhaust engines. The values obtained also showed good correlation with biodiesel values of 7.65 and $5.92 \text{ mm}^2 \text{ S}^{-1}$ from palm kernel oil and groundnut oil [30]. It was said to be somewhat higher than the values of $3.62 \text{ mm}^2 \text{ S}^{-1}$ reported in shear butter oil [28] and mango seed oil ($5.82 \text{ mm}^2/\text{S}$) [26]. Flash point refers to the lowest temperature at which the biodiesel produces enough vapour to ignite when exposed to thermal sources; it is also a measure of degree of flammability [31]. It is a basic criterion to consider when handling, storing and transporting fuel. The flash point of the biodiesel obtained from PKO and groundnut oil in this research was 98°C and 124°C. It was within the range of (100 – 170) °C set by ASTM. Therefore, the flash point value of the biodiesel from this research shows that it is safe, non-hazardous, and can hardly ignite at higher temperatures. The values obtained from this research for biodiesel from PKO was slightly lower than flash points of 120°C, 132°C, and 167°C reported by [32-33]. The biodiesel from this study is less volatile and free from basic impurities like methanol which could reduce the flash point of biodiesel.

Table 2. Palm Kernel Oil base FAME experimental results

Trans-esterification Temperature (°C)	Catalyst Concentration (Yield %)				
	0.25	0.5	1.0	1.5	2.0
50	76	82	54	0	0
55	50	84	68	62	40
60	66	66	52	62	48

Table 3. Groundnut Oil base FAME experimental results

Trans-esterification temperature (°C)	Catalyst Concentration (Yield %)				
	0.25	0.5	1.0	1.5	2.0
50	96	92	74	74	16
55	95	98	89	72	22
60	50	95	89	38	0

The fire point is the temperature at which the biodiesel may like burn for a few seconds after ignition in an open flame. The fire point of biodiesel of PKO and Groundnut oil obtained in this experiment are 108°C and 136°C, it is higher than ASTM values of 68°C for diesel [32]. This shows that biodiesel is very suitable for use as it can hardly burn even at higher temperatures after ignition. The pour point is a necessary criterion when evaluating the low-temperature Performance of fuel. It is considered as the operational capacity of the fuel under given weather, it shows how effective biodiesels can be utilized even in cold climatic regions. The ASTM specified value for the pour point of biodiesel is -5 to 10 and -35 to 15 for mineral diesel [27]. In this research the biodiesel pours point values obtained from palm kernel oil and groundnut oil were 9 and -1, respectively. These values are within the ASTM standard values and are in close range of 0.0°C, 2°C, 5°C, and 2°C pour point values [32-34]. The biodiesel produced from the palm kernel oil in this experiment has a high pour point value of 9 due to the degree of unsaturation of carbon to carbon (C-C) bond formed; this implies that it can improve the performance of an engine. Saponification value of biodiesel plays a vital role in assessing adulteration [35]. Saponification of

biodiesel can be defined as the mass in milligram of potassium hydroxide needed to saponify 1g of oil, and it is relatively dependent on the average molecular weight of fatty acids present in the primary oil [28]. Saponification value is a measure of degree on how the biodiesel oxidizes during storage, an increase in saponification value increase volatility of biodiesel. The saponification values of biodiesel produced from PKO and groundnut oil in this experimental study are 423.55 and 227.66 mg KOH g⁻¹ respectively. It is above the ASTM value of 120 mg KOH g⁻¹. The high saponification value is an indication that the primary oil had high amount of soap content, this might result to uneven combustion and increase emissions of thick fumes from exhaust engine. However, it also has an the advantage of purifying the internal component of the engine, and as such reduces friction between the surface parts of the engine [32]. Considering the yield of biodiesel, high saponification values should be reduced to the barest minimum as it would likely prevent the separation of biodiesel from glycerin. In comparison with other findings, the values in this study were obtained within the same range of saponification values of 229.9 mg KOH g⁻¹ and 226 mg KOH g⁻¹ obtained in biodiesel produced from oil and palm kernel oil reported by [32,34].

Table 4. Properties of biodiesel and mineral diesel compared to biodiesel produced from Palm kernel oil and Groundnut oil in this study.

Fuel properties	Mineral-diesel ASTM D975 Limits	Biodiesel ASTM D6751	Palm kernel	oil biodiesel Groundnut oil biodiesel
Kinematic viscosity (mm ² S ⁻¹) at 40°C	1.3 - 4.1	4.0-6.0	5.2	7.6
Specific gravity at 15°C.	0.85	0.88	0.8835	0.8815
Flash point (°C)	60-80	100 – 170 (ASTM D93)	98	124
Pour point (°C)	-35 to -15	-5 to -10 (ASTM D97)	9	-1
Acid value (mKOH/g)	-	0.5 (ASTM D-664)	0.673	0.48
Peroxide value (meq/kg)	-	-ASTM D37031-13	28	60
Iodine value (g/100)	-	7.5-8.6 (EN 14112)	8.04	17.11
Saponification value (mgKOH/g)	-	95 – 370 (ASTM D5558)	423.5	227.66
Fire point (°C)	-	68	108	136

Source: Biodiesel Handling and Use Guide (Fifth Edition). November 2016 for the standard properties for biodiesel and diesel fuels.

The acid content plays an important role when evaluating the quality of biodiesel. It determines how stable the biodiesel can stay over a long period of time. The acid value is defined by the amount of KOH in mg needed to neutralize 1.0 g of free fatty acids [36]. The acid value of biodiesel produced from palm kernel oil and groundnut oil in this present study are 0.673 and 0.48 mg KOH g⁻¹ which was in good correlation with ASTM D 664 value of 0.5 mg KOH g⁻¹. The acid values of biodiesel from this experiment was also in a close range with values of 0.37 mg KOH g⁻¹, 1.2 mg KOH g⁻¹, and 0.8 mg KOH g⁻¹ of biodiesel produced from Shea butter, mango seed oil, and palm kernel oil respectively [26,28,32]. The values obtained in this study shows that the biodiesel is not corrosive. Iodine value is a measure of degree of unsaturation resulting from the formation of carbon to carbon bonds. It is defined as the mass of iodine that is added to 100.0 g of oil [28]. Low iodine value signifies presence of saturation and vice versa, saturated oil has resistance against oxidation and deterioration. The iodine value for every biodiesel set by EN 14112 is (7.5-8.6) g per100. In this present study, the iodine value obtained from the biodiesel produced from palm kernel oil and groundnut oil were 8.04 and 17.11. The palm kernel oil biodiesel was within the specified range but that of the groundnut oil

was slightly above the range. This shows that PKO biodiesel is a suitable alternative fuel for diesel engines based specifically on the measure of iodine value. The PKO biodiesel possess low oxidative resistance unlike that of groundnut oil, although iodine value of biodiesel from groundnut oil is technically on a good range when compared with results of 65.09 g per 100, 34.24 g per100, 36.00g per100 of biodiesel from PKO, Shea butter oil, and palm oil [32,28,33]. Peroxide value plays a vital role on stability of biodiesel during storage. It is defined by the amount of peroxide oxygen per 1.0 kg of biodiesel. Peroxide value is directly proportional to the rate of oxidation which is greatly influenced by the level of saturation of the biodiesel. In other words, biodiesel with high peroxide value will easily oxidize, thus increasing the rate of biodegradation as well reducing its stability [37]. The rate at which biodiesel undergo oxidation is controlled by certain factors like heat, amount of Oxygen, light, water content, and temperature. Excessive heat, light and high temperature enhances the rate of oxidation. In this present study 28.0 meq kg⁻¹ and 60.0 meq kg⁻¹ was recorded for biodiesel produced from palm kernel oil and groundnut oil, this shows that biodiesel produced from groundnut oil will easily degrade compare to that from PKO.

3.3. Modeling of Data generated from Trans-esterification experimental result

Several models were used to fit the experimental data from the groundnut oil and PKO biodiesel. They are linear, interaction, pure quadratic, quadratic, 3rd order polynomial and 4th order polynomials with their respective regression coefficients of 0.6694, 0.6695, 0.8981, 0.8982, 0.9213, and 0.9926 for groundnut oil, while PKO was 0.4914, 0.7162, 0.5042, 0.7712, 0.8666, and 0.9773 as shown in (Table 5). The F test was carried out by comparing the variances of each model with the experimental

results, it shows that each of the models is actually adequate because their calculated F values are less than the F critical based on 14 degrees of freedom for both the numerator and denominator. However, regression coefficient of a model should be more than or approximately equal to 0.95 [38-39]. Hence, the 4th order polynomial is obviously the most suitable for both oils. The equation of the 4th order polynomial for groundnut oil is at Equation 7. Using the 4th order polynomial for both groundnut and PKO, were generated at a constant temperature (Figure 2(a) to Figure 2 (d))

$$y_{model} = a_0 + a_1x_1 + a_2x_2 + a_3x_1^2 + a_4x_1x_2 + a_5x_2^2 + a_6x_1^3 + a_7x_1^2x_2 + a_8x_1x_2^2 + a_9x_2^3 + a_{10}x_1^4 + a_{11}x_1^3x_2 + a_{12}x_1^2x_2^2 + a_{13}x_1x_2^3 + a_{14}x_2^4 \quad (\text{Eq.7})$$

$$\text{where } a_0 = -1702; a_1 = 35.48; a_2 = 79.3; a_3 = 1292; a_4 = -47.97; a_5 = -0.8628; a_6 = -581.6; a_7 = -7.308; a_8 = 0.9442; a_9 = 0; a_{10} = -49.42; a_{11} = 14.72; a_{12} = -0.4235; a_{13} = 0; a_{14} = 0$$

While for PKO;

$$y_{model} = a_0 + a_1x_1 + a_2x_2 + a_3x_1^2 + a_4x_1x_2 + a_5x_2^2 + a_6x_1^3 + a_7x_1^2x_2 + a_8x_1x_2^2 + a_9x_2^3 + a_{10}x_1^4 + a_{11}x_1^3x_2 + a_{12}x_1^2x_2^2 + a_{13}x_1x_2^3 + a_{14}x_2^4 \quad (\text{Eq.7})$$

Table 5. Data generated for different models used

0	X1	X2	Y _{expt}	Y _{model} (1)	Y _{model} (2)	Y _{model} (3)	Y _{model} (4)	Y _{model} (5)	Y _{model} (6)
Groundnut oil									
1	0.25	50	96	106.3	106.9	102.2	87.43	92.51	98.79
2	0.25	55	95	98.3	98.3	94.4	91.65	90.49	91.22
3	0.25	60	50	90.3	89.7	85.9	70.26	62.91	50.98
4	0.5	50	92	96.4	96.8	98.7	94.15	94.91	87.37
5	0.5	55	98	88.4	88.4	90.9	98.54	99.95	103.3
6	0.5	60	95	80.4	80.0	82.3	77.34	79.41	94.35
7	1.0	50	74	76.6	76.7	84.4	90.58	83.92	75.63
8	1.0	55	89	68.6	68.6	76.6	95.34	96.11	89.70
9	1.0	60	89	60.6	60.6	68.1	74.51	82.71	86.66
10	1.5	50	74	56.9	56.5	60.7	64.36	57.64	74.81
11	1.5	55	72	48.9	48.9	52.9	69.48	67.73	67.99
12	1.5	60	38	40.9	41.2	44.4	49.02	52.19	41.19
13	2.0	50	16	37.1	36.4	27.6	15.48	23.02	15.38
14	2.0	55	22	29.1	29.1	19.7	20.98	21.73	23.81
15	2.0	60	0	21.1	21.8	11.2	0.874	-5.21	-1.19
R ²				0.6694	0.6695	0.8981	0.8982	0.9213	0.9926
F				1.4939	1.4939	1.2561	1.1133	1.0854	1.0075

F CRITICAL = 2.4837

PKO									
1	0.25	50	76	65.38	83.02	61.91	76.30	77.40	72.593
2	0.25	55	50	73.58	73.58	69.59	77.06	62.36	53.121
3	0.25	60	66	81.78	64.14	77.99	57.42	57.89	66.286
4	0.5	50	82	59.26	71.39	59.86	68.33	77.25	89.138
5	0.5	55	84	67.46	67.46	67.54	74.61	72.91	77.801
6	0.5	60	66	75.66	63.53	75.94	60.48	69.46	65.061
7	1.0	50	54	47.02	48.13	51.68	48.69	51.58	47.491
8	1.0	55	68	55.22	55.22	59.35	65.99	68.28	72.941
9	1.0	60	52	63.42	62.32	67.76	62.88	66.52	53.368
10	1.5	50	0	34.79	24.87	38.03	24.10	14.18	3.5282
11	1.5	55	62	42.99	42.99	45.71	52.43	51.47	59.789
12	1.5	60	62	51.99	61.11	54.11	60.35	50.92	60.682
13	2.0	50	0	22.55	1.61	18.93	-5.43	-8.41	-0.7502
14	2.0	55	40	30.75	30.75	26.60	33.92	48.99	40.347
15	2.0	60	48	38.95	59.89	35.01	52.87	49.19	48.407
R ²				0.4914	0.7162	0.5042	0.7712	0.8666	0.9773
F				2.0352	1.3962	1.9834	1.2966	1.1539	1.0232

F CRITICAL = 2.4837

(1)=linear i.e. $a_0+a_1x_1+a_2x_2$
 (2)=interaction i.e. $a_0+a_1x_1+a_2x_2+a_3x_1x_2$
 (3)=pure quadratic i.e. $a_0+a_1x_1^2+a_2x_2^2$
 (4)=quadratic i.e. $a_0+a_1x_1+a_2x_2+a_3x_1^2+a_4x_1x_2+a_5x_2^2$
 (5)=3rd order polynomial i.e. $a_0+a_1x_1+a_2x_2+a_3x_1^2+a_4x_1x_2+a_5x_2^2+a_6x_1^3+a_7x_1^2x_2+a_8x_1x_2^2+a_9x_2^3$
 (6)= 4th order polynomial i.e. $a_0+...$
 X1=catalyst concentration as a percentage of weight of sample
 X2=transesterification temperature(°C)
 Y_EXPT=Yield from experiment (ml)

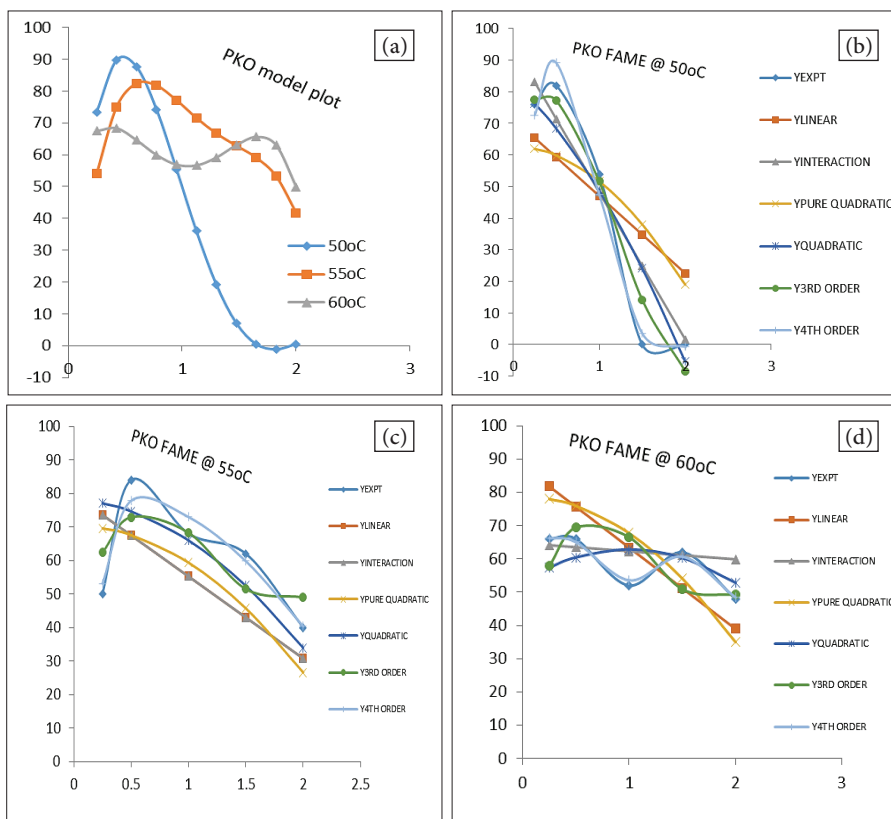


Fig. 2. (a) Varying catalyst concentration at constant temperature for PKO base FAME and comparison of the different groundnut oil base FAME models with the experimental data at (b) 50°C (c) 55°C (d) 60°C

3.4. Optimization of parameters

The main aim of optimization is to obtain the process parameter which gives the maximum FAME yield. This was done using different techniques namely: MATLAB optimization toolbox and response surface methodology (RSM)

3.4.1. MATLAB optimization toolbox

This optimization toolbox uses the principle of NEWTON RAPHSON's method of multivariable optimization technique. Firstly, a function was created in a function M-file as given below for groundnut oil and PKO base FAMES respectively.

Function f = projopt1(x)

$$f = -(-1702 + 35.48 * x(1) + 79.3 * x(2) + 1292 * x(1).^2 - 47.97 * x(1) .* x(2) - 0.8628 * x(2).^2 - 581.6 * x(1).^3 + 7.308 * x(1).^2 .* x(2) + 0.9442 * x(1) .* x(2).^2 - 49.42 * x(1).^4 + 14.72 * x(1).^3 .* x(2) + 0.4235 * x(1).^2 .* x(2).^2);$$

Function f = pkoopt(x)

$$f = -(4261 - 9215 * x(1) - 160.1 * x(2) + 1465 * x(1).^2 + 378.5 * x(1) .* x(2) + 1.498 * x(2).^2 + 874.3 * x(1).^3 - 108.5 * x(1).^2 .* x(2) - 3.709 * x(1) .* x(2).^2 - 56.99 * x(1).^4 - 10.67 * x(1).^3 .* x(2) + 1.315 * x(1).^2$$

$$.* x(2).^2);$$

Notice however that negative of the function was minimized, as this gives the negative of the maximum value of the function. Next, a program was written to minimize the functions respectively using the “fmincon” command as below table.

<code>x0 = [0.25 50]; A = [1 1]; B = 62; lb = [0.25 50]; ub = [2 60];</code>
<code>[x fval] = fmincon (@projopt1, x0, A, B, ,lb,ub)</code>
<code>x0 = [2 60]; A = [1 1]; B = 62; lb = [0.25 50]; ub = [2 60];</code>
<code>[x fval] = fmincon (@pkoopt,x0,A,B, lb,ub)</code>

The optimum/maximum value for groundnut oil FAME yield was obtained as 100.5141 with the corresponding independent variables (X_1 , X_2) of (0.25, 51.3463). On the other hand, the optimum/maximum value for PKO FAME yield was gotten as 90.7254 with the corresponding independent variables (X_1 , X_2) of (0.4843, 50).

3.4.2. MATLAB response surface methodology

The surface plots with the contour of the groundnut oil and PKO FAME model were plotted as indicated in Figure 3.

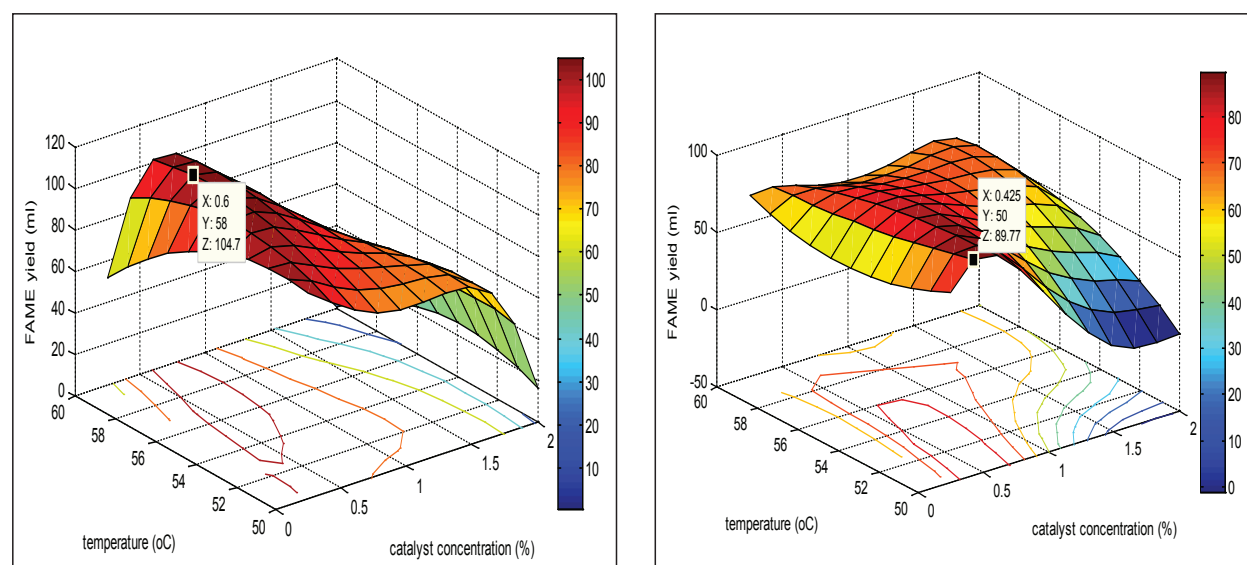


Fig. 3. Surface plot of the groundnut oil and PKO base FAME showing the optimal points

4. Conclusion

The results obtained from this present study showed that the optimum reaction conditions for the production of biodiesel from groundnut oil and palm kernel oil was obtained at a trans-esterification temperature of 55°C, 0.5 % w/v of CH₃ONa catalyst, mixing rate of 360 rpm and a reaction time of 90 minutes. At these conditions, an optimum yield of 98% and 84% by volume of FAME from groundnut and palm kernel oil was obtained. The biodiesel produced in this present study was characterized for fuel properties, and it gave good promising results; except for the pour points of biodiesel produced from palm kernel oil was found to be somewhat higher, which may point to potential difficulties in cold starts and filter plugging trouble. But however, the biodiesel from this experiment would be a better means in harnessing the supply of energy to the global economy as compared to mineral diesel. The 4th order polynomial model showed a good agreement with the experimental results, demonstrating that these methodologies were useful for modelling. Newton Raphson's multivariable optimization technique gave an optimum yield of 100.5 mL and 90.7 mL for groundnut oil and PKO FAME with a corresponding catalyst concentration and trans-esterification temperatures of (0.25%, 0.48%) and (51.3°C, 50°C). While the surface plots gave optimum yields of 104.8 mL and 89.8 mL with the catalyst concentration and trans-esterification temperatures of (0.6%, 0.425%) and (58°C, 50°C) for groundnut oil and Palm Kernel Oil (PKO) based Fatty Acid Methyl Esters (FAME). The findings obtained from this study showed that the Newton Raphson's multivariable optimization technique and Response Surface Methodology (RSM) were useful in enhancing the process parameters of the trans-esterification reaction.

5. Conflict of interest and Abbreviations

No conflict of interest to declare.

FAME: *Fatty Acid Methyl Ester*; PKO: *Palm Kernel Oil*; ASTM: *American Society of Testing and Materials*; KOH: *Potassium Hydroxide*; NaOH: *Sodium Hydroxide*; CH₃OH: *Methanol*; H₂SO₄: *Sulphuric Acid*; RSM: *Response Surface*

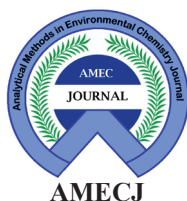
Methodology; FFA: *Free Fatty Acid*; CH₃ONa: *Sodium Methoxide*.

6. References

- [1] O.J. Adamu, T.A. Akintola, C. C. Enweremmadu, A.E. Adeleke, Characterization of palm-kernel oil biodiesel produced through NaCH-Catalysed trans-esterification process, *Sci. Res. Essay*, 3 (2008) 308-311. <http://www.academicjournals.org/SRE>
- [2] BP Energy Outlook 2035, BP PLC, 2016. <https://www.bp.com/content/dam/bp/pdf/energy-economics/energy-outlook-2016/bp-energy-outlook-2016>.
- [3] P.A. Owusu, S.A. Sarkodie, S. Dubey, A review of renewable energy sources, sustainability issues and climate change mitigation, *J. Cogent Eng.*, 3 (2016) 93-109. <https://doi.org/10.1080/23311916.2016.1167990>
- [4] D.P. Ho, H.H. Ngo, W. Guo, A mini review on renewable sources for biofuel, *Bioresour. Technol.*, 169 (2014) 742–749. <https://doi.org/10.1016/j.biortech.2014.07.022>
- [5] R. Gilbert, A. Perl, Transport oil. Earth scan, UK, 2008. <http://www.richardgilbert.ca/Files/2008/Summary%20of%20Transport%20Revolutions%204.pdf>
- [6] K. Bozbas, Biodiesel as an alternative motor fuel, production and policies in the European Union, *Renew. Sust. Energ. Rev.*, 12 (2008) 542-552. <https://doi.org/10.1016/j.rser.2005.06.001>
- [7] E.M. Shahid, Y. Jamal, Production of biodiesel: a technical review, *Renew. Sust. Energ. Rev.*, 15 (2011) 4732–4745. <https://doi.org/10.1016/j.rser.2011.07.079>
- [8] H. Fukuda, A. Kondo, H. Noda, Biodiesel fuel production by trans-esterification of oils: review, *J. Biosci. Bioeng.*, 92 (2001) 405–16. <https://doi.org/10.1263/jbb.92.405>
- [9] A. Demirbas, Importance of biodiesel as transportation fuels, *Energ. Policy*, 35 (2007) 4661–4670. <https://doi.org/10.1016/j.enpol.2007.04.003>
- [10] J. Orsavova, L. Misurcova J.V. Ambrozova, R.

- Vicha, J. Mlcek, Fatty acids composition of vegetable oils and Its contribution to dietary energy intake and dependence of cardiovascular mortality on dietary intake of fatty acids, *Int. J. Mol. Sci.*, 16 (2015) 12871-12890. <https://doi.org/10.3390/ijms160612871>.
- [11] A.W. Verla, C.E. Enyoh, F.C. Ibe, E.N. Verla, Status of liquid biofuels in Nigeria and tools for environmental sustainability assessment, *Int. J. Energ. Water Res.*, 3(4) (2020) 113-128. <https://doi.org/10.1007/s42108-020-00080-7>
- [12] C. E. Enyoh, A. W. Verla, E. C. Enyoh, E. N. Verla, A Review on the quality of palm oil (*Elaeis guineensis*) produced locally in Imo State, Nigeria, *Sustain. Food Prod.*, 4 (2018) 40-50. <https://doi.org/10.18052/www.scipress.com/SFP.4.40>
- [13] S. Nasreen, M. Nafees, L. A. Qureshi, M. S. Asad, A. Sadiq, S. D. Ali, Review of catalytic trans-esterification methods for biodiesel production, biofuels - state of development, Krzysztof Biernat, Chapter 6, Intech Open, 2018. <https://doi.org/10.5772/intechopen.75534>
- [14] O.J. Alamu, M.A. Waheed, S.O. Jekayinfa, Biodiesel production from Nigerian palm Kernel oil: effect of KOH concentration on yield, *Energ. Sust. Dev.*, 11 (2007) 77-82. [https://doi.org/10.1016/S0973-0826\(08\)60579-7](https://doi.org/10.1016/S0973-0826(08)60579-7)
- [15] C.E. Enyoh, B.O. Isiuku, Determination and human health risk assessment of heavy metals in floodbasin soils in Owerri, southeastern Nigeria, *Chem. Africa*, 5(3) (2020) 86-100. <https://doi.org/10.1007/s42250-020-00171-2>
- [16] A. Vonortas, N. Papayannakos, Comparative analysis of biodiesel versus green diesel, *Wiley Interdiscip. Rev. Energ. Environ.*, 3 (2014) 3-23. <https://doi.org/10.1002/wene.78>
- [17] J.C. Juan, D.A. Kartika, T.Y. Wu, Biodiesel production from jatropha oil by catalytic and non-catalytic approaches: an overview, *Bioresour. Technol.*, 102 (2011) 452-460. <https://doi.org/10.1016/j.biortech.2010.09.093>
- [18] O. Ogunkunle, O.O. Oniya, A.O. Adebayo, Yield response of biodiesel production from heterogeneous and homogeneous catalysis of milk bush seed (*Thevetia peruviana*) oil, *J. Energ. Policy Res.*, 4 (2017) 21-28. <https://doi.org/10.1080/23815639.2017.1319772>
- [19] M.Z. Kyari, M.M. Yunus, Optimization of trans-esterification of *Lophira lanceolata* (False Shea) seed oil to alkyl ester using response surface methodology, *Nigerian J. Chem. Res.*, 22 (2017) 88-94. <https://www.ajol.info/index.php/njcr/article/view/170990>
- [20] J.K. Efavi, A. Yaya, The Effect of NaOH catalyst concentration and extraction time on the yield and properties of *Citrullus vulgaris* seed oil as a potential biodiesel feed stock, *South African J. Chem. Eng.*, 25 (2018) 98-102. <https://doi.org/10.1016/j.sajce.2018.03.002>
- [21] M.A. Obianke, A.B. Mohammed, L.G. Hassan, A.A. Aliero, M.G. Liman, Optimization of reaction variables in situ trans-esterification of *Jatropha curcas* seed oil for biodiesel production, *Nigeria J. Basic Appl. Sci.*, 26 (2018) 102-114. <https://doi.org/10.4314/njbas.v26i2.15>
- [22] O.J. Alamu, M.A. Waheed, S.O. Jekayinfa, T.A. Akintola, Optimal trans-esterification duration for biodiesel production from Nigerian palm kernel oil, *Agri. Eng. Int. (CIGR)*, 9 (2007) 1-12. <https://cigrjournal.org/>
- [23] S. Athalye, S.R. Sharma, S. Peretti, Producing biodiesel from cottonseed oil using *Rhizopus oryzae* whole cell biocatalysts: culture media and cultivation period optimization, *Energ. Sust. Dev.*, 17 (2013) 331-336. <https://ui.adsabs.harvard.edu/abs/2012PhDT.....278A/abstract>
- [24] S. N. Naik, V.V. Goud, P.K. Rout, Production of first- and second-generation biofuels: a comprehensive review, *Renew Sust. Energ. Rev.*, 14 (2010) 578-597. <https://doi.org/10.1016/j.rser.2009.10.003>
- [25] E. C. Enyoh, C.E. Enyoh, C. E. Amaobi, Quality assessment of palm oil from different palm oil local factories in Imo State, Nigeria, *World Sci. News*, 88 (2017) 152-167. <http://www.worldscientificnews.com/wp-content/uploads/2017/08/WSN-882-2017-152-167.pdf>

- [26] J.O. Igbokwe, M.O. Nwafor, Synthesis and characterization of biodiesel from Nigerian palm kernel oil, *Am. J. Eng. Res.*, 3 (2014) 264-266. [https://www.ajer.org/papers/v3\(3\)/ZI33264266.pdf](https://www.ajer.org/papers/v3(3)/ZI33264266.pdf)
- [27] U. Musa, I.A. Mohammed, A.M. Sadi, M. Aliyu, B. Suleiman, S. Tasabi, Production and characterization of biodiesel from Nigerian mango seed oil, *World Congress on Engineering(WCE)*, 1 (2014) 645-649. http://www.iaeng.org/publication/WCE2014/WCE2014_pp645-649.pdf (2014).
- [28] Y. Datti, M. Ibrahim, I. Salihu, M. Abdulahi, S. Muhammad, A.S. Ado, U.U. Ahmad, Extraction, production and characterization of biodiesel from shea butter (*Vitellaria paradoxa* C.F. Gaertri) obtained from Hadejia, Jigawa State Nigeria, *J. Biol. Pharm. Sci.*, 11 (2020) 208-215. <https://doi.org/10.30574/gscbps.2020.11.3.0168>
- [29] J.V. Gerpen, B. Shank, R. Pruszko, D. Clement, G Knothe, Biodiesel production technology, national renewable energy laboratory 1617 Cole Boulevard, Golden, Colorado, 1-100, 2004. <https://www.nrel.gov/docs/fy04osti/36244.pdf>
- [30] S.J. Ojolo, A.O. Adelaja, G.M. Sabamowo, Production of biodiesel from palm kernel oil and Groundnut oil, *Adv. Mater. Res.*, 367 (2012) 501-506. <https://doi.org/10.4028/www.scientific.net/AMR.367.501>
- [31] P. Blomquist, F. Evergreen, O. Wellstrand, M. Avidson, Preliminary study of protection against fire in low-flash point fuel, Science partner report SP technical research institute of Sweden, 1-5, 2015. <http://www.diva-portal.org/smash/get/diva2:962918/FULLTEXT01.pdf>
- [32] E.I. Bello, B. Oguntuase, A. Osasona, T.I. Mohammed, Characterization and engine testing of palm kernel oil biodiesel. *Eur. J. Eng. Technol.*, 3 (2015) 1-8. <https://www.idpublications.org/wp-content/uploads/2015/02/Characterization-and-Engine-Testing-of-Palm-Kernel-Oil-Biodiesel.pdf>
- [33] A.A. Ayoola, P.A.Y. Arawe, M.E. Ojerumi, R.Y. Amaraibi, Comparison of the properties of palm oil and palm kernel oil biodiesel in relation to the degree of unsaturation of their oil feedstock, *Int. J. Appl. Nat. Sci.*, 5 (2016) 1-8. <https://core.ac.uk/download/pdf/95550242.pdf>
- [34] S.O. Kareem, Enzymatic biodiesel production from palm oil and palm kernel oil using free lipase, *Egypt. J. Pet.*, 26 (2017) 635-642. <https://doi.org/10.1016/j.ejpe.2016.09.002>
- [35] C.N. Ibeto, A.U. Ofoefule, H.C. Ezugwu, Analytic methods for quality assessment of biodiesel from animal and vegetable oil, *Trend Appl. Sci. Res.*, 6 (2011) 537-553. <https://doi.org/10.3923/tasr.2011.537.553>
- [36] B.M.W. Amo-Tanta, A.O. Onigbinde, Physicochemical properties and fatty acid profile of crude oil extract from three vegetable seed, *Pak. J. Nutr.*, 12 (2013) 647-650. <https://www.researchgate.net/profile/Bamidele-Amos-Tautua/publication/>
- [37] J.K. Ikaya, L.N. Umeigar, A. Lobee, Effect of extraction methods on the yield and quality characteristics of oil and nut, *J. Food Res. Sci.*, 2 (2013) 5-10. <https://doi.org/10.3923/jfrs.2013.1.12>
- [38] S.Yahaya, S.O. Giwa, M. Ibrahim, Extraction of oil from *Jatropha* seed kernels: optimization and characterization, *Int. J. Chem. Tech. Res.*, 9 (2016) 758-770. [https://www.sphinxσαι.com/2016/ch_vol9_no5/abstracts/A\(758-770\)V9N5CT.pdf](https://www.sphinxσαι.com/2016/ch_vol9_no5/abstracts/A(758-770)V9N5CT.pdf)
- [39] C.E. Enyoh, A.W. Verla, C.E. Duru, E.E. Enyoh, B. Setiawan, Curve estimation modeling for predictions of the novel coronavirus (Covid-19) epidemic in Nigeria, *Healthy-Mu J.*, 4 (2020) 1-35. <https://doi.org/10.35747/hmj.v4i1.545>.
- [40] C.E. Enyoh, Q. Wang, O. Prosper, Response surface methodology for modeling the adsorptive uptake of phenol from aqueous solution using adsorbent polyethylene terephthalate Microplastics. *Chem. Eng. J. Adv.*, 12 (2022) 100370. <https://doi.org/10.1016/j.cej.2022.100370>



Determination of cadmium in rice samples using amino-functionalized metal-organic framework by a pipette tip solid phase extraction

Mohammad Abbaszadeh^a, Ali Miri^a, and Mohammad Reza Rezaei Kahkha^{a,*}

^aDepartment of Environmental Health Engineering, Faculty of Health, Zabol University of Medical Sciences, Zabol, Iran

ARTICLE INFO:

Received 21 May 2022

Revised form 2 Aug 2022

Accepted 28 Aug 2022

Available online 29 Sep 2022

Keywords:

Cadmium,
Amino functionalized metal-organic framework,
Pipette tip extraction,
Rice samples,
Atomic adsorption spectrometer

ABSTRACT

In this study, the amino-functionalized metal-organic framework (NH₂-MOFs) was used as an adsorbent for the extraction of cadmium in rice samples based on the pipette tip solid phase extraction (PT-SPE) before determined by the flame absorption spectrometry (F-AAS). The pH of the sample solution, initial concentration of the cadmium, the volume of the sample, elution conditions, and the amount of adsorbent on the recovery of the cadmium were investigated and optimized. The results showed that the best extraction efficiency of cadmium was obtained at pH 5.0, 2500.0 μL of cadmium solution, and 20.0 μL of HCl (10% V/V) as eluent solvent. First, the cooking rice was transferred to a beaker and hydrochloric acid/nitric acid was added to it as a digestion process before analysis by the PT-SPE procedure. The limit of detection of this method was found to be 0.03 μg L⁻¹ with a relative standard deviation of ≤ 2.5 % (for seven replicate analyses of 50 μg L⁻¹ of cadmium). The linear and dynamic ranges were achieved at 0.3 -14.5 μg L⁻¹ and 0.3 -150 μg L⁻¹, respectively. The adsorption capacity of sorbent and enrichment factor was 175 mg g⁻¹ and 125 folds, respectively. The proposed method was successfully applied for the determination of cadmium in rice samples.

1. Introduction

Pollution of foods with heavy metals (HMs) is a serious problem for public health and the community due to its toxicity and carcinogenicity. Therefore, monitoring and controlling the amount of HMs in food samples is critical. Cadmium is one of the most dangerous HMs that enters food samples from various sources, including mining, industrial production and other ways such as agricultural runoff [1]. According to the US Environmental Protection Agency, the maximum acceptable level of cadmium in rice and wheat is 200 μg. kg⁻¹ [2]. On the other hand, the accumulation of cadmium

ions in food samples such as rice, wheat, and other species is unavoidable[3]. In these food samples, the effect of matrices is a serious problem for its measuring because of the low concentration of cadmium, therefore, a preconcentration technique is necessary before quantification[4]. Various techniques have been applied for this purpose such as dispersive liquid- liquid microextraction [5], cloud point extraction [6] and solid phase extraction (SPE) [7]. The pipette tip (PT), a micro-scale format of SPE, that used for the preconcentration and extraction of various samples[8]. Using a small amount of sorbent (insert into a pipette tip) and low solvent consumption without a special auxiliary device is the advantage of PT-SPE compared to conventional SPE cartridges [9,10].

*Corresponding Author: M. R. Rezaei Kahkha

Email: m.r.rezaei.k@gmail.com

<https://doi.org/10.24200/amecj.v5.i03.208>

Recently PT-SPE was applied for the determination and extraction of several analytes in food samples such as bisphenol a [11], estradiol in milk [12], and antibiotic residues Metal-organic frameworks (MOFs) are a new class of hybrid porous materials consisting of organic linkers coordinated to inorganic metal nodes that are used in solid phase extraction because of their thermal and chemical stability[14]. Recently, several adsorbents such as silica nanoparticles [15], molecularly imprinted polymer [16], and other sorbents were applied for determination of cadmium in food samples[17]. Hence, based on the above remarks and our research interest in applications of porous materials [18-21]we utilized the highly stable amino functionalized metal organic framework (Fig. 1) for the determination and extraction of cadmium in imported rice samples. Many other papers were presented about extraction methods by previous researchers [22-24]. Parameters affecting PT-SPE were studied and optimized. To the best of our knowledge, the MOF with the properties mentioned above was applied for the first time as a solid phase sorbent in a pipette-tip microextraction mode.

2. Material and methods

2.1. Reagents and instrument

All reagents and solutions were analytical grades. Methyl 4-formylbenzoate (CAS N: 1571-080, Sigma, Germany), pyrrole (CAS N: 109-97-7, pH >6, Merck), the trifluoroacetic acid (CAS N: 76-05-1, EC Number 200-929-3, TFA) from Sigma-Aldrich, propionic acid (CAS N: 79-09-4, MW: 74.08, Sigma-Aldrich), ZrOCl₂•8H₂O (CAS N.: 13520-92-8, 98%, Sigma-Aldrich), 1000 mg.L⁻¹ standard solution of cadmium (CAS N: 7440-43-9 Sharlou, Spain), *N,N'*-dimethylformamide (CAS N: 68-12-2, DMF), benzoic acid (>98%, CAS N: 65-85-0; EC N: 200-618-2, Sigma), acetone (≥99.5%; CAS N: 67-64-1, Sigma, Germany), tetrahydrofuran (THF, CAS N: 109-99-9 EC N: 203-726-8, Sigma), methanol (CAS N: 67-56-1), and KOH (CAS N: 1310-58-3, Sigma, Germany) were purchased from commercial sources and used as received. The flame atomic absorption spectrometer based on a double beam spectrophotometer (FAAS, AA7800, Shimadzu, Japan) was used for cadmium detection. The mixture of C₂H₂ gas and the D₂ was tuned for the cadmium determination by FAAS.

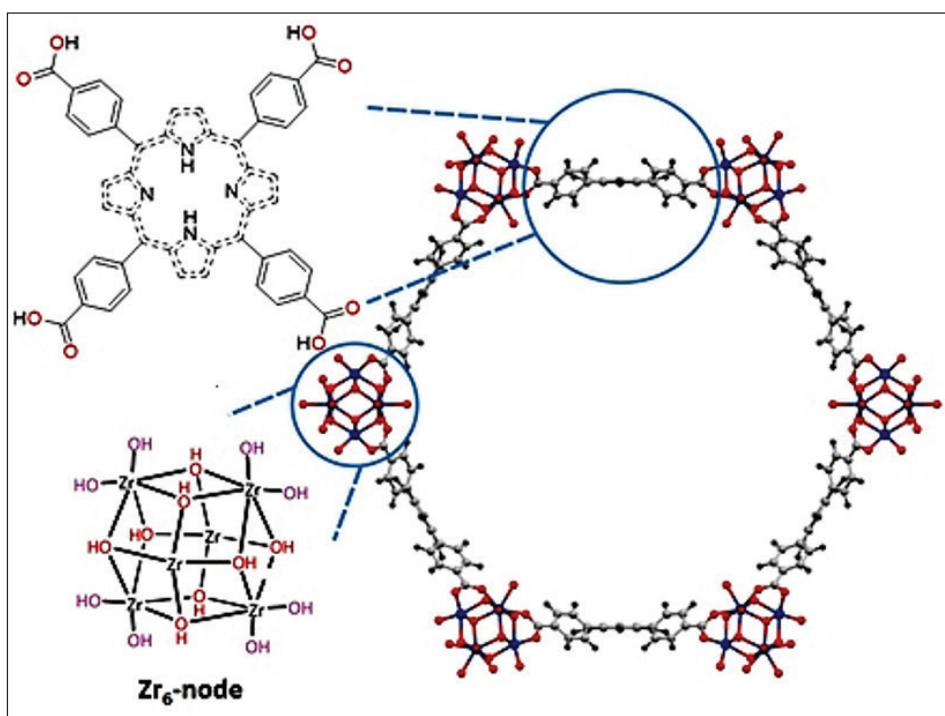


Fig.1. A schematic of amino functionalized MOF.

2.2. Synthesis of amino-functionalized metal-organic framework

The sorbent was synthesized in a similar way that we have previously reported [25]. Briefly, 200 mg of $\text{ZrOCl}_2 \cdot 8\text{H}_2\text{O}$, 3.0 g of benzoic acid, and 20 mL of DMF were added into a 30-mL vial (solution A); and in other 30- mL vial, 100 mg of H_2TCPP and 20 mL of DMF were added (solution B). Both solutions A and B were sonicated for 30 min and then incubated at 100 °C in an oven for 1 h. Next, 1 mL of A solution, 1 mL of B solution, and 0.05 mL of trifluoroacetic acid were added and mixed by swirling for 5 s. The vials were then incubated and immersed in an oven at 120 °C for 30 h. A dark purple precipitate started to form in the vials. After cooling to room temperature, the suspension was transferred into a centrifuge tube and centrifuged for 5 min (7500 rpm) to remove the supernatant. The solid was washed with fresh DMF (3×30 mL) before soaking in 40 mL of fresh DMF and 1.5 mL of 8 M HCl (activation with HCl). It was then heated at 120 °C for 12 h to remove the benzoic acid. The sample was subsequently washed with fresh DMF (3×30 mL), THF (3×30 mL), and acetone (3×30 mL). After soaking in acetone overnight, the solid was collected, and then dried in a vacuum oven

at 120 °C for 12 h to give the MOF. SEM of the amino-functionalized metal-organic framework is seen in Figure 2.

2.3. Pipette-tip extraction procedure

Appropriate amounts of sorbent were inserted into a pipette-tip (DRAGON, China) which was then attached to a 5000 μL micro pipette (DRAGONLAB, China). Then 2500 μL of the aqueous sample was withdrawn into the sorbent and dispensed back into the same tube for 20 cycles. Elution was performed by 20 μL of 10% HCl into a 1-mL vial. The desorption step was also performed by 20 aspirating/dispensing cycles. The extraction recovery of cadmium was calculated by comparing the absorbance of 50 $\mu\text{g L}^{-1}$ of cadmium standard solution by results of optimization experiments (Fig.3).

3. Results and discussion

3.1. Optimization of affecting parameter on the extraction procedure

To optimize the extraction conditions, parameters affecting extraction were optimized as below. All optimizations were performed on a 50 $\mu\text{g L}^{-1}$ of cadmium solution, made by diluting of 1000 mg L^{-1} standard solution.

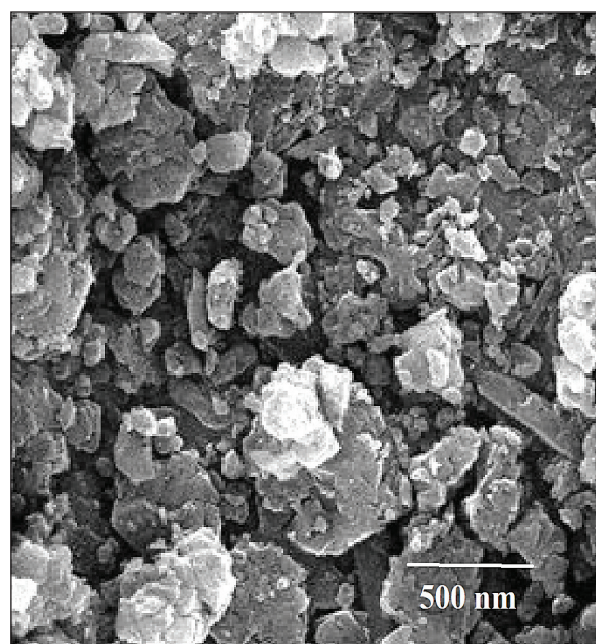
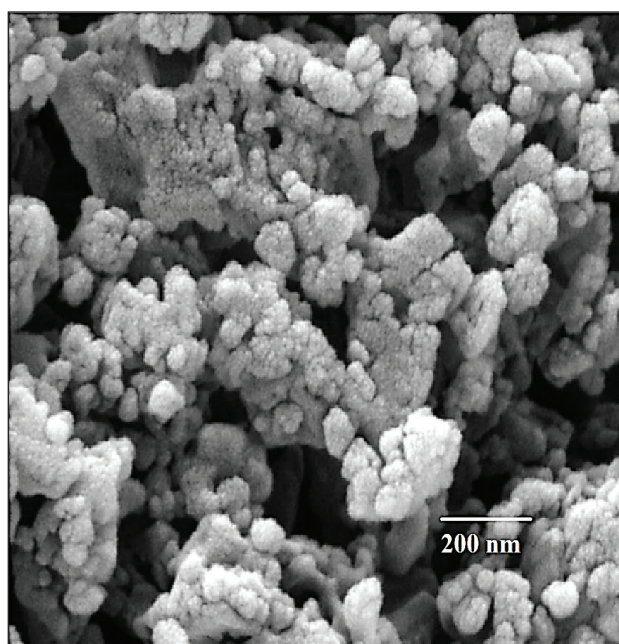


Fig.2. SEM images of synthesized NH_2 -MOFs

3.1.1. Effect of pH

The effect of sample pH on the extraction efficiency of cadmium was investigated by adjusting pH of it between 2.0 and 9.0. Either 0.1 M NaOH or 0.1 M HCl was used. As depicted in Figure 4, a solution with the pH values between 4.0 and 6.0 showed the highest

extraction efficiency (optimal pH = 5). In alkaline media, produced hydroxide ions can form a complex with cadmium ions, and a precipitation ($\text{Cd}(\text{OH})_2$) is created. Results showed that the extraction efficiency of cadmium based on NH₂-MOFs was decreased. So, pH 5.0 was selected as the optimum value.

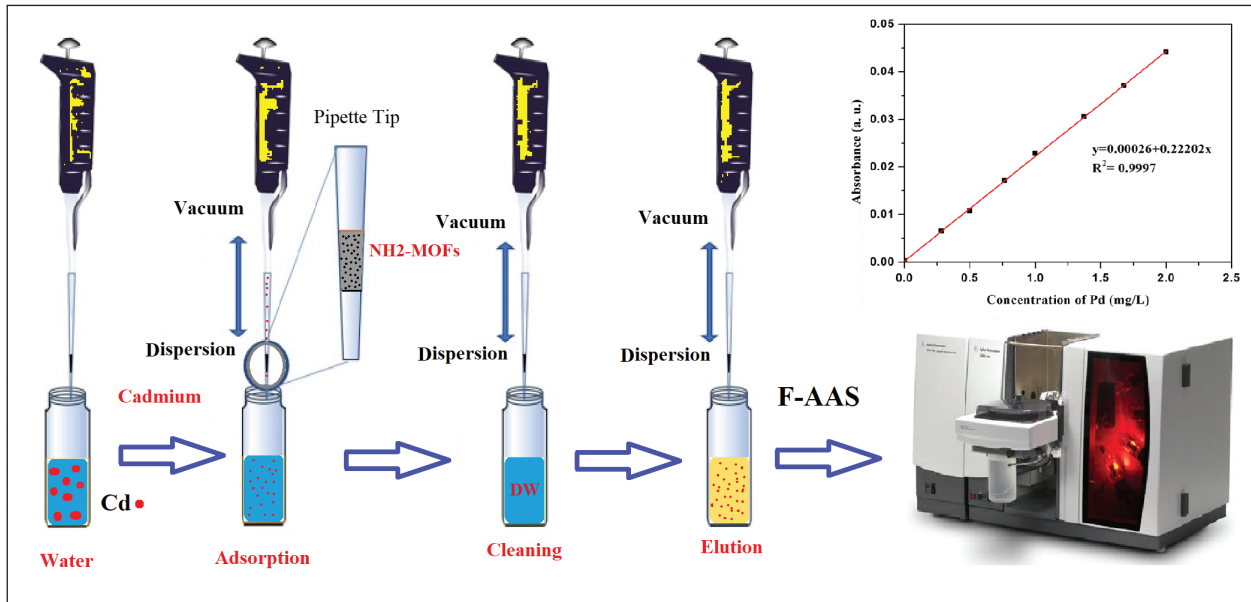


Fig. 3. Cadmium extraction based on NH₂-MOFs adsorbent and Pipette-tip- SPE procedure

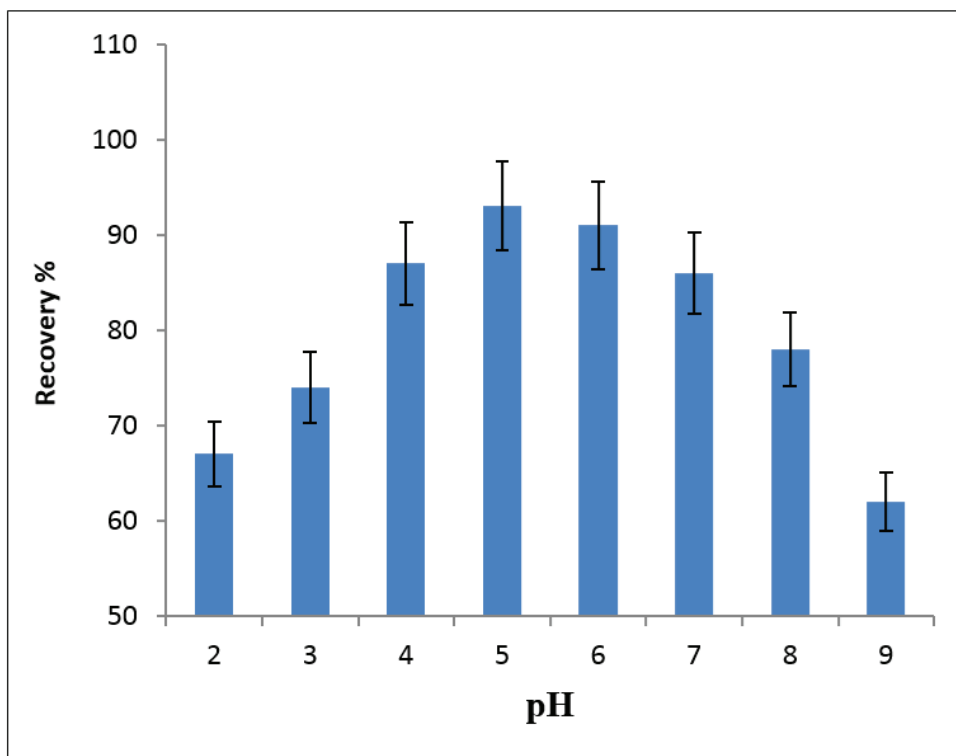


Fig. 4. Effect of pH on recovery of cadmium

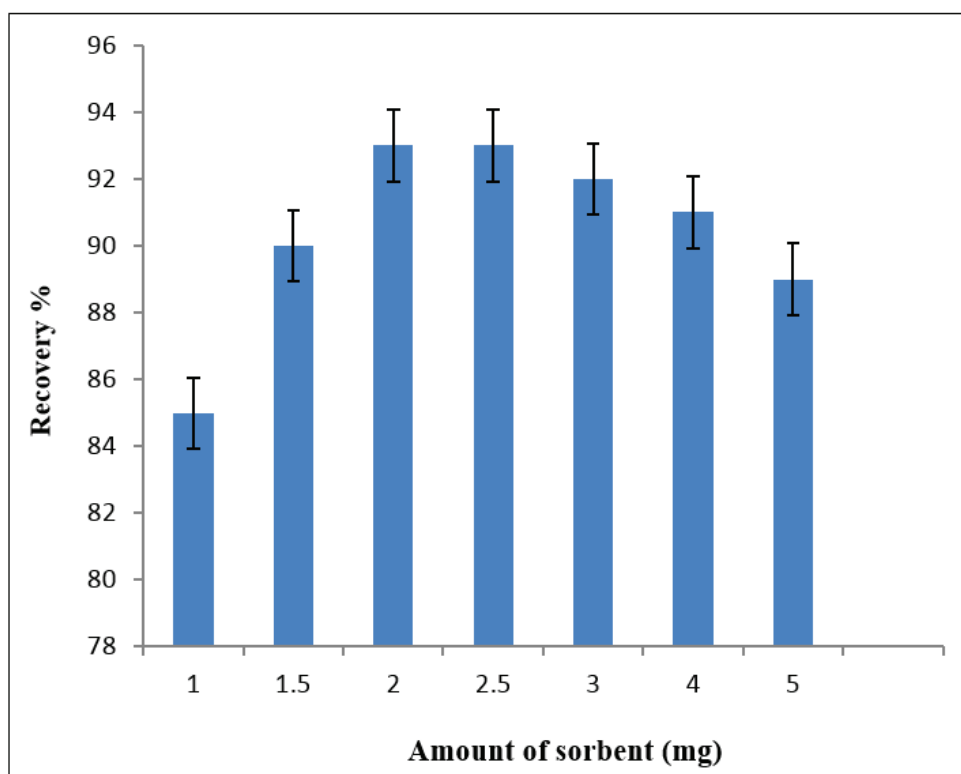


Fig. 5. Effect of amount of sorbent on recovery of cadmium.

3.1.2. Effect of amount of sorbent

To obtain the best extraction efficiency and good recoveries of cadmium ions, the amount of sorbent was examined between 1-5 mg. The adsorption ability of the adsorbent was increased by increasing the amount of sorbent up to 2 mg; therefore, the optimum amount of 2 mg was chosen (Fig. 5).

3.1.3. Effect of volume of the eluting solvent

Several strong acidic solvents including different concentrations of HNO_3 (2-10% V/V) and HCl (2-10% V/V) were studied to select an optimized eluting solvent. Among them HCl 10% showed the highest extraction efficiency for cadmium ions. To achieve the highest enrichment factor, we tried to obtain the smallest HCl volume of 10%. Volumes between 5 to 50 μL of HCl 10% were examined for the extraction of 1000 μL of a standard solution containing 50 $\mu\text{g L}^{-1}$ of the cadmium in deionized water. As shown in Figure 6, at the volume of 20 μL of the eluting solvent, the recovery of cadmium is at its highest value.

Therefore, the eluting volume of 20 μL was selected for further experiments.

3.1.4. Effect of volume of sample solution

Amount of sample solution taken for the analysis is an important parameter in solid phase extraction [5]. Different volumes of sample solution were tested at the range of 200 to 4000 μL containing 50 $\mu\text{g L}^{-1}$ of cadmium. As can be seen in Figure 7, the extraction recovery of cadmium increased with the increase of the volume up to 2500 μL . So, the extraction efficiency (more than 95%) and a preconcentration factor of 125 for cadmium extraction were achieved based on 20 μL of eluent with the PT-SPE procedure before determination by the F-AAS.

3.1.5. Effect of number of aspirating/dispensing of sample and elution solvent

The number of aspirating/dispensing cycles of eluent solvent and the volume of solution that passed through the extractor resembles the extraction time. The results showed the highest recoveries

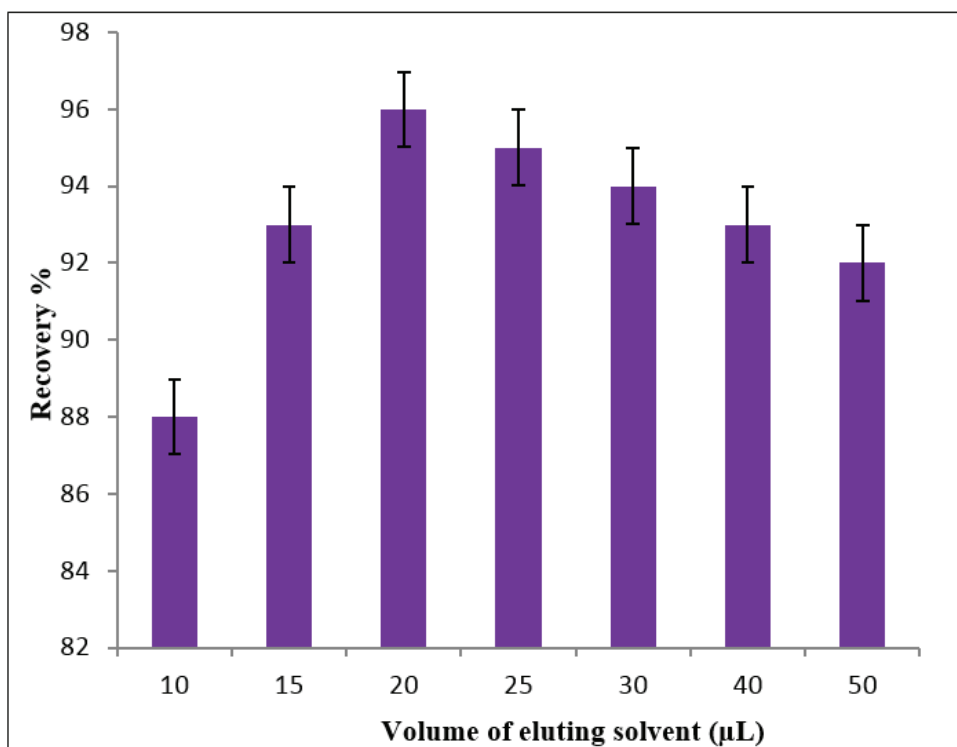


Fig. 6. Effect of volume of eluting solvent (HCl 10%) on recovery of cadmium

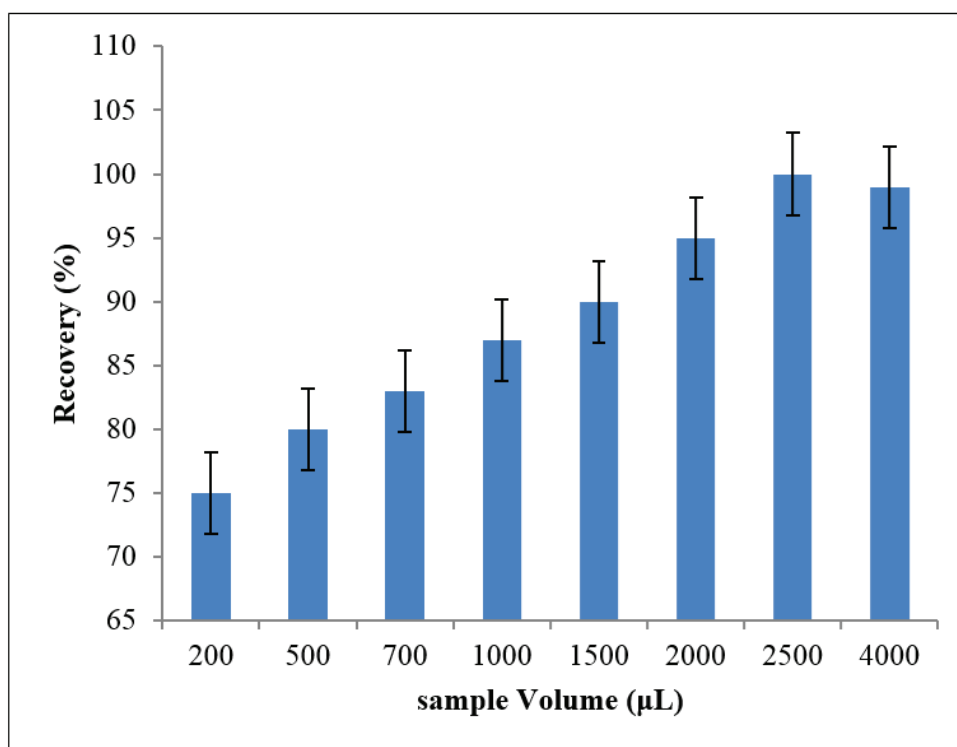


Fig. 7. Effect of sample volume on recovery of cadmium

for cadmium obtained at 20 cycles, when 2500 μL of a sample containing 50 $\mu\text{g L}^{-1}$ of the standard solution was used. During desorption, the analyte was eluted from the extractor into a 2.0 mL glass test tube by repetitive aspirating/dispensing of 20 μL of the HCl 10% (V/V) through the tip. The optimal number of aspirating/dispensing cycles for desorption of adsorbed analytes (provided the highest recovery) was found to be 20 cycles at 12min.

3.1.6. Reusability of the adsorbent

The reusability of the sorbent was investigated by washing of the column with HCl 10% V/V and then five cycles with deionized water. After that, several extraction and elution operation cycles were carried out under the optimized conditions. The results indicated that the amino functionalized MOF could be regenerated and reused at least ten times without significantly decreasing extraction recoveries.

3.1.7. Sorption capacity

To investigate of the adsorption capacity of the functionalized MOF, a standard solution containing 100 mg L^{-1} of cadmium ions was applied. The maximum sorption capacity is defined as the total amount of cadmium ions adsorbed per gram of the sorbent. The obtained capacity of the adsorbent was found to be 175 mg g^{-1} .

3.1.8. Effect of interfering ions

The effect of common co-existing ions that often companion with cadmium ions in real samples on cadmium determination was studied in optimum conditions by analyzing 100 $\mu\text{g L}^{-1}$ of cadmium after addition of varying concentrations of Na^+ , K^+ , Ca^{2+} , Cu^{2+} , Zn^{2+} , Ni^{2+} , Mn^{2+} , and Fe^{2+} . The concentration ratio of other ions was as follow: 1750 for Na^+ , K^+ ; 1500 for Ca^{2+} , Mg^{2+} ; 1250 for Cu^{2+} , Zn^{2+} , Fe^{2+} , Ni^{2+} , Mn^{2+} . Results showed that interference ions do not influence on extraction recovery of cadmium. Hence, the method was selective for preconcentration and extraction of cadmium (Table 1).

3.2. Analytical performance of suggested method

The analytical performance of the suggested pipette-tip solid phase extraction was evaluated, and the results are summarized in Table 2. The limit of detection (LOD) was obtained based on a signal-to-noise ratio of 3. The linearity range was studied by varying the concentration of the standard solution from 0.3 to 150 $\mu\text{g L}^{-1}$. The repeatability of the method, expressed as relative standard deviation (RSD), was calculated for seven replicates of the standard at an intermediate concentration (50 $\mu\text{g L}^{-1}$) of the calibration curve. The precision of the method was determined by repeatability (intraday precision) and intermediate precision (inter-day precision) of both standard and sample solutions.

Table 1. The effect of interfering ions on the recovery of Cd (II) ions in water samples by PT-SPE procedure coupled to F-AAS

Interfering Ions(M)	Mean ratio (C_M/C_{Cd})	Recovery (%)
	Cd(II)	Cd(II)
Al^{3+}	750	97.5
Na^+ , K^+	1750	97.8
Cu^{2+} , Zn^{2+} , Fe^{2+} , Ni^{2+} , Mn^{2+}	1250	98.2
I^- , Br^- , F^-	1100	97.7
Ca^{2+} , Mg^{2+}	1500	98.0
Co^{2+} , Pb^{2+}	950	97.9
Ag^+ , Au^{3+}	250	96.5

Table 2. Analytical figures of merit for proposed methods

Parameter	Analytical feature
Dynamic range ($\mu\text{g L}^{-1}$)	0.3 -150
R ² (determination coefficient)	0.99
Repeatability (RSD ^a %)	2.45
Limit of detection ^b (ng.L^{-1})	15
Enrichment factor (fold)	125
Total extraction time (min)	≤ 12

^aRSD, relative standard deviation, for 5 replicate measurements of $50 \mu\text{g.L}^{-1}$ of the analyte

^bLimit of detection was calculated based on the $3S_0/m$ criterion for 10 blank measurements

Precision was determined in seven replicates of both cadmium standard solution ($100 \mu\text{g L}^{-1}$) and sample solution ($100 \mu\text{g L}^{-1}$) on the same day (intra-day precision) and daily for 8 times over a period of one week (inter-day precision). The results are represented as % RSD and indicated that intra-day precision and inter-day precision of the method were 5.0% and 3.5%, respectively.

3.3. Determination and validation of cadmium in rice samples

Rice samples were purchased from several local markets. About 50 gr of rice was weighed and cooked in the oven for 8 hours at the temperature is 80°C with the aim of removing moisture

and determining weight It was dry. After drying and reaching constant weight, 10 gr of rice was transferred to a 250.0 ml beaker Samples for 48 hours at a temperature of 105°C it placed. Then 5 ml of 37% hydrochloric acid and 15 ml of 65% nitric acid were added to them and after 120 minutes at the laboratory temperature, it dissolved slowly and heated until its volume reached less than 20 ml. Then the obtained clear solution was cooled, filtered and used for the determination of cadmium according to the above PT-SPE method. As can be seen in Table 3 concentrations of cadmium in all samples in comparison to the maximum acceptable level ($200 \mu\text{g g}^{-1}$) are adequate.

Table 3. Determination of cadmium in different rice samples under optimized conditions^a

Rice Sample	Added ($\mu\text{g g}^{-1}$)	Found ($\mu\text{g g}^{-1}$)	Recovery (%)	RSD % (n=3)
1	0	45	-	-
	50	94.2	98.2	2.7
	150	194.5	74.3	3.2
2	0	40	-	-
	50	89.3	98.7	1.7
	100	139.2	98.1	2.8
3	0	55	-	-
	50	104.7	98.7	3.6
	100	154.5	98.5	2.8

^aThe maximum acceptable level of cadmium in the rice reported by WHO is $200 \mu\text{g g}^{-1}$

4. Conclusion

In this research, for the first time, we employed an amino functionalized MOF with a high surface area and large porosity for PT-SPE of cadmium. This method is very simple, fast, solvent-free and applicable for the extraction of cadmium. The total time of analysis, was less than 12 minutes and the functionalized-MOF sorbent was used for at least 10 extractions without any change in its capacity. Only 2mg of the sorbent was enough to fill the PT. Moreover, evaluation of intra-day and inter-day showed a notable precision with RSD below 5 and 3.5%, respectively. This method was applied successfully for the determination of cadmium in three rice samples. Real samples spiked with three concentration levels and results indicated that sorbent can be applied in the complicated matrix for analysis of heavy metals such as cadmium. Also, analysis of real samples showed that the concentration of cadmium in all samples is below the acceptable range.

5. Conflict of Interest and Ethical approval

The authors have declared no conflict of interest.

6. References

- [1] P.K. Rai, Heavy metals in food crops: Health risks, fate, mechanisms, and management, *Environ. Int.*, 125 (2019) 365-385. <https://doi.org/10.1016/j.envint.2019.01.067>.
- [2] Y. Mao, Research Progress of Soil Microorganisms in Response to Heavy Metals in Rice, *J. Agri. Food Chem.*, 70 (2022) 8513-8522. <https://doi.org/10.1021/acs.jafc.2c01437>.
- [3] C. Mao, Human health risks of heavy metals in paddy rice based on transfer characteristics of heavy metals from soil to rice, *Catena*, 175 (2019) 339-348. <https://doi.org/10.1016/j.catena.2018.12.029>
- [4] W.A. Khan, M.B. Arain, M. Soylak, Nanomaterials-based solid phase extraction and solid phase microextraction for heavy metals food toxicity, *Food Chem. Toxicol.*, 145 (2020)111704. <https://doi.org/10.1016/j.fct.2020.111704>
- [5] M.H. Habibollahi, Extraction and determination of heavy metals in soil and vegetables irrigated with treated municipal wastewater using new mode of dispersive liquid-liquid microextraction based on the solidified deep eutectic solvent followed by GFAAS, *J. Sci. Food Agri.*, 99 (2019) 656-665. <https://doi.org/10.1002/jsfa.9230>.
- [6] S.S. Arya, A.M. Kaimal, Novel, energy efficient and green cloud point extraction: technology and applications in food processing, *J. food Sci. Technol.*, 56 (2019) 524-534. <https://doi.org/10.1007/s13197-018-3546-7>
- [7] H.L. Jiang, N. Li, L. Cui, Recent application of magnetic solid phase extraction for food safety analysis, *TrAC Trends Anal. Chem.*, 120 (2019) 115632. <https://doi.org/10.1016/j.trac.2019.115632>
- [8] H. Sun, J. Fung, Recent advances in micro-and nanomaterial-based adsorbents for pipette-tip solid-phase extraction, *Microchim. Acta*, 188 (2021) 1-24. <https://doi.org/10.1007/s00604-021-04806-0>
- [9] M. Shirani, F. Salari, Needle hub in-syringe solid phase extraction based a novel functionalized biopolyamide for simultaneous green separation/preconcentration and determination of cobalt, nickel, and chromium (III) in food and environmental samples with micro sampling flame atomic absorption spectrometry, *Microchem. J.*, 152 (2020)104340. <https://doi.org/10.1016/j.microc.2019.104340>
- [10] M.A. Habila, Z.A. Alothman, Activated carbon cloth filled pipette tip for solid phase extraction of nickel (II), lead (II), cadmium (II), copper (II) and cobalt (II) as 1, 3, 4-thiadiazole-2, 5-dithiol chelates for ultra-trace detection by FAAS, *Int. J. Environ. Anal. Chem.*, 98 (2018) 171-181. <https://doi.org/10.1080/03067319.2018.1430794>
- [11] M.R.R. Kahkha, Fast determination of bisphenol a in spiked juice and drinking water samples by pipette tip solid phase extraction using cobalt metal organic framework as sorbent, *Bull. Chem. Soc. Ethiopia*, 32 (2018) 595-602. <https://doi.org/10.4314/bcse.v32i3.17>

- [12] Y. Zhang, Covalent organic framework Schiff base network-1-based pipette tip solid phase extraction of sulfonamides from milk and honey, *J. Chromatogr. A*, 1634 (2020) 461665. <https://doi.org/10.1016/j.chroma.2020.461665>
- [13] T.G. Aqda, Graphene oxide-starch-based micro-solid phase extraction of antibiotic residues from milk samples, *J. Chromatogr. A*, 1591 (2019) 7-14. <https://doi.org/10.1016/j.chroma.2018.11.069>
- [14] Y. Su, S. Wang, Zr-MOF modified cotton fiber for pipette tip solid-phase extraction of four phenoxy herbicides in complex samples, *Ecotoxicol. Environ. Safe.*, 201(2020)110764. <https://doi.org/10.1016/j.ecoenv.2020.110764>
- [15] A. Girgin, N. Atsever, Determination of cadmium in mineral water samples by slotted quartz tube-flame atomic absorption spectrometry after peristaltic pump assisted silica nanoparticle based pipette tip solid phase extraction, *Water Air Soil Pollu.*, 232 (2021) 1-10. <https://doi.org/10.1007/s11270-021-05386-8>
- [16] M.M. Moein, Advancements of chiral molecularly imprinted polymers in separation and sensor fields: A review of the last decade, *Talanta*, 224 (2021) 121794. <https://doi.org/10.1016/j.talanta.2020.121794>
- [17] M. Arjomandi, H. Shirkhanloo, A review: analytical methods for heavy metals determination in environment and human samples, *Anal. Methods Environ. Chem. J.*, 2 (2019) 97-126. <https://doi.org/10.24200/amecj.v2.i03.73>
- [18] M. Abbaszadehbezi, M. R. Rezaei Kahkha, A. Khammar, Application of pipette-tip solid-phase extraction technique for fast determination of levofloxacin from wastewater sample using cobalt metal-organic framework, *Anal. Methods Environ. Chem. J.*, 5 (2) (2022) 51-59. <https://doi.org/10.24200/amecj.v5.i02.185>
- [19] M.R.R. Kahkha, M. Kaykhaii, B. Rezaei Kahkha, H. Khosravi, Simultaneous removal of heavy metals from wastewater using modified sodium montmorillonite nanoclay, *Anal. Sci.*, 36 (2020) 1039–1043. <https://doi.org/10.2116/analsci.19P300>
- [20] M.R.R. Kahkha, Magnetic bentonite nanocomposite for removal of amoxicillin from wastewater samples using response surface methodology before determination by high performance liquid chromatography, *Anal. Methods Environ. Chem. J.*, 3 (03) (2020) 25-31. <https://doi.org/10.24200/amecj.v3.i03.108>
- [21] M.R.R. Kahkha, G. Ebrahimzadeh, A. Salarifar, Removal of Metronidazole residues from aqueous solutions based on magnetic multiwalled carbon nanotubes by response surface methodology and isotherm study, *Anal. Methods Environ. Chem. J.*, 3(03) (2020) 44-53. <https://doi.org/10.24200/amecj.v3.i03.110>
- [22] M. Tuzen, A. Sarı, Polyamide magnetic palygorskite for the simultaneous removal of Hg(II) and methyl mercury; with factorial design analysis, *J. Environ. Manage.*, 211 (2018) 323-333. <https://doi.org/10.1016/j.jenvman.2018.01.050>
- [23] T.A. Saleh, A. Sarı, M. Tuzen, Optimization of parameters with experimental design for the adsorption of mercury using polyethylenimine modified-activated carbon. *J. Environ. Chemical Eng.*, 5 (2017) 1079-1088. <https://doi.org/10.1016/j.jece.2017.01.032>
- [24] M. Tuzen, A. Sarı, M.R. Afshar Mogaddam, S. Kaya, K.P. Katin, N. Altunay, Synthesis of carbon modified with polymer of diethylenetriamine and trimesoyl chloride for the dual removal of Hg (II) and methyl mercury ([CH₃Hg]⁺) from wastewater: Theoretical and experimental analyses. *Mater. Chem. Phys.*, 277 (2022) 125501. <https://doi.org/10.1016/j.matchemphys.2021.125501>
- [25] M. R. Rezaei Kahkha, S. Daliran, The mesoporous porphyrinic zirconium metal-organic framework for pipette-tip solid-phase extraction of mercury from fish samples followed by cold vapor atomic absorption spectrometric determination, *Food Anal. Methods*, 10 (2017) 2175-2184. <https://doi.org/10.1007/s12161-016-0786-x>



A review: Total vaporization solid-phase microextraction procedure in different matrixes

Yunes M. M. A. Alsayadi ^{a*}, and Saahil Arora ^b

^a University Institute of Pharmaceutical Sciences, Chandigarh University, Punjab-140413, India

^b University Institute of Pharmaceutical Sciences, Chandigarh University, Punjab-140413, India

ARTICLE INFO:

Received 21 May 2022

Revised form 2 Aug 2022

Accepted 28 Aug 2022

Available online 29 Sep 2022

Keywords:

Solid-phase microextraction,
Headspace solid-phase microextraction,
Total vaporization solid-phase
microextraction,
Vacuum-assisted total vaporization
solid-phase microextraction,
Method optimization

ABSTRACT

Total vaporization solid-phase microextraction (TV-SPME) is a type of extraction technique in which a specific solvent dissolves the analyte. Then a tiny amount of solvent is taken to the vial of SPME. Then, the solvent vaporizes in the SPME vial, and sampling is carried out on the headspace of the SPME fiber. As a result, the partitioning phase of the analyte between the headspace and liquid sample is omitted. The equilibrium phase remains the analyte partitioning between the headspace and SPME. TV-SPME was introduced in 2014 by Goodpaster to increase the recovery compared to the liquid injection method. This review discusses different aspects of TV-SPME, including its impact on sampling techniques, theoretical part, sampling procedure, and method optimization. Special attention was paid to its applications. A comprehensive literature study was conducted in the relevant databases to summarize the research work that has been done on this technique. In TV-SPME, the liquid samples completely vaporized and had a less matrix effect and better adsorption. This method needs no sample preparation, consumes less supply, and can be done automatically. Also, TV-SPME enables a cost-effective and efficient extraction for different matrixes. This review summarizes aspects related to TV-SPME including its sampling procedure, method optimization, and its preference for conventional liquid methods. Special attention was paid to its applications of the vacuum-assisted total vaporization solid-phase microextraction procedure (VA-TV-SPME).

1. Introduction

Solid-phase microextraction technique (SPME) is widely used for pre-concentration/separation of analyte from the sample, analytes are absorbed on a fiber and then, it desorbed before determined by analytical instrument such as GC-FID [1,2]. SPME was introduced in 1989, and since then, it has been used extensively in the field of environmental chemistry, with more than 1500 publications. SPME

is a technique with off-column pre-concentration sampling that facilitates the trace analysis of the occurring abundance of matrices and samples. This technique depends on a polymer fiber with surface chemistry designed to increase targeted compounds' adsorption [3, 4, 5]. SPME was initially presented as a solvent-free technique combining the prepared sample into one-step sampling, sample introduction extraction, and concentration [1,6]. Two processes are involved in the SPME extraction: (1) the analytes partitioning between the fiber coating and the sample, and (2) the desorption process occurs by the concentrated analytes from the coated fiber

*Corresponding Author: Yunes M. M. A. Alsayadi

Email: yunes20171@gmail.com

<https://doi.org/10.24200/amecj.v5.i03.190>

to the instrument to be used for the analysis. The extraction is performed by placing a solid sample containing volatile analytes and an aqueous sample containing organic analytes into a vial, then closed with a septum and cap [7]. The main advantages of SPME are a simple extraction method, efficient, selective, and fast. SPME followed with less amount of sample volumes and no-solvent consumption. For those advantages, it was implemented quickly in many disciplines of analytical chemistry, like bioanalysis, environmental science, and chemical analysis [8,9,10]. In addition, SPME can be coupled and automated with instruments like gas chromatography, which easily estimates the organic compound [11]. Direct analysis of complex matrixes mostly cannot be performed in a manner that attains the sensitivity and selectivity needed for many trace analysis applications. To solve this issue, SPME techniques were used so that preconcentrating of analytes occurs selectively before placing it into ion trap mass spectrometric/gas chromatographic analysis. This approach was introduced to be used in the trace analysis of the metabolites of explosives in seawater [6]. The SPME technique includes exposing a fiber of fused silica coated with a solid phase to an aqueous solution containing organic compounds [12]. It involves using a silica fiber coated with a polymer film to adsorb compounds of interest from their matrices. Such a technique is a solvent-free, reliable, and inexpensive method that can be used practically for aqueous sample analysis/headspace and shows good sensitivity and excellent selectivity [13]. The SPME technique is used for multiple sampling, and sample preservation leads to minimizing the risk of contamination of the sample because the technique affords a simplified sample handling [14]. SPME is mainly carried out in one of the two modes; either headspace or immersion technique. In headspace SPME mode, the extraction of analytes by fibers occurs from the headspace above a sample. While in immersion SPME mode, the extraction of analytes by the fiber takes place directly from a liquid sample [15]. In headspace SPME, the partition of analytes occurs between the headspace above the

sample and the coating fiber of SPME [16,17]. The main criteria for applying headspace solid-phase microextraction (HS-SPME) was to prevent the fiber of SPME coatings from being tricked by the components of sample matrices [18]. In HS-SPME, the fiber is placed into the vial of the sample, the volatile organic compounds that are available in the headspace, are bound to the coating, and then the fiber is to be taken to the site of injection of the Gas Chromatography (GC) for desorption and further analysis [13]. HS-SPME compounds having analytes with low volatility from complex aqueous samples can be used by the manner of increasing the temperature of the sample. Still, some SPME coatings made from some adsorbent substances may face difficulties due to their low stabilities, particularly in a hot medium like a steam of hot water. It is the preparation of super hydrophobic metal-organic framework (MOF) that is obtained from decoration nodes of the amino-functionalized UiO-66(Zr) with phenyl silane was needed and then successfully improved to be used in a novel fiber coating of SPME [15]. The scientists of food flavors have appreciated the ease of use and sensitivity of the headspace technique mode by using it in analyzing the volatile compounds in many food products [19]. Headspace SPME sampling was widely used in analyzing of some intact explosives like triacetone triperoxide (TATP) which was detected from headspace applying planar SPME with the help of an ion mobility spectrometer [20]. HS-SPME is a pre-sampling technique that does not need complicated apparatus or solvents [21]. HS-SPME can integrate the concentration, extraction, and introduction in a single step. Combining HS-SPME with GC-MS is employed to determine the volatile components in different plants like tea samples [22]. In the immersion SPME sampling technique, the fiber is directly placed into a liquid sample and the compounds of interest adsorb/adsorb to the fiber coating. After the absorption/adsorption, the fiber is then placed for desorption in the inlet of a LC or GC for further analysis [23]. Immersion SPME sampling has been utilized practically in the applications of environmental

studies for extracting organic explosives that are present in aqueous soil extracts and/or water to be later analyzed by GC-MS and GC-electron capture detection [6,16]. Some explosives examples that have been detected and recognized in this method like PETN, 2,6-dinitrotoluene, RDX (composition C-4), TNT, and NG (dynamite) [24,25]. Both the techniques either headspace or immersion SPME cannot be smoothly applied to the detection and identification of some explosive residues especially those present on post-blast debris, regardless of many previously reported descriptions of its unique use, for example, the detection of a single particle of smokeless powder [2] or the residue extraction of the explosives that obtained from soil samples collected from the blast site after an explosion [25,26]. In fact, headspace and immersion SPME methods have been used to analyze a various analytes [27]. TV-SPME is almost a new technique that is being utilized in analytical chemistry. It is always in comparison with conventional techniques including HS-SPME in the motive of determination of the superior technique. That comparison is highly appreciated as it plays a critical turn in the superiority of the method that is to be adopted. And in the case of TV-SPME and HS-SPME, it is important to compare them to see if one is superior, as it helps to choose a method with specific samples [28]. These two methods are among the advanced micro extraction methods as they require least to almost no sample preparation compared to other liquid methods which require a high amount of

the sample [29]. They involve placing the samples directly into the headspace in place of placing them to do individual extraction techniques to a sample ahead of being directly injected into the GC. Table .01 shows the differences between the HS-SPME and TV-SPME [30]. The comparison concentrates on the sample volumes, analysis time, and matrix effects as these parameters are critical for analysis samples.

Environmentally, TV-SPME has been used to analyze drugs and their metabolites in saliva, urine, and hair. This valuable simple technique has also been used in analyzing lipids, fuel samples, street drugs, lipids, and pollutants in water and post-blast explosive residues [30], [33], [36-38]. TV-SPME has been used to identify illegal adulterants in tiny samples (microliter quantities) of alcoholic beverages [39-40]. Both gamma-butyrolactone (GBL) and gamma-hydroxybutyrate (GHB) were identified at levels that would be found in spiked drinks [34]. There were techniques being used, including Membrane protected micro-solid-phase extraction (μ -SPE), which was used for the first time in 2006 with the motive of replacing multistep SPE. The principle of μ -SPE lies in taking a minimal amount of the sorbent and packing it inside a porous membrane paper having edges that are heat sealed for the fabrication of a μ -SPE device. This device can perform pre-concentration and extraction in a single step. Such techniques seem to have the best extracting method, especially for complex

Table 1. Differences between the HS-SPME and TV-SPME

Parameter	HS-SPME	TV-SPME
Sample volumes	Sample utilization is at least 1mL.[29,31-33].	**Almost 1 μ l - 100 μ l as TV-SPME vaporizes the sample completely [31,34].
Matrix effect	The effect of matrix is higher as it is between two phases only [32, 33].	less matrix effects are there as it results in fully vaporizing the analyte and its matrix[34].
Analysis time.	***HS-SPME and other liquid injection, need that the analyte to be reacted with the derivatizing agent in solution [33, 35].	As TVSPME allows for the analyte to be derivatized during the extraction process which reduces analysis time [27, 34].

**Almost 1 μ l - 100 μ l as TV-SPME vaporizes the sample completely, analyte partitioning will be there between the vapor and only the fiber, which lead forcing more amount of the sample to adsorb into the fiber and large amount of the sample can be exposed to the vapor. And that can cause minimizing the sample size [31,34].

***Other methods including HS-SPME and other liquid injections, need that the analyte to be reacted with the derivatizing agent in solution prior to being injected into the GC. And that lead to minimize the time of analysis[33, 35].

samples, since extraneous matter does not adsorb over the sorbent as it is protected effectively inside the Membrane [39]. Direct Immersion-Solid Phase Microextraction (DI-SPME) is preferred for aqueous samples as the fiber is introduced directly to the sample solution. However, when applied to a complex matrix, the sample must be pretreated; otherwise, some interfering substances from the matrix can bind irreversibly to the fiber. As a result, choosing the mode is not preferred in the case of complex samples, including samples arising from food, sludge, and biological origin

[39-40]. To overcome such issues, HS-SPME can be used, although it has some limitations, including it can work better only for volatile compounds and that compounds having good volatility even with almost moderate heat. Therefore, nonvolatile or low volatile compounds cannot be extracted by applying such an approach. So, something should be developed for extracting compounds with less or no volatility from complex samples by adopting a mode of direct immersion [41]. Differences between DI-SPME, HS-SPME, and Membrane Protected SPME, are shown in Figures 1 (a and b).

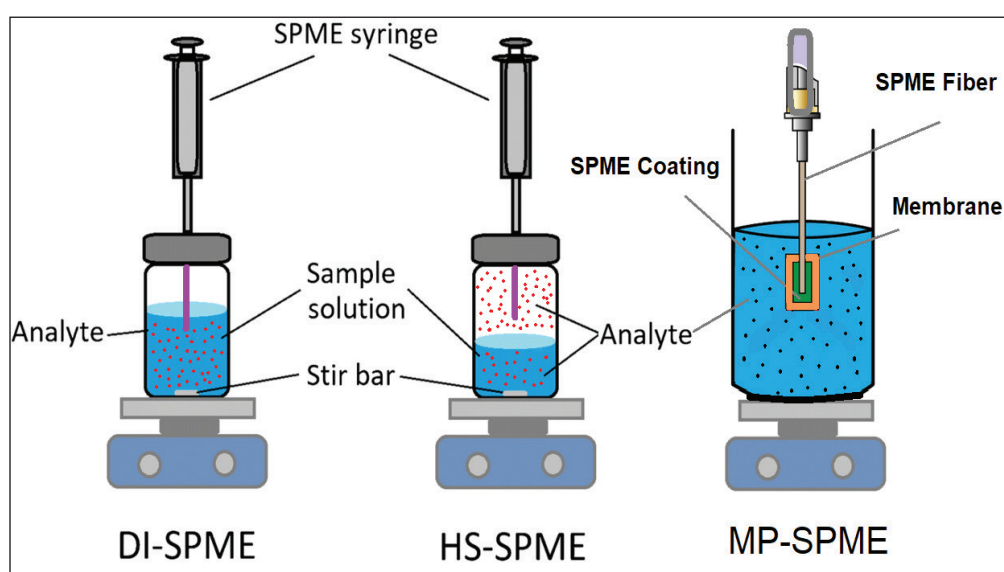


Fig. 1a. DI-SPME, HS-SPME and membrane protected SPME

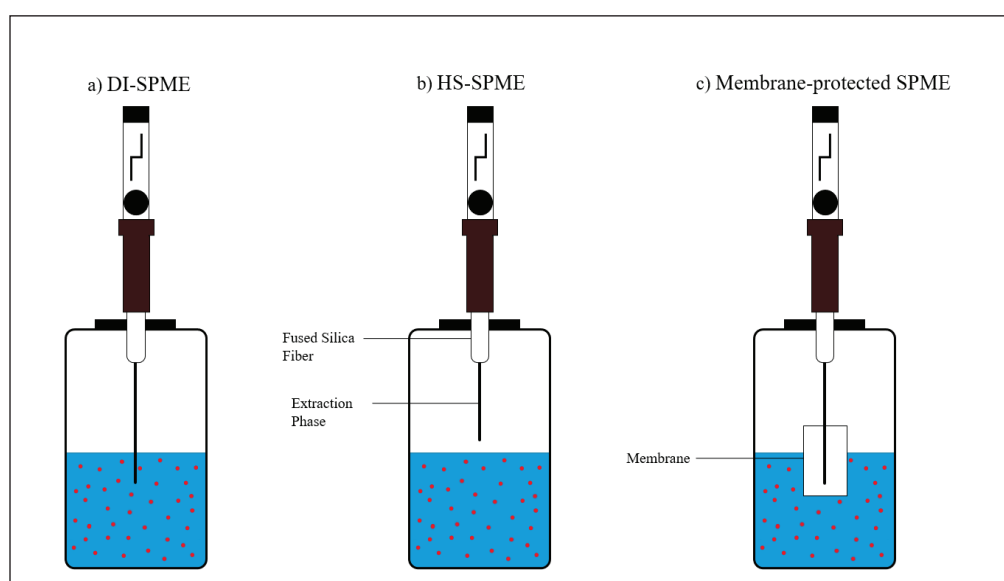


Fig. 1b. DI-SPME, HS-SPME and membrane protected SPME

SPME and its derivative techniques are a well-recognized method of extraction which utilize zero solvents and has a wide scope and applications, including biomedical, food, forensic, and environment [35,41]. Moreover, they can be applied in organic contaminants extraction like; pesticides, Pharmaceutical compounds, emerging pollutants, and persistent organic pollutants [42-53]. Total vaporization (TV) is a technique that can be practically utilized in conjunction fused with headspace sampling. The residual solvents will be released from the matrix by applying TV to a solid sample. Furthermore, applying it to the liquid samples allows the whole sample to be vaporized before the headspace sampling [54]. TV technique applies to many samples like solid samples (e.g., residual solvents), [55], aqueous solutions (e.g., odor compounds) [56] and fermentation liquor (e.g. ethanol) [57]. The approach of coupling TV and SPME (TV-SPME) offered great sensitivity and even low detection limits for compounds present in the hair of some users of tobacco such as nicotine and cotinine. In the TV-SPME technique, a sample extract needs to be heated until it gets vaporized and fiber of SPME is utilized for pre-concentrating analytes from the produced vapor [53]. In TV-SPME, a complete vaporizing of the liquid samples gives a fewer matrix effect and better adsorption. This method does not need any sample preparation, utilizes less supplies and can be done automatically, enabling it to be both a cost-effective and efficient method [58]. SPME is a sensitive technique where the liquid portion is totality vaporized before being placed for sampling, easing to attain equilibria inside the sample vial and increasing the analyte's availability in the headspace, leading to making the analyte quantity more [53,59]. TV-SPME is an effective technique that does not require derivatization while being used to analyze controlled substances, either with or without on-fiber. Total vaporization is a technique that has been utilized in simple headspace sampling. Still, matrix effects that result between two phases in headspace sampling are a matter of concern. One important method to remove matrix

effects is completely evaporating the analyte and its matrix. Total vaporization headspace is applicable in determining ethanol in fermentation liquor, methanol in wood pulp, odor compounds in aqueous samples, and volatile organic compounds in biological samples [56,60-62]. The matrix effects in SPME can be eliminated by extracting analytes (quantitatively) from complex matrixes. This method is known as cooled fiber SPME, and it has been applied for extracting polycyclic aromatic hydrocarbons (PAHs) from heated soil samples [3]. Also, the urine extracts in solvent and have been evaporated in a headspace vial. The residue was heated until analytes derivatize, vaporize, and absorb to a SPME fiber [63].

2. Experimental

2.1. TV-SPME sampling procedure and practical TIPS

SPME fiber format was one of the most commonly used forms of the technique for many years [64]. In SPME fiber format, a small amount of the extracted phase is coated by a thin and short fused-silica rod, which is revealed for a specific time directly to the headspace above the sample or to the sample itself. Analytes of interest were taken from the sample to be analyzed in the SPME fiber coating, and then the sample was extracted till the point when the quantity of analyte extracted by the fiber remained constant even if the sampling time increased i.e., the analyte concentration attained partition equilibrium state between the fiber coating and sample [65]. Generally, the time needed to attain equilibrium relies on the characteristics of the fiber coating, matrix, and target analyte, and its range varies from a few minutes to many hours [66]. SPME sampling includes two stages of the equilibrium mechanism, which occur between the headspace/sample (first stage) and the fiber coating/headspace (second stage). In the TV-SPME technique, the equilibrium process between the sample/headspace is no longer needed since the analytes can be directly partitioned from the fiber coating and headspace [67]. **Figure 2** shows the sample preparation of HS-SPME and TV-SPME. For HS-SPME, the extraction of volatile analytes

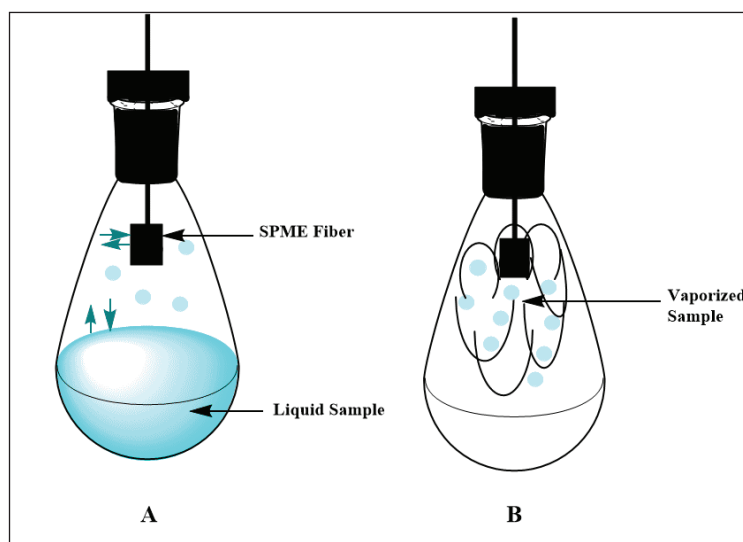


Fig. 2. Samples preparation of HS-SPME and TV-SPME

is noticed to happen faster than analytes with semi volatiles nature [15]. For that, the longer equilibration times could be less in various ways, including agitating the sample, heating the sample, maximizing the headspace/sample interface, and implementing the cold fiber HS-SPME proposal to cool the fiber coating and heating the sample matrix occurs simultaneously [13]. The effects of the matrix that can be produced between two phases while sampling in the headspace technique is a matter of concern. An important method to remove such effects from the matrix is applying heat to evaporate the analyte and its matrix fully. An excellent example of the use of total vaporization headspace involves estimation of volatile organic

compounds in biological samples, methanol in wood pulp, odor compounds in aqueous samples, and ethanol in fermentation liquor [27]. In TV-SPME, the extracted aliquot of the sample is sentenced for heating till the point where both the analytes and solvent are completely vaporized; after that, the analytes partition between the SPME fiber and the vapor phase [16]. TV-SPME extraction of analytes from a sample of interest was performed by applying a specific solvent in this approach. Then, a small part of this extract is fully vaporized inside a headspace vial inserted into an SPME fiber. Also, the VOCs in water samples based on fiber coating on the needle were determined after HS-SPME and TV-SPME were coupled to the GC-MS (Fig.3).

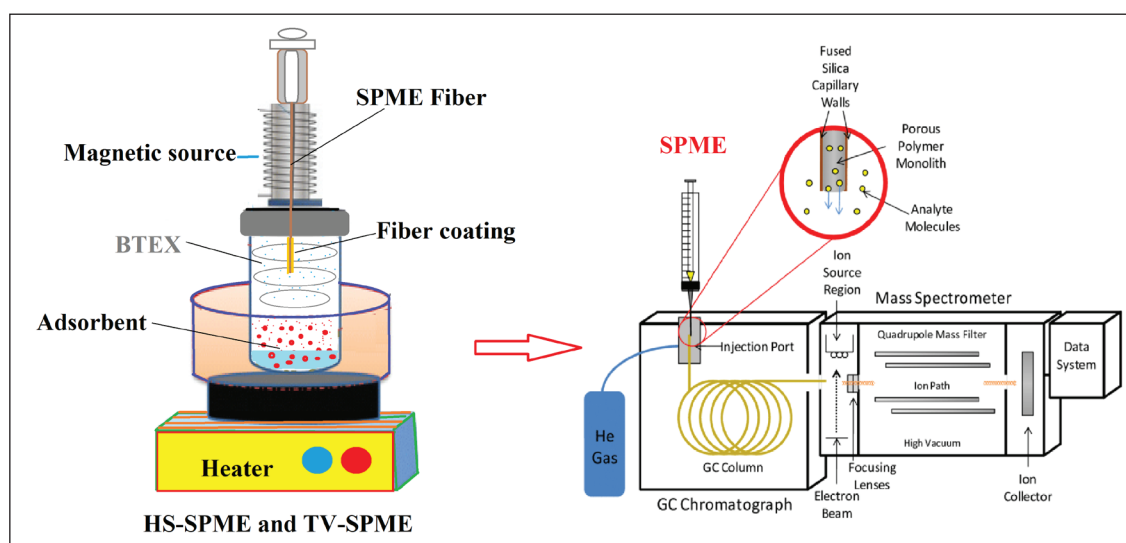


Fig.3. Determination VOCs in water samples based on fiber coating on needle after HS-SPME and TV-SPME coupled to the GC-MS

These results are a simple two-phase system. In particular, patterns occur when the analytes partition between the extract and the headspace is removed and when the analyte partitioning occurs directly between the vapor phase and the SPME fiber. In general, combining the total vaporization technique with SPME increase preconcentrating analytes onto the fiber. For example, the estimation of an organic analyte in an organic solvent is not accessible by either immersion or headspace SPME. For that, the solvent should get vaporized and the analyte absorbed into the fiber of SPME. So, when the analyte gets distributed (in TV-SPME) at a solid/vapor interface, it has been found that the extraction time is less important than the sample volume and extraction temperature for the analytes to be recovered efficiently. In TV-SPME, extracts of the sample do not have to get filtered, which gives it a significant advantage compared to liquid injection. Nonvolatile compounds or solids that may have the chance to be laid within an extract of the sample will stay on the surface of the vial. That may lead to minimize extensively the contamination and the quantity of buildup that may take place in the inlet and the column of GC. Furthermore, the boiling point of the analytes plays an essential role in the selectivity of the GC inlet in liquid injection. TV-SPME can add a level of chemical selectivity because of the advantage of the fiber that can enable it to select the targeted analyte specifically. Finally, the volumes for the liquid injection are almost 1 to 2 μL ; thus, only a tiny portion of the sample extract is needed for the injection. The Large-volume injection (LVI) techniques have thus been developed to be used in the GC. However, LVI needs some changes to meet the requirements for the instrument and other analysis parameters. So, TV-SPME needs no modification in instruments and other parameters, enabling the use of large volumes of the sample for the analysis in GC, which ultimately concluded in great sensitivity over the liquid injection [27]. The idea of combining total vaporization with SPME is almost similar to that of LVI techniques in those large volumes of the sample (e.g., 200

mL) which lead to an increase the sensitivity. However, TV-SPME is an essential technique because it does not require any modification in the GC instrument, such as exits for solvent vapor or adding retention gaps.

Additionally, the sample extracts require no filtration as any non-volatile or volatile components float above and within the surface of the vial. A critical feature of TV-SPME is that although it evaporates the liquid sample completely, resulting in a much larger volume, it plays a vital role in preconcentrating the analytes more than compensates for this dilution. In addition, a clear choice of fiber chemistry used in SPME can add remarkable selectivity to the analysis [16].

2.2. TV-SPME method optimization

HS-SPME is a process of multi-stage equilibrium [68] where the extracted analytes in the headspace partition with the adsorptive surface on the fiber after the compounds get extracted from the matrix to the sample headspace by the help of some external force, including ultrasound, agitation and rising the temperature. These strategies shorten the time needed to attain equilibrium. In 2014, a novel separation technique was introduced by Goodpaster in which sampling was to be performed only in the headspace [53]. In this technique, the extraction of the analyte occurs by a solvent. Then a tiny amount of the solvent is taken to the SPME vial by total vaporization of the transferred solvent in the vial used in SPME, and sample processing is taken place on the SPME fiber from the headspace [23]. Therefore, the phase of partitioning the analyte extracts between the headspace and liquid sample is omitted, and the only equilibrium phase that remains is the partitioning of the analyte between the headspace and SPME [69]. Reflecting that the partitioning process of the analyte is to occur between the vapor and solid, it was noticed that in comparison with extraction temperature and sample volume, the extraction time parameter has less significance [67]. In addition, all non-volatile and solid compounds stay on the surface of the

SPME vial and are not taken to the injection portion or the GC column. Therefore, it reduces contamination in GC, and the sample extracts require no filtration [16]. Also, the evaporation of the sample is almost more, and a proper fiber of SPME is used for the preconcentration of the analytes to enable the TV-SPME technique to have a greater sensitivity compared to the traditional SPME [69]. The TV-SPME method depended on the vaporization of the total portions of the sample, containing volatile, non-volatile, and semi-volatile components. Therefore, it is noticed that semi-volatile and non-volatile compounds require more heat, and the sample volume needed is a more significant amount. Consequently, it was reported that the SPME fiber is heated and that heat does not cause any fault in the absorption of the analytes on the SPME fiber [67]. Maybe this is one of the limitation factors, but it is considered to be among the main reasons why this valuable technique is not more widely used. As a result, few publications based on TV-SPME have been written [70]. The TV-SPME technique should be coupled with another method to ease the vaporization; surpassing the preparation steps and minimizing the required heat would be helpful [71]. Various factors must be investigated and optimized, such as the desorption temperature, the extraction time and temperature, and the salt concentration. Such factors significantly affect thermal desorption and extraction efficiencies [15]. For controlled substances that are not thermally stable and not sufficiently volatile while being analyzed by GC-MS, derivatization is used to improve their characteristics to match the required conditions in the method optimization in GC-MS. The performance of GC-MS is significantly improved by the use of such derivatizing compounds [71]. Although derivatization has many benefits, techniques of the conventional solution phase work are time-consuming and intensive. However, derivatization was adapted to a sampling technique that is called TV-SPME to automate and simplify the process. SPME is

a technique in which the analytes of interest are placed for pre-concentration onto a fiber coated in adsorptive or absorptive material. TV-SPME is a unique and novel technique in which a tiny amount of solution is poured into a vial and heated until complete vaporization occurs [53]. A fiber of SPME is then introduced, and the adsorption of the sample onto the fiber coating takes place. TV-SPME belongs to immersion SPME in that both are two-phase systems which differ from headspace SPME, which is a three-phase system [69]. Calculating the maximum volume for total vaporization of a given solvent can be easily obtained by the vial volume, molecular weight, solvent vapor pressure, and temperature [53]. For example, the calculated maximum volume of methanol for total vaporization in a 20-mL vial at 60°C is 24 μ L [53].

When TV-SPME is used for sampling, it can be streamlined the process of derivatization by enabling it to be taken place simultaneously with the extraction step in a process called on-fiber derivatization (Fig.4). This On-fiber derivatization was used before in conjunction with immersion or headspace SPME [72]. However, it could be desirable to use the advantages brought by TV-SPME to bear for on-fiber derivatization. In the process of derivatization on-fiber with TV-SPME, an SPME fiber is introduced to the headspace of a vial that contains a small aliquot of liquid derivatization agent. The fiber is then taken to the heated headspace of a vial that contains the sample. The reaction between the derivatization agent and analyte takes place directly in the headspace surrounding the fiber or on the SPME fiber. After sufficient time for adsorption and reaction, the fiber is taken to the inlet of the GC for desorption. The use of an autosampler can make this a fully automated process wherein the only sample prep necessary is to dissolve the sample in a suitable solvent and place an aliquot into the vial [73]. Several parameters are in direct touch with TV-SPME method, involving desorption time, SPME fiber type, extraction time, sample volume and desorption temperature [16,69].

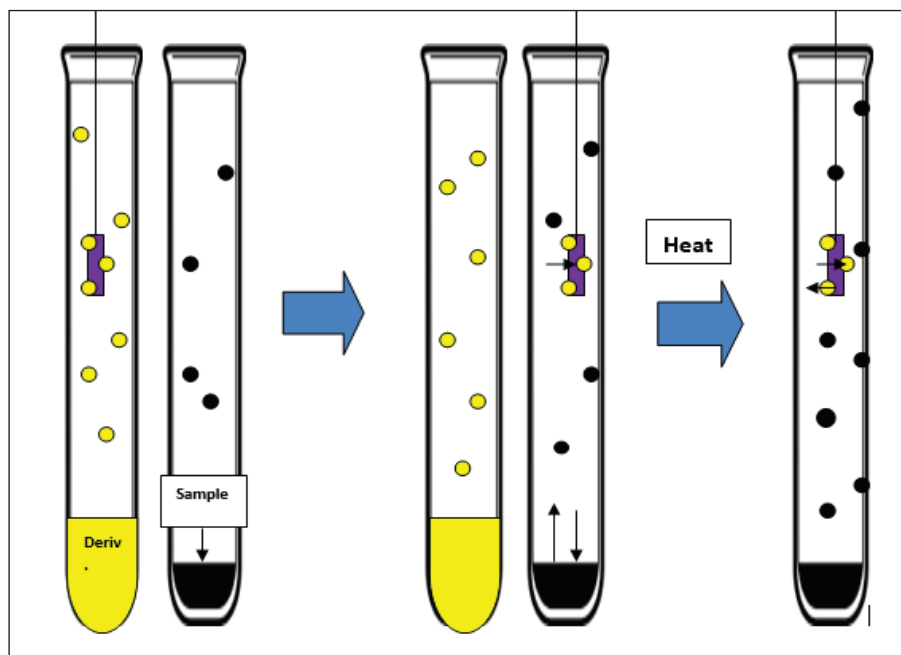


Fig. 4. Derivatization on-fiber in TV-SPME

2.3. TV-SPME based on liquid method

Although Gas Chromatography – Mass Spectrometry (GC-MS) is considered to be one of the most frequently used techniques in the laboratories, it has some limitations since compounds need to be volatile as well as thermally stable. Without these two characteristics, GC-MS cannot be used for regular routine analysis. For that some compounds have to undergo derivatization before injecting them into the gas chromatograph (GC) to meet and satisfy these requirements of thermostability and volatility. In SPME technique, a sample is taken into a vial and then heat is applied on the vial to initiate a site of the analyte to get vaporized into the headspace. A polymeric material such like polydimethylsiloxane-divinylbenzene (PDMS/DVB) used to coat SPME fiber, the coated SPME fiber is placed into the headspace of the sample or immersed graphene- Fe_3SO_4 -SPME Fiber in water samples and the analyte is adsorbed onto the fiber concluding that the formation of a thin coating of the analyte on the fiber (Fig.5). The fiber is then introduced to the inlet of the GC for desorption [74]. TV-SPME technique is almost similar to that of headspace SPME but it differs by the complete vaporization of a liquid sample prior getting adsorbed onto the fiber. Such adsorption

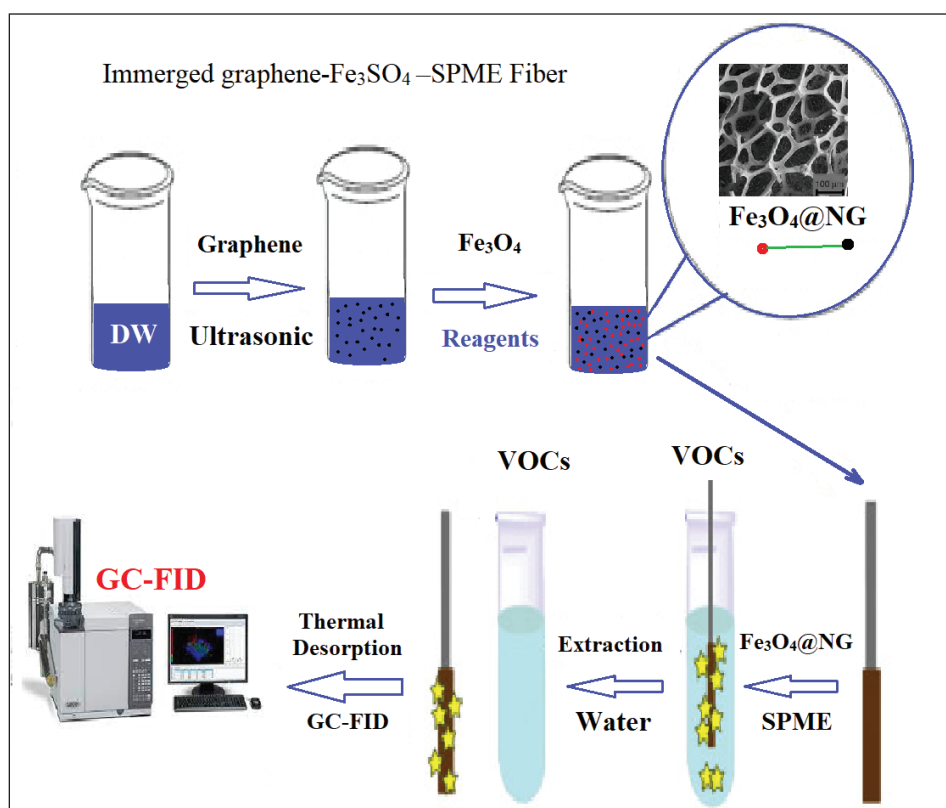
permits the occurrence of partitioning of the analyte between only the coating of the fiber and the vapor. By this technique, more portion of the sample is exposed for the adsorption onto the fiber lead to minimize the sizes of the sample (e.g., 1 – 200 μL) can be utilized [75-76].

TV-SPME showed its ability to be an efficient technique especially when used for the analysis of controlled substances in both the ways either with or without on-fiber derivatization. A summarized table for the results is presented below: Table 2. Brief of results for TV-SPME and liquid injection methods. + denotes that a single chromatographic peak is formed. 0 denotes that multiple chromatographic peaks are formed, and – denotes that no any chromatographic peak is formed [72,77].

even it could not be applied for all analytes, TV-SPME with on-fiber derivatization can serve as a powerful technique for amine, GHB and hydroxylamine-controlled substances [78]. The technique can increase the efficiency of the analyst by minimizing the time required for preparation of the sample for these types of analytes. Since GHB cannot be analyzed directly in its native state by GC/MS, this method is particularly well-suited to overcome such limitation [72,79].

Table 2. liquid injection methods based on V-SPME

Drug	TV-SPME	Liquid Injection
Methamphetamine	+	+
Amphetamine	+	+
Methamphetamine + TFAA	+	+
25I-NBOH	0	-
Gabapentin	+	+
Psilocin	+	+
25I-NBOH + TFAA	+	+
Pregabalin	+	-
Ephedrine	+	+
Ephedrine + TFAA	0	+
Lorazepam	+	+
Vigabatrin	-	-
GHB	-	-
Gabapentin + DMF-DMA	0	+
GHB + BSTFA + 1% TMCS	+	+
Vigabatrin + DMF-DMA	-	+
Pregabalin + DMF-DMA	-	0

**Fig.5.** Immersed (graphene- Fe_3SO_4 -SPME Fiber) in water and adsorbed the BTEX from water onto the fiber

2.4. Application of TV-SPME procedure

2.4.1. Ascertainments of lipid profiles of *Phormia regina*

Pupae of *Phormia regina* was the sample used in this study which basically belongs to a kind of blow fly species; while doing the inquiries of death, the forensic entomologists commonly found this type, which is commonly found by forensic entomologists during the investigations of death. Conventionally, the insect species analysis in a forensic backdrop has been falling within the prospect of biologists along with entomologists. Nevertheless, considerable effect has been done by the chemistry domain for the evaluation of these specimens by LC-MS, GC-MS and likely analytical techniques [80]. Studies that rely on liquid extraction are more commonly used for such analysis. Usually, the pest is placed in a non-polar solvent by the mean immersion for a particular time, allowing the extraction process of the cuticular and internal lipids. Derivatization is a kind of needful for these excerpts to improve performance and sensitivity within subsequent separation steps [81-82]. Unavoidably, single or multifold rounds of chromatography follows: liquid chromatography (LC), gas chromatography (GC) and thin layer chromatography (TLC) are some of the techniques that have been used. This wide-ranging method has been applied to the analysis of pupae [83-86].

Some experiments have been sought for the evaluation of the Volatile Organic Compounds (VOCs) that emitted by pupae using HS-SPME at elevated temperatures, unfortunately, the experiments were unsuccessful. For that, attentions have been exerted towards developing a new technique for the liquid extraction of pupae in order for the isolation of any hydrocarbons and lipids subsequent to TV-SPME analysis. The derivatization by trimethylsilyl was also performed internally within the sample vial immediately before GC-MS analysis took place, such derivatization would come very handy and with potential advantage to future analysts in order to rundown on blow fly pupae [23].

A new-fangled technique has been developed for the evaluation of sterols, fatty acids and

other naturally occurring lipids within pupae of the blow fly *Phormia regina*. Such method counted on liquid extraction in a solvent (non-polar), followed by derivatization using N,O-bis(trimethylsilyl)trifluoroacetamide (BSTFA) w/ 1% trimethylchlorosilane (TMCS) carried out inside the sample vial. The facilitation of this rundown was done by total vaporization solid-phase microextraction (TV-SPME), along with gas chromatography-mass spectrometry (GC-MS) which served as the instrumentation for analysis. The TV-SPME delivery technique was considered to be sensitive and effective approximately five times more than traditional liquid injection, this higher sensitivity may ease the reconstitution requirement, rotary evaporation, and collection of high-performance liquid chromatography fractions, and many of the other pre-concentration steps that are commonplace in the current literature. In addition to that, the ability of this method to derivatize the liquid extract in just single step while ensuring good sensitivity represents an improvement over present derivatization method. Various saturated and unsaturated fatty acids were the lipids present by and large in fly pupae, ranging from lauric acid (12:0) to arachidonic acid (20:4), as well as cholesterol. The concentrations of myristic acid (14:0), palmitelaidic acid (16:2), and palmitoleic acid (16:1) emerged as the most reliable indicators of the age of the pupae [23, 87-88].

2.4.2. Detection of γ -butyrolactone (GBL) and γ -hydroxybutyric acid (GHB) in alcoholic beverages via TV-SPME and GC-MS

γ -butyrolactone (GBL) and γ -Hydroxybutyric acid (GHB) are important drugs since they can be spiked into a victim's beverage to facilitate sexual assault (surreptitiously). These drugs may cause sedation, memory loss, and are difficult to be detected especially in plasma and biological samples. The challenge related to their analysis of these drugs lies on that they may be prone to readily interconvert in aqueous samples, which was showed in samples that required longer time to stand at room temperature. A volume required

for the study of GBL in water was performed with volumes that ranged from 1 μ l to 10mg as compared to the efficacy of headspace SPME, immersion SPME and TV-SPME. Lastly, water, liquor, wine beer, and mixed drinks were spiked with either GBL or GHB along with realistic concentrations (mg/ml) and microliter quantities were analysed using a combination of the TV-SPME and GC/MS method. The volume study of GBL exhibited a great sensitivity in the detection of GBL when TV-SPME was used. In addition to that, GBL and GHB were recognized in many beverages at realistic concentrations. Overall, TV-SPME is a method of benefits since it does not require sample preparation and uses lesser sample volume as compared to the immersion and headspace SPME [73].

2.4.3. Detection of both cotinine and nicotine in hair

TV-SPME can be used in detection of both cotinine and nicotine in hair as biomarkers of tobacco users whereas the cotinine detection was not possible in the past by using conventional SPME [89]. Only few research papers have published in using headspace SPME in the detection of nicotine in human hair by using. It was reported for first time that both cotinine and nicotine are efficiently detected using TV-SPME from a hair sample collected from a tobacco user. Incidentally, full scan data detect many other important compounds relied on a library search [53]. These involves phenacetin (an analgesic), squalene (a hair lipid that occurs naturally), 1,4-benzenediamine (a precursor of hair dye), and homosalate (type UV filter seen in shampoos). The hair taken from a two more smokers had nicotine concentrations of 21 and 29 ng mg⁻¹ hair, which is almost same as that the concentrations reported from other studies [24,25]. A detailed studies of validating the TV-SPME for the use of hair analysis showed its ability to detect both the cotinine and nicotine even in a small portion of the hair from the tobacco users which could serve as a good method for the researchers of toxicology and other medical backgrounds [53].

2.4.4. Tracking explosive residues on the places of bombing

The detection of the residues seen on bombing places and that arising from a debris of post-blast has a great role for the explosive's investigators. This can be used on the determining of explosive type, which may be used to catch a link about some suspect. To solve the issue of not finding a particle of explosives, some standard methodology can be used including the extraction of some pieces of debris with specific solvent (i.e., acetone and/ or dichloromethane) and then the extract(s) is to be analyzed via liquid injection GC/MS and/or infrared spectroscopy [16,90]. A TV-SPME method for the analysis of explosive residues on pipe bomb fragments has been designed and optimized. Optimization of this method was done by the following parameters incubation temperature, extraction time, and sample volume of the TV-SPME method. For the nitroglycerin, method optimization parameters were a 70 mL sample volume, a 30-minute extraction time and a 65 C incubation temperature. In addition to that, TV-SPME showed great sensitivity as compared to conventional liquid extraction methods as it was found to be 13-fold more sensitive and it has a very low detection limit (i.e., less than 10 ng mL⁻¹). When this developed method was used to actual pipe bombs, the recovery of the estimated NG mean mass was 1.0 mg and the mean concentration of NG on the fragments of steel was almost 0.26 ppm (w/w). It was noticed that end caps fragments yielded higher amount of NG and DPA. These findings could contribute to understand how IEDs functioning and it help the analysts regarding the required sensitivity for the analysis smokeless powder from post-blast fragments.

Fragments from the end caps yielded the highest amount of DPA and NG. These results of this study contributed by the meaning of understanding of how small IEDs function as well as inform analysts regarding the sensitivity that is required for post-blast analysis of smokeless powder. It is expected that many other types of smokeless powder could be analyzed by this technique. This technique also can be used for the analysis of some other types of containers like PVC [16].

2.4.5. Identification and Automated Derivatization of Controlled Substances via TV-SPME and Gas Chromatography/Mass Spectrometry (GC/MS)

Due to polarity, many compounds that present in biological and environmental samples are not suitable to be analyzed by GC. In addition to that, some compounds have the tendency to have decomposing and adsorbing properties on the injector or columns and to show non-reproducible peak areas, shapes and heights [91]. To overcome such issues, the need of introducing derivatization reactions arises [92]. The importance of derivatization comes from its ability to decrease the polarity of the compounds of interest and increase the volatility and improve the analytes thermo stability. The derivatization also can improve the process of selecting of compounds behavior towards selective detectors, such as the spectrometry (MS) and electron capture detector (ECD). One of the main purposes from the formation of derivatives is to enhance the selectivity of the compounds, limit of detection (LOD) or both [93]. Before applying the analytical method, the targeted compounds placed for a procedure of sample preparation that involves a derivatization, concentration, or clean-up step procedures [26]. Combining extraction technique with derivatization result in enhancing the separation characteristics, detectability, and analyte recovery [94]. Generally, derivatization has been performed to promote the extractability of the analytes, reduce polarity, improve the GC characteristics of compounds, and make them compatible with the analytical system and/or to increase the detection sensitivity [91]. In forensic science laboratories, controlled substances units are placed under pressure for analyzing samples adapting methods that can show cost-effectiveness and high throughput. Additional to that, it is recommended in the field of analytical chemistry that that new chemical compounds appear in forensic chemists and exhibits must react to this by developing instrumental methods have great selectivity and high specificity [95]. It was observed that TV-SPME offering greater sensitivity for controlled substances as compared

to traditional liquid injection. Additionally, TV-SPME technique was easily applied to involve either a post-extraction or a pre-extraction on-fiber derivatization step species with thermally labile. Promising results were obtained for almost all categories of drugs that were analyzed successfully by the meaning of on-fiber derivatization as solutions. This important discovery may increase the use of this novel technique, because controlled substances are existed mostly in their solid forms in the laboratories of forensic science. This technique can be applied in the determination of solid drug powders and beverage sample, since these applications include a significant decrease in the amount of sample preparation. Although not applicable ideally for all analytes, TV-SPME with on-fiber derivatization could serve as an important technique for the determination of hydroxylamine and amine, controlled substances, and GHB. Thus, this work results in a set of optimized derivatization methods that can serve in TV-SPME and even in liquid injection. This approach presents a possible method for automated derivatization and sampling for a wide variety of thermally labile compounds and for analyzing compounds that need no derivatization [72,74,96]. Many applications exist for extraction analyte by the TV-SPME which was shown in Figure 6.

2.4.6. VA-TV-SPME procedure

Considering that SPME is that method depended on vaporizing the whole portion of the sample of interest, including volatile, nonvolatile and semi-volatile components. However semi-volatile and non-volatile compounds needs more heat, for that more amount of the sample volume is required. As a resultant of that, the SPME fiber get heated and that fiber has not affected the absorption of the analytes on the SPME fiber [53]. It could be a limiting factor, and considered to be the main reason behind this important extraction technique is not more used widely. For that reason, publication studies based on TV-SPME technique are less [23,69,70]. To solve such limitations, TV-SPME is coupled with another technique to encourage the analytes vaporization

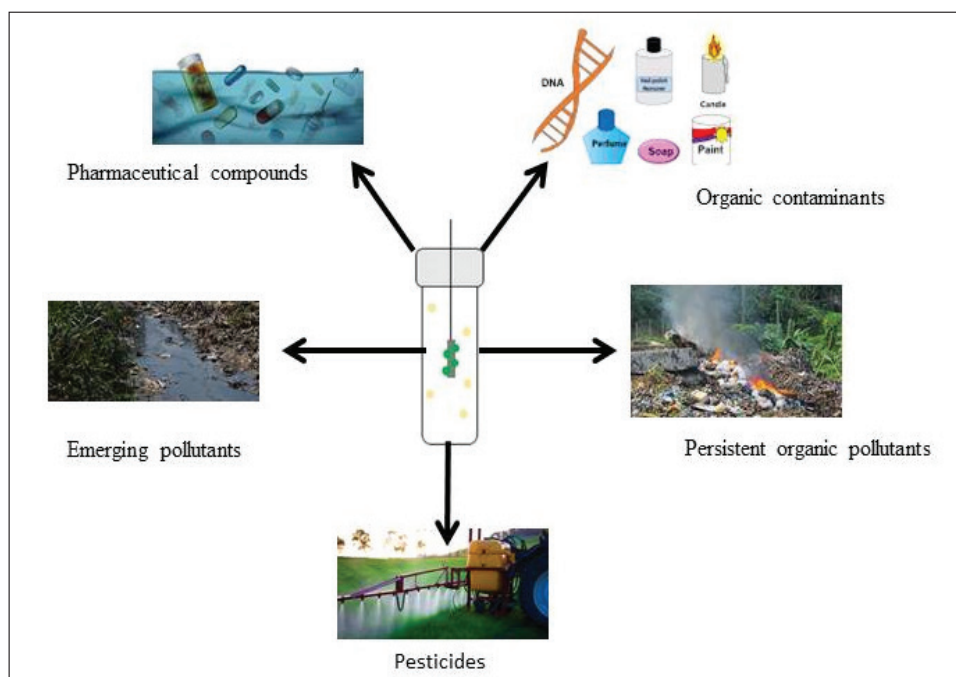


Fig. 6. Some applications of TV-SPME

and the preparation steps are omitted lead to a great reduction in the required heat which would assist a great benefit. In 2001, Brontun explained that when there is inhibition of the vessel pressure, it will lead to effect positively on the sampling [19]. One more explanation revealed that by decreasing the pressure, the analytes gets released from the matrix of the sample. Additional to that, decreased pressure reduces the boundary layer that attached to the fiber and strengthens the analyte absorption on the surface of the absorbent [49]. Recently, new extraction technique was introduced by Psillakis called Vac-HS-SPME as a new method depends on reduction of the pressure of the vessel used for sampling [76]. They revealed that when the vacuum conditions are applied, HS-SPME the extraction rate of analyte will be increased by speeding up the conversion from the aqueous matrix to the headspace. As a result of that, the vaporization of the analytes increased attributed to vacuum removal and faster equilibrium of the air from the headspace. This technique could not be able to extract analytes from the sample in solid phase and soil without preparation [77]. The sample may be lost due to the direct contact between the vacuum and the sample while evacuation period occurring.

To overcome such risk, the need of using a novel setup for the sampling vessel, Vacuum Assisted HS-SPME (VA-HS-SPME) was introduced to be used in the extraction of Polycyclic Aromatic Hydrocarbons (PAHs) from polluted soil without the need of preparation and the risk of analytes loss is less [52]. In that proposed technique, for the first time, a low-cost, sample, reliable and fast setup was developed by using both VA-HS-SPME (low pressure) [78] and TV-SPME techniques. One of the main advantages of VA-TV-SPME, more temperature can be applied for the extraction of analyte from the matrix of the sample without increasing the fiber temperature, which results in the increasing the of analyte extraction, as compare to conventional TV-SPME. One more advantage is that the time of sample vaporization is shorter. Also, when vacuum-assistance and total vaporization are simultaneously used, it maximizes the rate of analyte extraction in a complex matrix, with no need of any preparation. To evaluate the PAHs extraction from polluted water samples, a PDMS fiber is used, then the determination is done by GC-FID [67]. The main purpose of coupling TV-SPME with the VA-TV-SPME system (Fig.7) was to increase the sensitivities

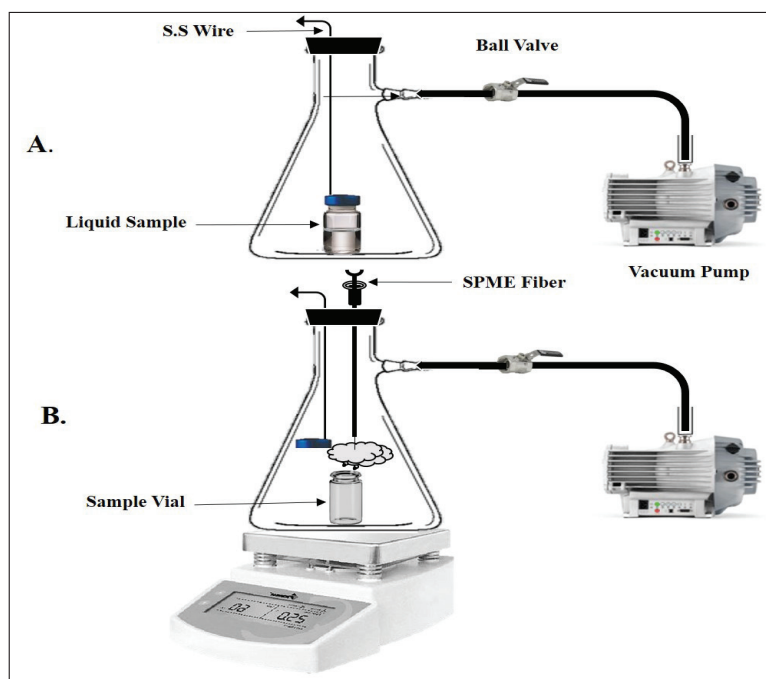


Fig. 7. Diagram of the VA-TV-SPME Assembly: in [A.] the cap of the sample is capped in close system while in [B.] the cap of the system is opened

in shorter times, which lead to lower extraction time and temperature, as compared to the conventional TV-SPME technique [67]. Such technique offers a new method to solve the warm of the SPME fiber caused by the heating process needed for separating the analyte from the matrix avoiding the use of complicated equipment and the sample is vaporized totally with lower duration as well as low heat energy. Additional to that, the total vaporization of the sample presents highly efficiency due to the increasing of the mass transfer in just one step. In addition to that, it is possible to use of homemade and commercial SPME fiber, and there is potential for coupling with other SPME techniques and automation, such as an inside needle capillary adsorption trap (INCAT) or a needle trap device (NTD [79].

2.5. Estimation of BTEX Compounds present in Polluted water using GO-APTES Fiber and Novel VA-TV-SPME Method

Isomers of benzene, toluene, ethylbenzene and xylene, all together known as BTEX (Fig.8), are highly volatile aromatic hydrocarbons and considered to be among the most serious human health and environmental risk issues.[32,97-98].

When these organic compounds are exposed in higher concentrations, they cause a harmful effects on central nervous systems, respiratory and skin [89-100]. Leakage of oil pipelines may be resulted by accidental fuel spills, and the disposal contamination of oil companies effluents and petrochemical, such pollutants have been released into groundwater and other water sources [97]. As a result of that, many analytical methods were developed such as a consequence, a wide variety of analytical methods, such as narrow-bore tube DLLME [38], ultrasound-assisted emulsification microextraction [101] and in syringe dispersive liquid-liquid microextraction (IS-DLLME). These methods have been developed with motive of extracting and determining of BTEX compounds from water [102]. For the determination of BTEX from contaminated water without using ant additional steps for the extraction and the preparation of the aqueous samples, microextraction techniques were used. VA-SPME removed one of the most partitioning steps in the conventional HS-SPME and that can increase the speed and the sensitivity of the method [102]. A novel and reliable microextraction technique was used for the fast determination of

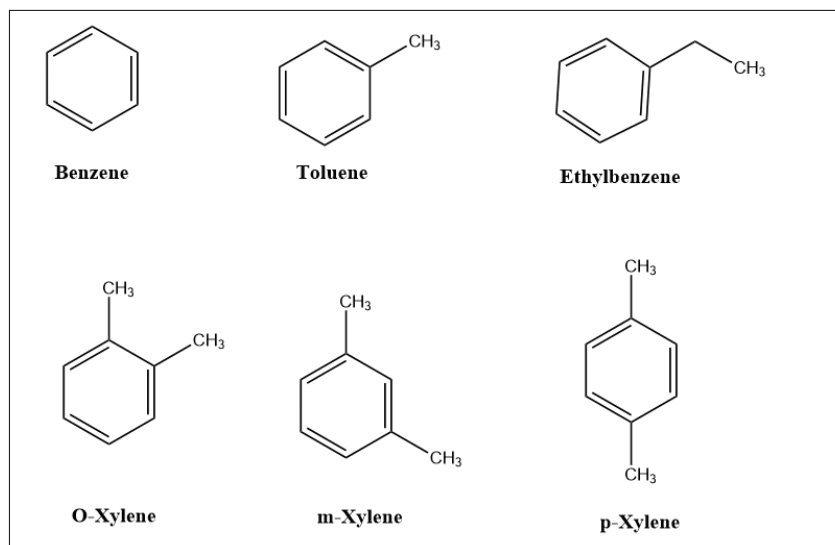


Fig. 8. Structures of BTEX

benzene, toluene, ethylbenzene and xylenes (BTEX) from contaminated water without any extra steps for the preparation or extraction of the aqueous sample. Vacuum-assisted-total vaporization-solid-phase microextraction (SPME) eliminated one of the partitioning steps in conventional headspace SPME and caused an increase in the sensitivity and speed of the method. A special nanocomposite SPME fibre made of graphene oxide/3-aminopropyl-triethoxysilane fiber was utilized as the extraction phase to attain an efficient extraction. Numerous parameters were considered for the optimization, the extraction time, temperature, and desorption conditions. The optimized method exposed acceptable a good validity aspects according to the ICH guidelines with acceptable range. In this study, BTEX that present in aqueous samples were determined by the use of VA-TV-SPME method. It was observed that effect of adsorption time is less in the extraction efficiency of VA-TV-SPME [102]. Additional to that, in order to preconcentrate and extract the analytes, an affordable and home-made GO-APTES SPME fiber was utilized and it was observed that it has reliable and a powerful sorbent, compared with that fibres obtained from the market commercially. For achieve a précised analyte determination, this method was hyphenated with a GC-FID instrument. According the outcomes of this method, an analytical parameters such as LDR,

LOD and RSD were within the acceptable range, and it was observed this method is suitable for the determination of BTEX in polluted water[32,47,59].

3. Conclusion

The coupling TV with SPME arises from the need for a technique where a complete vaporizing of the liquid samples gives a fewer matrix effect and better adsorption. Such a method requires less sample preparation, utilizes the least supplies, and can be done automatically, enabling it to be both a cost-effective and efficient method. TV-SPME is a sensitive technique where the liquid aliquot is totality vaporized prior to sampling, easing to attain the equilibria inside the sample vial and increasing the quantity of analyte available in the headspace. TV-SPME is an effective technique for analyzing controlled substances with and without on-fiber derivatization. The approach of coupling TV and SPME (TV-SPME) offered great sensitivity and even low detection limits for compounds present in the hair of tobacco users, such as nicotine and cotinine. A sample extract needs to be heated until it gets vaporized, and fiber of SPME is utilized for pre-concentrating analytes from the matrix.

4. Acknowledgement

The authors are heartily thankful to management of Chandigarh University for constant encouragement, support and motivation.

5. List of abbreviation

TV-SPME: Total Vaporization Solid Phase microextraction
 SPME: Solid Phase Microextraction
 GC: Gas Chromatography
 HS-SPME: Headspace Solid Phase Microextraction
 MOF: Metal-Organic Framework
 TATP: triacetone triperoxide
 I-SPME: Immersion Solid Phase Microextraction
 LC: Liquid Chromatography
 IR: Infrared Spectroscopy
 UV: Ultraviolet Spectroscopy
 TV: Total Vaporization
 PAHs: Polycyclic Aromatic Hydrocarbons
 LVI: Large-Volume Injection
 MS: Mass spectrometry
 GC/MS: Gas Chromatography/ Mass Spectrometry
 PDMS/DVB: Polydimethylsiloxane-divinylbenzene
 LC-MS: Liquid Chromatography- Mass Spectrometry
 TLC: Thin Layer Chromatography
 VOCs: Volatile Organic Compounds
 BSTFA: Bis(trimethylsilyl)trifluoroacetamide
 TMCS: Trimethylchlorosilane
 GLB: γ -butyrolactone
 GHB: γ -hydroxybutyric acid
 DPA: Diphenylamine
 NG: Nitroglycerin
 ECD: Electron Capture Detector
 LOD: Limit of Detection
 VA-TV-SPME: Vacuum Assisted Total Vaporization Solid Phase Microextraction
 VA-HS-SPME: Vacuum Assisted Headspace Solid Phase Microextraction
 PDMS: Polydimethylsiloxane
 GC-FID: Gas Chromatography Flame Ionization Detector
 CAT: Capillary Adsorption Trap
 INCAT: Inside Needle Capillary Adsorption Trap

6. References

- [1] C. L. Arthur, J. Pawliszyn, Solid phase microextraction with thermal desorption using fused silica optical fibers, *Anal. Chem.*, 62 (1990) 2145-2148. <https://doi.org/10.1021/ac00218a019>.
- [2] M. Lashgari, V. Singh, J. Pawliszyn, A critical review on regulatory sample preparation methods: Validating solid-phase microextraction techniques, *TrAC Trends Anal. Chem.*, 119 (2019). <https://doi.org/10.1016/j.trac.2019.07.029>.
- [3] E. Martendal, E. Carasek, A new approach based on a combination of direct and headspace cold-fiber solid-phase microextraction modes in the same procedure for the determination of polycyclic aromatic hydrocarbons and phthalate esters in soil samples, *J. Chromatogr., A* 1218 (2011) 1707-1714. <https://doi.org/10.1016/j.chroma.2011.01.074>.
- [4] E. Yiantzi, N. Kalogerakis, E. Psillakis, Vacuum-assisted headspace solid phase microextraction of polycyclic aromatic hydrocarbons in solid samples, *Anal. Chim. Acta.*, 890 (2015) 108-116. <https://doi.org/10.1016/j.aca.2015.05.047>.
- [5] J. S. Elmore, M. A. Erbahadir, D. S. Mottram, Comparison of dynamic headspace concentration on Tenax with solid phase microextraction for the analysis of aroma volatiles, *J. Agric. Food Chem.* 45 (1997) 108-116. <https://doi.org/10.1021/jf960835m>.
- [6] S. A. Barshick, W. H. Griest, Trace analysis of explosives in seawater using solid-phase microextraction and gas chromatography/ion trap mass spectrometry, *Anal. Chem.*, 70 (1998) 3015-3020. <https://doi.org/10.1021/ac980060b>.
- [7] S. A. Scheppers Wercinski, J. Pawliszyn, *Solid Phase Microextraction Theory*, Solid Phase Microextraction., Boca Raton, 257 pages, 1999. <https://doi.org/10.1201/9780367803223>
- [8] S. Huang, Monitoring of persistent organic pollutants in seawater of the Pearl River Estuary with rapid on-site active SPME sampling technique, *Environ. Pollut.*, 200 (2015) 149-158. <https://doi.org/10.1016/j.envpol.2015.02.016>.
- [9] S. Risticvic., Protocol for solid-phase microextraction method development,

- Nat. Protoc., 5 (2010) 122-139. <https://doi.org/10.1038/nprot.2009.179>.
- [10] É. A. Souza-Silva., A critical review of the state of the art of solid-phase microextraction of complex matrices III, *Bioanalytical and clinical applications. TrAC Trends Anal. Chem.*, 71 (2015) 249-264. <https://doi.org/10.1016/j.trac.2015.04.017>.
- [11] S. Lv, The study of fingerprint characteristics of Dayi pu-erh tea using a fully automatic HS-SPME/GC-MS and combined chemometrics method, *PLOS ONE*, 9 (2014) e116428. <https://doi.org/10.1371/journal.pone.0116428>
- [12] C. L. Arthur, Automation and optimization of spme. *Anal. Biochem.*, 64 (1992) 1960-1966. <https://doi.org/10.1021/ac00041a034>
- [13] J. Ai, Solid phase microextraction for quantitative analysis in nonequilibrium situations, *Anal. Chem.*, 69 (1997) 1230-1236. <https://doi.org/10.1021/ac9609541>.
- [14] K. G. Furton, Application of solid-phase microextraction to the recovery of explosives and ignitable liquid residues from forensic specimens, *J. Chromatogr., A* 885 (2000) 419-432. [https://doi.org/10.1016/s0021-9673\(00\)00368-x](https://doi.org/10.1016/s0021-9673(00)00368-x).
- [15] G. Liu, Headspace solid-phase microextraction of semi-volatile ultraviolet filters based on a superhydrophobic metal-organic framework stable in high-temperature steam, *Talanta* 219 (2020) 121175. <https://doi.org/10.1016/j.talanta.2020.121175>.
- [16] D. Bors, J. Goodpaster, Mapping explosive residues on galvanized pipe bomb fragments using total vaporization solid phase microextraction (TV-SPME), *Anal. Methods*, 7 (2015) 9756-9762. <https://doi.org/10.1039/C5AY02358K>.
- [17] R. Technologies, A review of: Static headspace – Gas chromatography theory and practice, *J. Liq. Chromatogr. Relat. Technol.*, 21 (1998) 434-436, <https://doi.org/10.1080/10826079808000503>.
- [18] M. Tabibpour, Carbon fibers modified with polypyrrole for headspace solid phase microextraction of trace amounts of 2-pentyl furan from breath samples, *J. Chromatogr. A*, 1609(2020) 460497. <https://doi.org/10.1016/j.chroma.2019.460497>.
- [19] N. P. Brunton, D. A. Cronin, F. J. Monahan, The effects of temperature and pressure on the performance of Carboxen/PDMS fibres during solid phase microextraction (SPME) of headspace volatiles from cooked and raw turkey breast, *Flavour Fragr. J.* 16 (2001) 294-302. <https://doi.org/10.1002/ffj.1000>.
- [20] A. Mehdinia, M. O. Aziz-Zanjani, Advances for sensitive, rapid and selective extraction in different configurations of solid-phase microextraction, *TrAC Trends Anal. Chem.*, 51 (2013) 13-22. <https://doi.org/10.1016/j.trac.2013.05.013>.
- [21] W. Q. Xie, Y. Gong, K. Yu, Enhancing the sensitivity of full evaporation technique using multiple headspace extraction analysis, *Chromatographia*, 80 (2017) 1263-1268. <https://doi.org/10.1007/s10337-017-3343-x>.
- [22] C. Wang, Oolong tea made from tea plants from different locations in Yunnan and Fujian, China showed similar aroma but different taste characteristics, *Springerplus*, 5 (2016) 576. <https://doi.org/10.1186/s40064-016-2229-y>.
- [23] W. Kranz, Optimization of total vaporization solid-phase microextraction (TV-SPME) for the determination of lipid profiles of *Phormia regina*, a forensically important blow fly species, *Anal. Bioanal. Chem.*, 409 (2017) 6349-6357. <https://doi.org/10.1007/s00216-017-0573-6>.
- [24] J. L. Thomas, Application of a co-polymeric solid phase extraction cartridge to residues containing nitro-organic explosives, *Forensic Chem.*, 11 (2018) 38-46. <https://doi.org/10.1016/j.forc.2018.08.006>.
- [25] S. Calderara, D. Gardebas, F. Martinez, Solid phase micro extraction coupled with on-column GC/ECD for the post-blast analysis of organic explosives, *Forensic Sci. Int.*, 137 (2003) 6-12. [https://doi.org/10.1016/s0379-0738\(03\)00256-1](https://doi.org/10.1016/s0379-0738(03)00256-1).

- [26] A. Jim, Application of solid-phase microextraction to Virgin olive oil quality control, *J. Chromatogr. A*, 1121 (2006) 140-144. <https://doi.org/10.1016/j.chroma.2006.05.005>.
- [27] C. L. Rainey, D. E. Bors, J. V. Goodpaster, Design and optimization of a total vaporization technique coupled to solid-phase microextraction, *Anal. Chem.*, 86 (2014) 11319-11325. <https://doi.org/10.1021/ac5030528>.
- [28] K. G. Furton, Application of solid-phase microextraction to the recovery of explosives and ignitable liquid residues from forensic specimens, *J. Chromatogr. A*, 885 (2000) 419-432. [https://doi.org/10.1016/s0021-9673\(00\)00368-x](https://doi.org/10.1016/s0021-9673(00)00368-x).
- [29] M. A. LeBeau, M. A. Montgomery, M. L. Miller, S. G. Burmeister, Analysis of biofluids for gamma-hydroxybutyrate (GHB) and gamma-butyrolactone (GBL) by headspace GC-FID and GC-M, *J. Anal. Toxicol.*, 24 (2000) 421-428. <https://doi.org/10.1093/jat/24.6.421>.
- [30] K. E. Davis, L. D. Hickey, J. V. Goodpaster, Detection of γ -hydroxybutyric acid (GHB) and γ -butyrolactone (GBL) in alcoholic beverages via total vaporization solid-phase microextraction (TV-SPME) and gas chromatography-mass spectrometry, *J. Forensic Sci.* 66 (2021) 846-853. <https://doi.org/10.1111/1556-4029.14660>.
- [31] D. N. Konanov, UniQPy: A tool for estimation of short-chain fatty acids composition by gas-chromatography/mass-spectrometry with headspace extraction, *J. Pharm. Biomed. Anal.*, 212 (2022) 11468. <https://doi.org/10.1016/j.jpba.2022.114681>.
- [32] M. Beiranvand, Determination of BTEX compounds in contaminated water using the novel vacuum-assisted-total vaporization SPME method and GO-APTES fiber, *J. Chromatogr. Sci.*, 60 (2022) 486-492. <https://doi.org/10.1093/chromsci/bmab111>.
- [33] K. E. Davis, J. V. Goodpaster, Gas chromatography-mass spectrometry paired with total vaporization solid-phase microextraction as a forensic tool, *J. Vis. Exp.*, 171 (2021) 1-6. <https://doi.org/10.3791/61880>.
- [34] M. Llompарт, M. Celeiro, C. García-Jares, T. Dagnac, Environmental applications of solid-phase microextraction, *TrAC Trends Anal. Chem.*, 112 (2019) 1-12. <https://doi.org/10.1016/j.trac.2018.12.020>.
- [35] G. Sauzier, Optimisation of recovery protocols for double-base smokeless powder residues analysed by total vaporisation (TV) SPME/GC-MS, *Talanta*, 158 (2016) 368-374. <https://doi.org/10.1016/j.talanta.2016.04.048>.
- [36] L. Hickey, Automated derivatization and identification of controlled substances in solution via total-vaporization solid-phase microextraction (TV-SPME), *SSRN Electron. J.*, (2021), <https://doi.org/10.2139/ssrn.3888661>.
- [37] O. M. Fayemiwo, M. O. Daramola, K. Moothi, BTEX compounds in water – Future trends and directions for water treatment. *Water South Africa*, 43 (2017) 602-613. <https://doi.org/10.4314/wsa.v43i4.08>.
- [38] M. Rahmani, M. Kaykhahi, E. Ghasemi, M. Tahernejad, Application of in-syringe dispersive liquid-liquid microextraction and narrow-bore tube dispersive liquid-liquid microextraction for the determination of trace amounts of BTEX in water samples, *J. Chromatogr. Sci.*, 53 (2015) 1210-1216, <https://doi.org/10.1093/chromsci/bmu163>.
- [39] M. Sajid, Porous membrane protected micro-solid-phase extraction: A review of features, advancements and applications, *Anal. Chim. Acta.*, 965 (2017) 36-53. <https://doi.org/10.1016/j.aca.2017.02.023>.
- [40] M. Sajid, Development of natural sorbent based micro-solid-phase extraction for determination of phthalate esters in milk samples, *Anal. Chim. Acta*, 924 (2016) 35-44. <https://doi.org/10.1016/j.aca.2016.04.016>.
- [41] C. Basheer, H. K. Lee, Hollow fiber membrane-protected solid-phase microextraction of triazine herbicides in bovine milk and sewage

- sludge samples, *J. Chromatogr., A* 1047. (2004) 189-194. <https://doi.org/10.1016/j.chroma.2004.06.130>.
- [42] S. Merkle, K. Kleeberg, J. Fritsche, Recent developments and applications of solid phase microextraction (SPME) in food and environmental analysis—A review, *Chromatogra. 2* (2015) 293-381. <https://doi.org/10.3390/chromatography2030293>
- [43] H. Piri-Moghadam, F. Ahmadi, J. Pawliszyn, A critical review of solid phase microextraction for analysis of water samples, *TrAC Trends Anal. Chem.*, 85 (2016) 133-143. <https://doi.org/10.1016/j.trac.2016.05.029>.
- [44] X. Wang, Zinc(II)-based metal-organic nanotubes coating for high sensitive solid phase microextraction of nitro-polycyclic aromatic hydrocarbons, *Talanta*, 186 (2018) 561-567. <https://doi.org/10.1016/j.talanta.2018.02.062>.
- [45] M. Merdivan, V. Pino, J. L. Anderson, Determination of volatile polycyclic aromatic hydrocarbons in waters using headspace solid-phase microextraction with a benzyl-functionalized crosslinked polymeric ionic liquid coating, *Environ. Technol.*, 38 (2017) 1897-1904. <https://doi.org/10.1080/09593330.2016.1240242>.
- [46] H. Mokbel, Simultaneous analysis of organochlorine pesticides and polychlorinated biphenyls in air samples by using accelerated solvent extraction (ASE) and solid-phase micro-extraction (SPME) coupled to gas chromatography dual electron capture detection, *Environ. Sci. Pollut. Res. Int.*, 23 (2016) 8053-8063. <https://doi.org/10.1007/s11356-016-6072-z>.
- [47] M. Espina-Benitez, Development of a new microextraction fiber combined to on-line sample stacking capillary electrophoresis UV detection for acidic drugs determination in realwater samples, *Int. J. Environ. Res. Public Health.*, 14 (2017) 1-16. <https://doi.org/10.3390/ijerph14070739>.
- [48] R. López-Serna, Multiresidue analytical method for pharmaceuticals and personal care products in sewage and sewage sludge by online direct immersion SPME on-fiber derivatization – GCMS, *Talanta*, 186 (2018) 506-512. <https://doi.org/10.1016/j.talanta.2018.04.099>.
- [49] N. Ochiai, K. Sasamoto, A. Hoffmann, K. Okanoya, Full evaporation dynamic headspace and gas chromatography-mass spectrometry for uniform enrichment of odor compounds in aqueous samples, *J. Chromatogr. A*, 1240 (2012) 59-68. <https://doi.org/10.1016/j.chroma.2012.03.097>.
- [50] S. R. Kim, Method validation for measurement of hair nicotine level in nonsmokers, *Biomed. Chromatogr.*, 23 (2009) 273-279. <https://doi.org/10.1002/bmc.1110>.
- [51] J. Kim, Association between secondhand smoke in hospitality venues and urinary 4-(methylnitrosamino)-1-(3-pyridyl)-1-butanol concentrations in non-smoking staff, *Int. J. Environ. Res. Public Health*, 13 (2016) <https://doi.org/10.3390/ijerph13111101>.
- [52] C. L. Arthur, J. Pawliszyn, Solid phase microextraction with thermal desorption using fused silica optical fibers, *Anal. Chem.*, 62 (1990) 2145-2148. <https://doi.org/10.1021/ac00218a019>,
- [53] J. You, BTEX degradation by a newly isolated bacterium: Performance, kinetics, and mechanism, *Int. Biodeterior. Biodegrad.*, 129 (2018) 202-208. <https://doi.org/10.1016/j.ibiod.2018.02.012>.
- [54] N. De Giovanni, D. Marchetti, A systematic review of solid-phase microextraction applications in the forensic context, *J. Anal. Toxicol.*, 44 (2020) 268-297. <https://doi.org/10.1093/jat/bkz077>.
- [55] D. M. Mana Kialengila, Full evaporation headspace gas chromatography for sensitive determination of high boiling point volatile organic compounds in low boiling matrices, *J. Chromatogr. A*, 1315 (2013) 167-175. <https://doi.org/10.1016/j.chroma.2013.09.058>.
- [56] N. Ochiai, K. Sasamoto, A. Hoffmann, K. Okanoya, Full evaporation dynamic headspace

- and gas chromatography-mass spectrometry for uniform enrichment of odor compounds in aqueous samples, *J. Chromatogr. A*, 1240 (2012) 59-68. <https://doi.org/10.1016/j.chroma.2012.03.097>.
- [57] E. Goudsmits, The analysis of organic and inorganic gunshot residue from a single sample, *Forensic Sci. Int.*, 299 (2019) 168-173. <https://doi.org/10.1016/j.forsciint.2019.03.049>.
- [58] S. Dugheri, N. Mucci, Advanced solid-phase microextraction techniques and related automation: A review of commercially available technologies *J. Anal. Methods Chem.*, 2022(2022) 8690569. <https://doi.org/10.1155/2022/8690569>
- [59] D. Bors, J. Goodpaster, Mapping smokeless powder residue on PVC pipe bomb fragments using total vaporization solid phase microextraction, *Forensic Sci. Int.*, 276 (2017) 71-76. <https://doi.org/10.1016/j.forsciint.2017.04.002>.
- [60] Q. Guan, Rapid determination of total acid content of oils resulting from sub/supercritical water liquefaction of lignite by headspace gas chromatography, *Energy Fuels*, 27 (2013) 5135-5137. <https://doi.org/10.1021/ef401020c>.
- [61] M. Chan , H. Sy, Determination of ethanol content in kombucha using headspace gas chromatography with mass spectrometry detection: Single-laboratory validation, *J. AOAC Int.*, 5 (2021) 122-128. <https://doi.org/10.1093/jaoacint/qsaa094>.
- [62] J. Schuberth, A. Full, A full Evaporation headspace technique with capillary GC and ITD: A means for quantitating volatile organic compounds in biological samples, *J. Chromatogr. Sci.*, 34 (1996) 314-319. <https://doi.org/10.1093/chromsci/34.7.314>.
- [63] C. Pistos, J. T. Stewart, Direct injection HPLC method for the determination of selected benzodiazepines in plasma using a Hisep column, *J. Pharm. Biomed. Anal.*, 33 (2003) 1135-1142. [https://doi.org/10.1016/s0731-7085\(03\)00426-6](https://doi.org/10.1016/s0731-7085(03)00426-6).
- [64] J. Pawliszyn, S. Pedersen-Bjergaard, Analytical microextraction: Current status and future trends, *J. Chromatogr. Sci.*, 44 (2006) 291-307. <https://doi.org/10.1093/chromsci/44.6.291>.
- [65] J. Pawliszyn, Theory of solid-phase microextraction, *J. Chromatogr. Sci.*, 38 (2000) 270-278. <https://doi.org/10.1093/chromsci/38.7.270>
- [66] G. Vas, K. Vékey, Solid-phase microextraction: A powerful sample preparation tool prior to mass spectrometric analysis, *J. Mass Spectrom.*, 39 (2004) 233-254. <https://doi.org/10.1002/jms.606>.
- [67] M. Beiranvand, A. Ghiasvand, Design and optimization of the VA-TV-SPME method for ultrasensitive determination of the PAHs in polluted water, *Talanta*, 212 (2020) 120809. <https://doi.org/10.1016/j.talanta.2020.120809>.
- [68] X. Sun, Detection of polycyclic aromatic hydrocarbons in water samples by annular platform-supported ionic liquid-based headspace liquid-phase microextraction, *J. Anal. Methods Chem.*, 2018 (2018) 3765682. <https://doi.org/10.1155/2018/3765682>.
- [69] D. Bors, J. Goodpaster, Chemical analysis of racing fuels using total vaporization and gas chromatography mass spectrometry (GC/MS), *Anal. Methods*, 8 (2016) 3899-3902. <https://doi.org/10.1039/C6AY00539J>.
- [70] G. Sauzier, Optimisation of recovery protocols for double-base smokeless powder residues analysed by total vaporisation (TV) SPME/GC-MS, *Talanta*, 158 (2016) 368-374. <https://doi.org/10.1016/j.talanta.2016.04.048>.
- [71] C. Jurado et., Rapid analysis of amphetamine, methamphetamine, MDA, and MDMA in urine using solid-phase microextraction, direct on-fiber derivatization, and analysis by GC-MS, *J. Anal. Toxicol.*, 24 (2000) 11-16. <https://doi.org/10.1093/jat/24.1.11>.
- [72] L. D. Hickey, Automated derivatization and identification of controlled substances via total vaporization solid phase microextraction (TV-SPME) and gas chromatography/mass spectrometry (GC/MS), forensic and

- investigative science program, Thesis, 2019. <http://dx.doi.org/10.7912/C2/2387>
- [73] K. E. Davis, L. D. Hickey, J. V. Goodpaster, Detection of γ -hydroxybutyric acid (GHB) and γ -butyrolactone (GBL) in alcoholic beverages via total vaporization solid-phase microextraction (TV-SPME) and gas chromatography–mass spectrometry, *J. Forensic Sci.*, 66 (2021) 846-853. <https://doi.org/10.1111/1556-4029.14660>.
- [74] A.V. de Bairros, Determination of low levels of benzodiazepines and their metabolites in urine by hollow-fiber liquid-phase microextraction (LPME) and gas chromatography–mass spectrometry (GC–MS), *J. Chromatogr. B*, 975 (2015) 24-33. <https://doi.org/10.1016/j.jchromb.2014.10.040>
- [75] G.S. Groenewold, J.R. Scott, C. Rae, Recovery of phosphonate surface contaminants from glass using a simple vacuum extractor with a solid-phase microextraction fiber, *Anal. Chim. Acta*, 697 (2011) 38-47. <https://doi.org/10.1016/j.aca.2011.04.034>.
- [76] E. Psillakis, Vacuum-assisted headspace solid-phase microextraction: A tutorial review, *Anal. Chim. Acta*, 986 (2017) 12-24. <https://doi.org/10.1016/j.aca.2017.06.033>.
- [77] N. Reyes-Garcés, Advances in solid phase microextraction and perspective on future directions, *Anal. Chem.*, 90 (2018) 302-360. <https://doi.org/10.1021/acs.analchem.7b04502>.
- [78] M. Beiranvand, A. Ghiasvand, Simple, Low-cost and reliable device for vacuum-assisted headspace solid-phase microextraction of volatile and semivolatile compounds from complex solid samples, *Chromatographia*, 80 (2017) 1771-1780. <https://doi.org/10.1007/s10337-017-3422-z>.
- [79] A. Ghiasvand, F. Zarghami, M. Beiranvand, Ultrasensitive direct determination of BTEX in polluted soils using a simple and novel pressure-controlled solid-phase microextraction setup, *J. Iran. Chem. Soc.*, 15 (2018) 1051-1059. <https://doi.org/10.1007/s13738-018-1302-6>.
- [80] R. Telles-Romero, Effect of temperature on pupa development and sexual maturity of laboratory *Anastrepha obliqua* adults, *Bull. Entomol. Res.*, 101 (2011) 565-571. <https://doi.org/10.1017/S0007485311000150>.
- [81] B. Frere, GC-MS analysis of cuticular lipids in recent and older scavenger insect puparia. An approach to estimate the postmortem interval (PMI), *Anal. Bioanal. Chem.*, 406 (2014) 1081-1088. <https://doi.org/10.1007/s00216-013-7184-7>.
- [82] J. E. Baker, D. R. Nelson, C. L. Fatland, Developmental changes in cuticular lipids of the black carpet beetle, *Attagenus megatoma*. *Insect Biochem.*, 9 (1979) 335-339. [https://doi.org/10.1016/0020-1790\(79\)90015-5](https://doi.org/10.1016/0020-1790(79)90015-5).
- [83] M. Gołębiowski, Comparison of free fatty acids composition of cuticular lipids of *Calliphora vicina* larvae and pupae, *Lipids*, 47 (2012) 1001-1009. <https://doi.org/10.1007/s11745-012-3702-1>.
- [84] M. Gołębiowski, Cuticular and internal n-alkane composition of *Lucilia sericata* larvae, pupae, male and female imagines: Application of HPLC-LLSD and GC/MS-SIM, *Bull. Entomol. Res.*, 102 (2012) 453-460. <https://doi.org/10.1017/S0007485311000800>.
- [85] M. Gołębiowski, The composition of the cuticular and internal free fatty acids and alcohols from *Lucilia sericata* males and females, *Lipids*, 47 (2012) 613-622. <https://doi.org/10.1007/s11745-012-3662-5>.
- [86] M. Gołębiowski, M. I. Boguś, M. Paszkiewicz, P. Stepnowski, Cuticular lipids of insects as potential biofungicides: Methods of lipid composition analysis, *Anal. Bioanal. Chem.*, 399 (2011) 3177-3191. <https://doi.org/10.1007/s00216-010-4439-4>.
- [87] J. A. Yoder, G. J. Blomquist, D. L. Denlinger, Hydrocarbon profiles from puparia of diapausing and nondiapausing flesh flies (*Sarcophaga crassipalpis*) reflect quantitative rather than qualitative differences, *Arch. Insect Biochem. Physiol.*, 28 (1995) 377-385. <https://doi.org/10.1002/arch.940280407>.

- [88] S. R. Kim, Method validation for measurement of hair nicotine level in nonsmokers, *Biomed. Chromatogr.*, 23 (2009) 273-279. <https://doi.org/10.1002/bmc.1110>.
- [89] J. Kim, Association between secondhand smoke in hospitality venues and urinary 4-(methylnitrosamino)-1-(3-pyridyl)-1-butanol concentrations in non-smoking staff, *Int. J. Environ. Res. Public Health*, 13 (2016) 1101. <https://doi.org/10.3390/ijerph13111101>.
- [90] TWGFEX, Laboratory explosion group standards and protocols, Recommended guidelines for forensic identification of intact explosives, 2007. https://moodle.cranfield.ac.uk/pluginfile.php/408151/mod_resource/content/0/Guidelines_for_ident_of_post_blast_expl_residues-TWGFEX.pdf (2007) 1-9.
- [91] M. A. Farajzadeh, N. Nouri, P. Khorram, Derivatization and microextraction methods for determination of organic compounds by gas chromatography, *TrAC Trends Anal. Chem.*, 55 (2014) 14-23. <https://doi.org/10.1016/j.trac.2013.11.006>.
- [92] F. Pena-Pereira, I. Lavilla, C. Bendicho, Miniaturized preconcentration methods based on liquid-liquid extraction and their application in inorganic ultratrace analysis and speciation: A review, *Spectrochim. Acta, B*, 64 (2009) 1-15. <https://doi.org/10.1016/j.sab.2008.10.042>.
- [93] R. M. Smith, Before the injection- Modern methods of sample preparation for separation techniques, *J. Chromatogr. A*, 1000 (2003) 3-27. [https://doi.org/10.1016/s0021-9673\(03\)00511-9](https://doi.org/10.1016/s0021-9673(03)00511-9).
- [94] A. Balinova, R. Mladenova, D. Shtereva, Solid-phase extraction on sorbents of different retention mechanisms followed by determination by gas chromatography-mass spectrometric and gas chromatography-electron capture detection of pesticide residues in crops, *J. Chromatogr. A*, 1150 (2007) 136-144. <https://doi.org/10.1016/j.chroma.2007.02.002>.
- [95] J. M. DuBois, A mixed-method analysis of reports on 100 cases of improper prescribing of controlled substances, *J. Drug Issues.*, 46 (2016) 457-472. <https://doi.org/10.1177/0022042616661836>.
- [96] M. Lashgari, Y. Yamini, An overview of the most common lab-made coating materials in solid phase microextraction, *Talanta*, 191 (2019) 283-306. <https://doi.org/10.1016/j.talanta.2018.08.077>.
- [97] T. O. Egbuchunam, G. Obi, F. E. Okieimen, F. Tihminlioglu, Removal of BTEX from aqueous solution using Organokaolinite, *Int. J. Appl. Environ. Sci.*, 11 (2016) 505-513. <http://www.ripublication.com>
- [98] M. H. Dehghani, Source apportionment of BTEX compounds in Tehran, Iran using UNMIX receptor model, *Air Qual. Atmos. Health*, 10 (2017) 225-234. <https://doi.org/10.1007/s11869-016-0425-0>.
- [99] K. Khodaei, BTEX biodegradation in contaminated groundwater using a novel strain (*Pseudomonas* sp. BTEX-30), *Int. Biodeterior. Biodegrad.*, 116 (2017) 234-242. <https://doi.org/10.1016/j.ibiod.2016.11.001>.
- [100] M. Hashemi, N. Jahanshahi, A. Habibi, Application of ultrasound-assisted demulsification microextraction for determination of benzene, toluene, ethylbenzene and o-xylene in water samples by gas chromatography, *Desalination.*, 288 (2012) 93-97. <https://doi.org/10.1016/j.desal.2011.12.017>.
- [101] W. S. Khayoon, Micro-solid phase extraction with liquid chromatography-tandem mass spectrometry for the determination of aflatoxins in coffee and malt beverage, *Food Chem.*, 147 (2014) 287-294. <https://doi.org/10.1016/j.foodchem.2013.09.049>.
- [102] F. Leusch, M. Bartkow, A short primer on benzene, toluene, ethylbenzene and xylenes (BTEX) in the environment and in hydraulic fracturing fluids, *Smart Water Res. Cent.*, (2010) 1-8. <https://www.ehp.qld.gov.au/management/coal-seam-gas/pdf/btex-report.pdf>